AWARD NUMBER: W81XWH-18-1-0086

TITLE: Novel Postpartum Liver Biology Has Implications for Breast Cancer Liver Metastasis

PRINCIPAL INVESTIGATOR: Pepper Schedin

CONTRACTING ORGANIZATION: OHSU
3181 SW Sam Jackson Park Road
Portland, OR 97239

REPORT DATE: JULY 2022

TYPE OF REPORT: Final

PREPARED FOR: U.S. Army Medical Research and Development Command
Fort Detrick, Maryland 21702-5012

REPORT DOCUMENTATION PAGE

Form Approved
OMB No. 0704-0188

1. REPORT DATE	2. REPORT TYPE	3. DATES COVERED
JULY 2022	Final	03/15/2018-03/14/2022

4. TITLE AND SUBTITLE

Novel Postpartum Liver Biology Has Implications for Breast Cancer Liver Metastasis

5a. CONTRACT NUMBER
W81XWH-18-1-0086

5b. GRANT NUMBER
BC170206

5c. PROGRAM ELEMENT NUMBER

6. AUTHOR(S)
Pepper Schedin
Phae Ochs

E-Mail:

5d. PROJECT NUMBER

5e. TASK NUMBER

5f. WORK UNIT NUMBER

7. PERFORMING ORGANIZATION NAME(S) AND ADDRESS(ES)
OHSU
3181 SW Sam Jackson Park Road
Portland, Oregon 97239

8. PERFORMING ORGANIZATION REPORT NUMBER

9. SPONSORING / MONITORING AGENCY NAME(S) AND ADDRESS(ES)

U.S. Army Medical Research and Development Command
Fort Detrick, Maryland 21702-5012

10. SPONSOR/MONITOR'S ACRONYM(S)

11. SPONSOR/MONITOR'S REPORT NUMBER(S)

12. DISTRIBUTION / AVAILABILITY STATEMENT

Approved for Public Release; Distribution Unlimited

13. SUPPLEMENTARY NOTES

14. ABSTRACT

Women diagnosed with breast cancer within 10 years of a completed pregnancy are 2~3x more likely to develop liver metastases than never-pregnant (nulliparous) patients, even after controlling for prognostic variables. This finding suggests a unique biology in the postpartum liver, a putative pre-metastatic niche, which makes postpartum patients more susceptible to liver metastases. Here we tackle the problem of defining the liver-breast cancer tumor cell niche in models of postpartum breast cancer and explore relevance to women, laying the foundation for rational drug design to treat metastatic BrCa to the liver.

In rodent models, we previously reported increased liver size, hepatocyte proliferation, and anabolic metabolism during pregnancy and lactation. Within one week post-weaning, the rodent liver returned to its pre-pregnant size via a coordinated cell death and tissue remodeling process we call liver involution.

To explore a potential relationship between liver involution and liver metastasis, we utilized an immune competent murine model of postpartum breast cancer (Aim 1). In this model, liver metastases are induced by portal vein injection of mammary tumor cells into nulliparous or involution hosts. Using two different mammary tumor cell lines, we find that the process of involution supports overt liver metastasis. To investigate if increased metastatic burden in the involuting liver is due to increased tumor cell seeding, the number of tumor cells that extravasated into the liver parenchyma was evaluated over time. Seeding was not enhanced in involution hosts. Time-course experiments show the metastatic advantage in the postpartum host emerges ~2 weeks after tumor cell injection. This time frame is consistent with differential tumor cell clearance via cytotoxic immunity, which we hypothesize differs between nulliparous and involution hosts. Data in support of this hypothesis includes our recent results showing impaired T naïve T cell priming in the involution host, suggestive of immune suppression in the involution liver microenvironment. These data are published.

To investigate relevance of weaning-induced liver involution in women, we recruited healthy pregnant women to undergo MRI liver scans at first and third trimester, in addition to other imaging and lab tests (Aim 3). In a cohort of 47 women we find, overall, increased liver volume with pregnancy (average 15% increase). A subset of participants (n=17) underwent an MRI liver scan at >3 months post-weaning to ask if liver size decreases after weaning. Post-weaning liver volumes were reduced compared to third trimester liver volumes, and were similar to baseline liver sizes. These data are consistent with the occurrence of weaning-induced liver involution in women, and may shed light into the high rates of liver metastases observed in young breast cancer patients. These data are published.

To better understand the liver metastatic niche in women with breast cancer metastasis to the liver (BCML), we established an IRB to obtain formalin fixed, paraffin embedded cases of BCML, collected 28 cases with complete clinical data and sufficient tissue (from 34 cases total), performed multiplex immunohistochemistry (mIHC) to characterize tumor phenotypes, and proximity extracellular matrix, and immune milieu (Aim 2). We find that BCML are more likely to occur in younger patients (<45 years of age); associate with recent pregnancy in younger women; be luminal and ER+ in biomarker expression; show evidence of tumor differentiation; have relatively low to modest ki67 expression, low desmoplasia, vascularity or lymphatic involvement; and strongly associate with the extracellular matrix protein collagen IV. These data analyses are incomplete and remain unpublished at the end of the grant funding period. We are pursuing additional funding sources to complete these objectives.

15. SUBJECT TERMS

NONE LISTED

16. SECURITY CLASSIFICATION OF:			**17. LIMITATION OF ABSTRACT**	**18. NUMBER OF PAGES**	**19a. NAME OF RESPONSIBLE PERSON**
					USAMRDC
a. REPORT	**b. ABSTRACT**	**c. THIS PAGE**	Unclassified	**84**	**19b. TELEPHONE NUMBER** *(include area code)*
Unclassified	Unclassified	Unclassified			

Standard Form 298 (Rev. 8-98)
Prescribed by ANSI Std. Z39.18

TABLE OF CONTENTS

1. **INTRODUCTION:** *Narrative that briefly (one paragraph) describes the subject, purpose and scope of the research.*

The poor prognosis of young women diagnosed with BrCa is highest in women diagnosed postpartum, up to 10 years out from a completed pregnancy. Our newer data show that this poor prognosis can be tracked to increased liver metastasis; data that argues strongly for the development of treatments that are effective at blocking metastatic lesions in the liver. Recently, the concept of targeting the metastatic cell niche has gained momentum. However, this approach is seriously hampered by difficulties in finding and characterizing disseminated tumor cells. Here we tackle the problem of defining the liver-BrCa tumor cell niche in models of postpartum breast cancer and explore relevance to women, laying the foundation for rational drug design to treat metastatic BrCa to the liver. **Objective/Specific Aims:** We identify the lack of understanding of postpartum liver biology as a major obstacle to identifying therapeutic targets aimed at destabilizing the liver metastatic niche in postpartum breast cancer patients. To advance this goal, mechanistic studies and stronger translational rationale are needed. To fill these critical gaps, we propose the following: **Aim 1)** Use liver metastasis mouse models to decipher the post-intravasation steps of the metastatic cascade that are supported by the involuting liver. **Aim 2)** Explore the liver metastatic niche in breast cancer patients utilizing tumor and adjacent normal liver tissue obtained from breast cancer patients with liver metastases. **Aim 3)** Obtain first-of-kind evidence for weaning-induced liver involution in women via a serial MRI imaging study of livers in healthy women across pregnancy and weaning. This final report covers accomplishments achieved over the duration of the entire funding period.

2. **KEYWORDS:** Young women's breast cancer, pregnancy, postpartum breast involution, postpartum breast cancer, metastatic niche, liver growth, tumor microenvironment

3. ACCOMPLISHMENTS: What was accomplished under these goals?

Brief Summary by Year of Funding:
Aim 1) **Use liver metastasis mouse models to decipher the post-intravasation steps of the metastatic cascade that are supported by the involuting liver**. Aim 1 tasks: 90% complete at end of funding period, as follows:

<u>Liver Metastasis Model -Balb C mice/ D2A1-GFP mammary tumor cells</u>

Year 1, months 1-6: animal studies: *100% complete*
Year 1, months 7-12: tissue sectioning *100% complete*
Year 2, months 1-6: Immunohistochemistry (IHC) data capture and IHC quantitation: IHC endpoint terminated due to inability to detect the variant of GPT transfected into these cells by multiple ant-GFP antibodies (as presented in Yr 1 final report). For this D2A1-GFP model, we will rely exclusively on histological evidence of tumor mass. *100% complete*
Year 2, manuscript preparation
Year 3 data published*. Task if 100% complete*

<u>Liver Metastasis Model - Balb C mice/ D2OR-GFP mammary tumor cells (time course of 90 min, 1, 3, and 14 days post tumor cell injection)</u>

Year 1, months 6-12: animal studies: 100% complete
Year 2, months 1-6: tissue sectioning 100% complete, multiplex IHC: 100% complete
Year 2, months 7-12: IHC data capture and quantitation: 100% complete
Year 3, manuscript preparation
Year 3, data publication. Task is *100% complete*

<u>Liver Metastasis Model- Balb C mice/ D2OR-GFP mammary tumor cells anti CD8 -treatment study</u>

Year 2, validation studies to optimize dose and delivery of anti-CD8 blocking antibody studies
Year 2, blocking peptide metastases studies
Year 2-3, data capture, quantitation,
Year 3, manuscript preparation
Year 3, data publication. Task is 100% complete

NEW Metastasis model (added Yr 1Q4) Model 3 – Nude mice/D2OR mammary tumor cells

Year 2, months 9-12: animal studies *100% complete*
Year 2, months 1-3: functional evidence for immune suppression-in vivo T cell activation assays: 100% complete
Year 3, determine that the novel findings of this study (i.e., lack of liver metastases in the nude hosts) remain outside the scope of this DOD application and was not further pursed with this grant mechanism.

Aim 2) Explore the liver metastatic niche in breast cancer patients utilizing tumor and adjacent normal liver tissue obtained from breast cancer patients with liver metastases. Aim 2 tasks 75% complete at end of funding period, as follows:

Year 1, months 1-6: IRB submission and approval: *100% complete*
Year 1-4, 34 cases were accrued [overall goal by study end was 40-56 total accrual], so *85% complete*. However, only 28 cases completed through to tissue acquisition, so 70*% complete*
Year 2, months 1-6: First tissue batch of block sectioning- *100% complete*; multiplex IHC: *66% complete*
Year 2, months 7-12: batch #1 (n=18 cases) IHC mIHC panel #1 ("Discovery Panel") data capture and quantitation: *100% complete*
Year 2, months 7-12: development of mIHC panel #2 (ECM and integrin panel) - *100% complete*
Year 2, months 7-12: Batch #1, mIHC panel #2 staining *100% complete*
Year 2, months 7-12: Second tissue batch of blocks (n=6) sectioning, multiplex IHC: 100% *complete*
Year 3, months 1-6: batch #2 IHC data capture and quantitation: 75*% complete*
Year 3, months 1-6: Third tissue batch of block sectioning (n=4), multiplex IHC: *100% complete*
Year 3, months 7-12, batch #3, data capture and quantitation: *50% complete*
Year 3, manuscript preparation: *30% complete*

Aim 3) **Obtain first-of-kind evidence for weaning-induced liver involution in women via a serial MRI imaging study of livers in healthy women across pregnancy and weaning.** Aim 3 tasks: 100% complete at end of funding period, as follows:

Year 1**,** Continue to enroll new participants to the Moms LIVEr study by contacting participants enrolled in the parent Baby Bump study: *100% complete*
Years 2-3**,** Continue monthly contact with enrolled participants to determine their anticipated time of weaning: *100% complete*
Years 1-2, Interim data analyses-including compilation of liver volumetric data, body composition, dietary and physical activity surveys, lactation survey data collection and calculation of breast/liver work load during lactation: *100% complete*
Years 2-3, At time of weaning, schedule their postpartum liver MRI scan, Bodpod for body composition analysis, and dietary, physical activity and lactation questionnaire visits: *100% complete*
Years 2-3, manuscript preparation
Year 4, manuscript publication, 100% complete, manuscript published

Detailed Report:

Aim 1: Use liver metastasis mouse models to decipher the post-intravasation steps of the metastatic cascade that are supported by the involuting liver

1. **Summary of Significant Results and Key Conclusions are published:** Bartlett, A.Q., Pennock, N.D., Klug, A., Schedin, P. Immune Milieu Established by Postpartum Liver Involution Promotes Breast Cancer Liver Metastasis. Cancers 2021, 13, 1698. https://doi.org/10.3390/cancers13071698

   In rodents, we identified a physiologic process within the normal liver that creates a pre-metastatic niche. This physiology is weaning-induced liver involution, characterized by hepatocyte cell death, immune influx, and extracellular matrix remodeling. Here, using weaning-induced liver involution as a model of a physiologically regulated pro-metastatic niche, we investigate how liver involution supports breast cancer metastasis. Liver metastases were induced in Balb/c immune competent hosts by portal vein injection of D2OR (low metastatic) or D2A1 (high metastatic) mouse mammary tumor cells. Tumor incidence and multiplicity increased in involution hosts with no evidence of a proliferation advantage. D2OR tumor cell extravasation, seeding, and early survival were not enhanced in the involuting group compared to the nulliparous group. Rather, the involution metastatic advantage was observed at 14 days post tumor cell injection. This metastatic advantage associated with induction of immune tolerance in the involution host liver, reproductive state dependent intra-tumoral immune composition, and CD8-dependent suppression of metastases in nulliparous hosts. Our findings suggest that the normal postpartum liver is in an immune suppressed state, which can provide a pro-metastatic advantage to circulating breast cancer cells. Potential relevance to women is suggested as a postpartum diagnosis of breast cancer is an independent predictor of liver metastasis. Further, these data establish physiologic liver involution as a model to understand the liver metastatic niche, and suggest future research into whether the immune milieu identified in the involuting liver could be targeted to treat metastases more generally.

   Aim 1: Major Activities and Specific Objectives

   - Mouse metastasis studies with D2OR-GFP tumor cells delivered via the portal vein to investigate if the involution metastatic advantage
   - At early time points after tumor cell injection, we find data contrary to our initial hypothesis, i.e., that the metastatic advantage in the involution host is NOT due to an advantage early after tumor cells enter the liver.
   - Found that the overt metastatic advantage found in the involution host liver emerged ~2 weeks post-injection, a time point consistent with a role for the adaptive immune system, and suggestive of an alternative hypothesis of differential immune cell clearance of tumor cells between nulliparous and involution hosts.
   - Developed and preformed mouse adoptive cell transfer studies to demonstrate that the involution liver is immune suppressed
   - Mouse metastasis studies in immunocompromised hosts with D2OR tumor cells to investigate the role of T cells in establishment of overt liver metastasis nulliparous and involution hosts
   - Multiplex IHC studies in liver tissues from mice injected with D2OR-GFP tumor cells to investigate how tumor cells interact with the involuting liver environment

   Aim 1: Significant Results and Key Conclusions

   We first validated our portal vein injection method for human relevance. Demonstration that the portal vein injection model recapitulates morphological patterns of human breast cancer metastasis to the liver, including epithelial, mesenchymal and metaplastic morphologies, and pushing, replacement, desmoplastic and sinusoidal growth patterns (**Aim 1 Figure 1**). We next found that the overt metastatic advantage found in the involution

host liver is NOT observable at early time points after tumor cell injection, as we had predicted (**Aim 1 Figure 2**), but rather emerged between 7-10 days post tumor cell injection, consistent with differential tumor cell clearance due to T cell activation, and thus we pursed this alternative hypothesis. Next, using multiplex IHC to characterize the immune milieus of tumors evolving in nulliparous host livers compared to livers undergoing weaning-induced involution, we found the immune milieu of liver metastasis differ by host reproductive state (**Aim 1 Figure 3**). Specifically, involution tumors were T cell "cold, and myeloid cell "hot", data consistent with immune suppression occurring in the involuting liver.

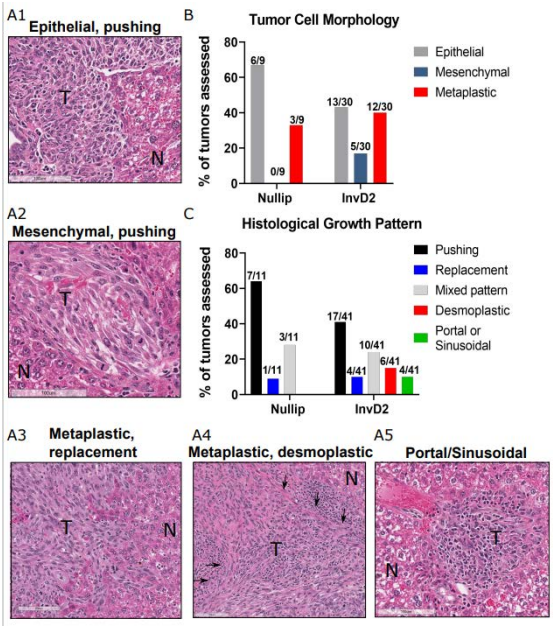

Aim 1 Figure 1. Histology of murine mammary liver metastases resembles human disease and shows increased histological heterogeneity in involution hosts Representative hematoxylin and eosin stained images from D2OR tumors classified as (a1) epithelial, pushing, (a2) mesenchymal, pushing, (a3) metaplastic, replacement, (a4) metaplastic, desmoplastic with desmoplastic areas noted by black arrows, and (a5) portal/sinusoidal pattern. Tumors are denoted by "T" and adjacent normal liver by "N"; (b) Quantitation of D2OR tumor cell morphology and (c) histological growth pattern by host reproductive stage.

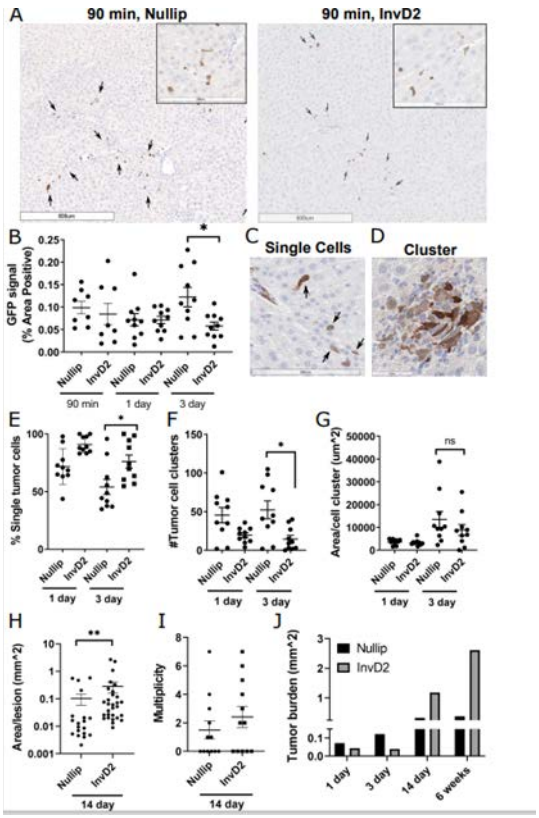

Aim 1 Figure 2. Involution metastatic advantage is observed by 2 weeks post-injection but not at earlier time points. (a) Representative low and high magnification IHC images of liver FFPE sections stained to identify GFP-tagged D2OR cells, arrows indicate tumor cells; (b) IHC quantification of GFP+ tumor cells in liver FFPE sections from mice euthanized 90 minutes (n=4 mice/group), 1 day (n=5 mice/group), and 3 days (n=5 mice/group) after intraportal injection of 500,000 D2OR-GFP tumor cells per liver. Two sections >200µm apart were assessed per mouse to quantify independent tumor cells; One-way ANOVA; Representative high magnification images showing GFP+ tumor cells as (c) single cells (1 day time point) or, (d) clusters, defined as >3 tumor cells, i.e. micro-metastases, (3 day time point); Quantification of GFP+ (e) single tumor cells as a percent of total tumor cell signal, (f) number of tumor cell clusters, and (g) size of tumor cell clusters at 1 and 3 days post-injection; One-way ANOVA; IHC quantification of GFP+ (h) tumor area and (i) multiplicity from mice euthanized 14 days after intraportal injection of 500,000 D2OR-GFP tumor cells; Two-tailed Mann-Whitney test; (j) Timeline of tumor burden in nullip (black) and InvD2 (grey) mouse groups, showing "switch" from early (3 day) advantage in nullip to later (≥14 days) advantage in involution. *p<0.05, **p<0.01.

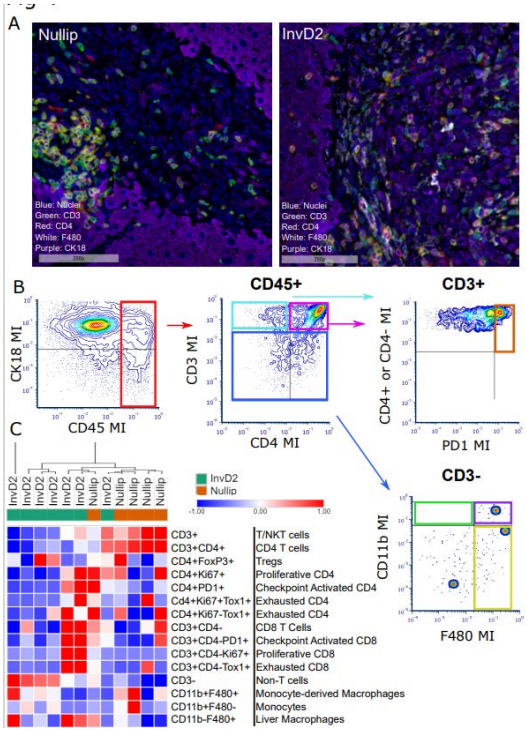

Aim 1 Figure 3. Immune milieu of liver metastases differs by host reproductive state. (a) Representative pseudo-colored multiplex IHC images of liver metastases in nullip and InvD2 mice euthanized 14 days after intraportal tumor cell injection showing select biomarkers: nuclei (blue), CD3 (green), CD4 (red), F480 (white), and CK18 (purple); (b) Representative image cytometry gating schema, showing the identification of CD45+, CD3+/-, CD4+/-, and PD1+ populations; (c) Hierarchical-clustered heat-map of intra-tumoral immune cell populations (%CD45+) identified by image cytometry of multiplex IHC staining for 9 biomarkers (CD45, CD3, CD4, FoxP3, Ki67, PD1, Tox1, CD11b, and F480). Tumor data are reported as average per mouse.

We next directly tested the hypothesis that the involution liver is immune suppressed. Specifically, we hypothesized that antigen-specific T cells responses are inhibited in the involuting compared to nulliparous liver. To test this hypothesis we designed an in vivo assay where ovalbumin-specific CD4 T cells were delivered systemically. Subsequently, mice were intra-hepatically injected with ovalbumin (e.g. the cognate antigen) or PBS. After 5 days, sufficient time for antigen presentation, T cell priming, and T cell activation, mice were euthanized. The frequency of ovalbumin (ova) specific CD4 T cells was measured in the liver and the spleen by flow cytometry. We find significantly increased ova-specific T cells in the nulliparous host liver when antigen is given ("Nullip OVA") compared to PBS, indicating T cell activation. However, the involution group mice do not show signs of T cell activation when antigen is given as there is no difference in frequency of ova-specific T cells between PBS and OVA treated mice (**Aim 1 Figure 4)**.

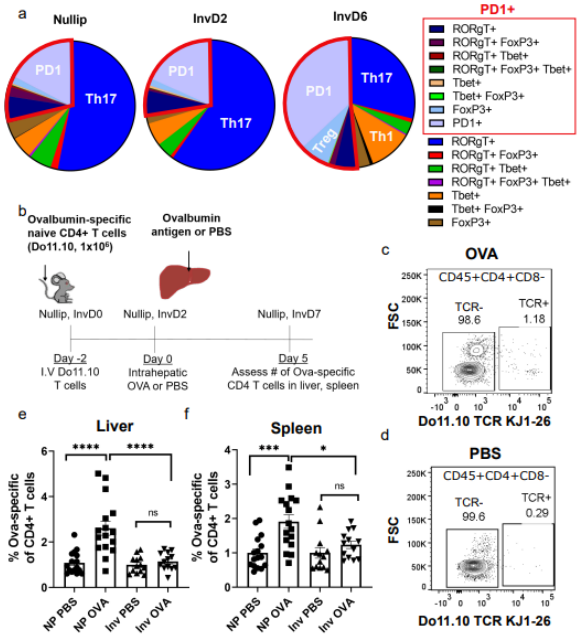

Aim 1 Figure 4. CD4+ T cell polarization is reproductive stage dependent with implications for antigen-specific activation. (a) Flow cytometry phenotyping of CD45+ CD4+ T cells from livers of mice at nullip, InvD2, and InvD6 reproductive stages (nullip n=8, InvD2 n=5, InvD6 n=6). Only CD45+ CD4+ T cells that expressed at least one of the four phenotyping markers RORgT, Tbet, PD1, or FoxP3 are shown (see SFig3 for total CD45+CD4+ T cell polarization); (b) Experimental schema for the in vivo T cell activation assay (SFig X shows transferred CD4+ Do11.10 cells); Representative flow cytometry plots showing expression of ova-specific Do11.10 T cell receptor (TCR) in CD45+ CD4+ CD8- cells from mice intra-hepatically injected with (c) ovalbumin (OVA) antigen or (d) PBS; Flow cytometry quantification of ova-specific CD4+ T cells (Do11.10 TCR+) as %CD4+ in (e) whole liver or (f) spleen across 2 independent experiments (nullip PBS n=16, nullip OVA n=15, InvD2 PBS n=13, InvD2 OVA n=13). Data normalized to PBS average for reproductive group, One-way ANOVA. *p<0.05, ***p<0.001, ****p<0.0001.

These results are supportive of the hypothesis that antigen-specific T cell responses are inhibited in the involution liver. In sum, these data are the first, to our knowledge, to demonstrate reproductive control of T cell responses in the liver, with implications for breast cancer metastasis to the liver. We next depleted CD8 T cells in nulliparous hosts in our portal vein breast cancer metastasis to the liver model, and increased liver metastasis to involution host levels; data consistent with increased immune surveillance being protective in nulliparous hosts, but lacking in involution hosts (**Aim 1 Figure 5**).

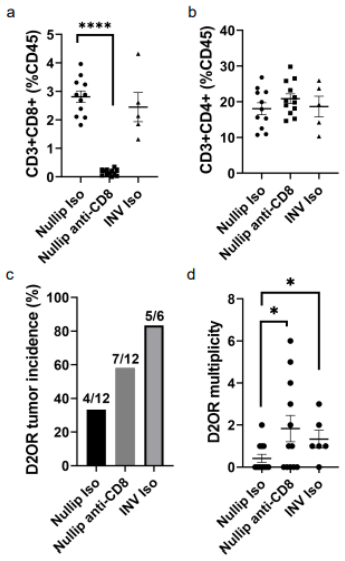

Aim 1 Figure 5. Depletion of CD8+ T cells in the nulliparous host recapitulates the involution metastatic advantage. Flow cytometry quantification of **(a)** CD8 and **(b)** CD4 T cells from livers of mice at endpoint of 6 week metastases study where mice were treated with CD8-depleting or isotype control antibody demonstrating effective CD3+CD8+ T cell depletion; **(c)** Incidence and **(d)** multiplicity of D2OR liver metastases 6 weeks after intraportal injection of 50,000 D2OR tumor cells with and without CD8 depletion in nulliparous hosts. Nullip iso n=12, Nullip anti-CD8 n=12, INV iso n=6. One-way ANOVA. *p<0.05, ****p<0.0001.

To investigate the role of T cells in our liver metastasis model, we repeated the overt metastases experiments in the background of immune compromised mice, and find – surprisingly- that no liver metastases grew in nude hosts of either nulliparous (n=16) or involution (n=6) groups. Yet, our wildtype (WT) controls behaved as we expected with ~3x increased overt liver metastatic incidence in involution compared to nulliparous WT mice. Furthermore, in the nude model, we performed tumor cell injection into the mammary gland. Within the same mouse, tumor cells grew out in the mammary gland, but not in the liver, demonstrating that the tumor cells were viable. These data demonstrate that the lack of liver tumors in the nude hosts cannot be accounted for by the trivial explanation that the tumor cells were compromised. Overall, the expected liver metastases in the control WT group and observed mammary tumor growth in nude hosts help us rule out experimental confounders and add rigor. While these data support a key role for immune milieu in establishing liver metastases, the surprising, and novel findings of lack of liver metastases in the nude hosts remain outside the scope of this DOD application and was not pursued further within the context of this grant mechanism.

Aim 1 Significance Statement: Cancer becomes lethal when it metastasizes to secondary sites, and for breast cancer metastasis to the liver is a serious clinical problem, as it essentially means survival time is limited to months. Liver metastasis is promoted, in part, by changes to the liver environment that occur after a completed pregnancy, resulting in the formation of a metastatic niche that supports circulating tumor cells. Understanding how the liver niche support breast cancer cells may lead to development of treatments for patients with metastatic breast cancer. Here, we report that the developmentally regulated process of weaning-induced liver involution increases liver metastasis in cancer cells with otherwise low metastatic potential. Increased metastasis associates with unique immunological properties in the involuting liver, including reduced ability to activate T cells required for tumor cell clearance. These data establish physiologic liver involution as a model to understand the liver metastatic niche, and suggest future research into whether the immune milieu identified in the involuting liver could be targeted to treat metastases more generally. Potential relevance to women is suggested as a postpartum diagnosis of breast cancer is an independent predictor of liver metastasis.

Aim 2: Aim 1: Major Activities and Significant Results: Explore the liver metastatic niche in breast cancer patients utilizing tumor and adjacent normal liver tissue obtained from breast cancer patients with liver metastases (BCLM)

- Aim 2 IRB protocol, consent and authorization forms were approved by both OHSU's IRB office and HRPO. As per HRPO request, we have identified an independent research monitor (Sarah Ward), as our protocol is deemed greater-than-minimal risk for individuals who received research-only liver biopsies.
- We have received 34 cases of breast cancer liver metastases and 4 matched primary breast cancers, 21 cases from the OHSU tissue biorepository, 3 prospective cases from patients receiving a clinically indicated liver resection, and 10 biopsies from women enrolled in the OHSU SMMART trial, a targeted, personalized therapeutics clinical trial for metastatic cancer patients. No subjects were enrolled for research-only liver biopsies, and thus we did not require monitoring from our independent resarch monitor.
- Of the 34 cases received, 6 cases were deemed unusable for the following reasons: liver biopsy did not contain tumor and or any tissue on the slides (n=4); patient data is incomplete (n=1), and 1 cases was a repeat case, leaving n=28 cases for subsequent analysis.
- BCML are more likely to occur in younger patients (<5 years of age); associate with recent pregnancy in younger women; be luminal and ER+ in biomarker expression; show evidence of tumor differentiation; have relatively low to modest ki67 expression, low desmoplasia, vascularity or lymphatic involvement; and strongly associate with the extracellular matrix protein collagen IV.

Aim 2: Significant Results and Key Conclusions

Objective 1-characterize human breast cancer liver metastasis for demographic data and tumor characteristics. For the BCLM study, we took "all available cases", and while our cohort is relatively small, we have demographic and clinical characteristics for n=28 cases completed, with patterns that appear to be not random (Table 1). Specifically, 50% of our cases are from women under the age of 45%. Since only ~20% of all breast cancers are diagnosed in women under the age of 45, these data suggest a >2 fold enrichment in young cases with liver metastasis. Of the patients under age of 45, 10/14 (70%) are women diagnosed with PPBC, whereas overall the cohort is 35% PPBC. This cohort is also enriched in ER+ primary breast cancer, with 22/28 (78%) being ER+.

Table 1. Demographics of Human BCLM cases

	N (%)
Age at diagnosis	
<45	14 (50.0%)
45-60	12 (42.9%)
>60	2 (7.1)
PPBC	
Yes	10 (35.7%)
No	18 (64.3%)
Race	
White	26 (92.9%)
Black	0 (0%)
Asian	1 (3.6%)
Hispanic	1 (3.6%)
Estrogen	
Positive	22 (78.6%)
PR+	17 (77.3%)
PR-	5 (22.7%)
Negative	5 (17.9%)
Unknown	1 (3.6%)

Table 2
Differentiation & Ki67 status BCLM cases.

Tumor Differentiation	cancer ER status	% tumor Ki67+	Chemotherapy treated?
Well	+	1	No
Well	+	20	Yes
Well	+	20	Yes
Moderately	+	10	No
Moderately	+	20	No
Moderately	+	30	Yes
Moderately	+	4	No
Moderately	unknown	unknown	unknown
Poorly	+	5	No
Poorly	+	80	Yes
Poorly	+	30	Yes
Undifferentiated	+	20	No
Undifferentiated	+	5	Yes
Undifferentiated	-	80	No
Undifferentiated	+	5	Yes
Undifferentiated	-	90	Yes
Mixed	+	1	Yes
Mixed	-	30	Yes

Characterized tumor differentiation status of the metastatic lesions (n=18), using 5 classifications: 3 classifications for tumors that retained some breast tissue histology (duct like structures or small tumor clusters reminiscent of filled ducts), referred to as Well, Moderately, or Poorly differentiated; a 4th class that lacked any discernable mammary gland histology, referred to as undifferentiated; and a 5th class where tumor differentiation state was heterogeneous, containing regions with some residual mammry gland histology and other regions with no evidence of differentiation, that we refer to as mixed. 14 cases were ER+ and 10/14 of these cases (71%) showed some evidence of mammary gland differentiation, whereas 1/3 ER- cases had evidence of differentiation (33%). Lower differentiation status correlated with higher ki67 expression, but not with prior chemotherapy exposure (**Table 2 & Aim2 Figure 1**).

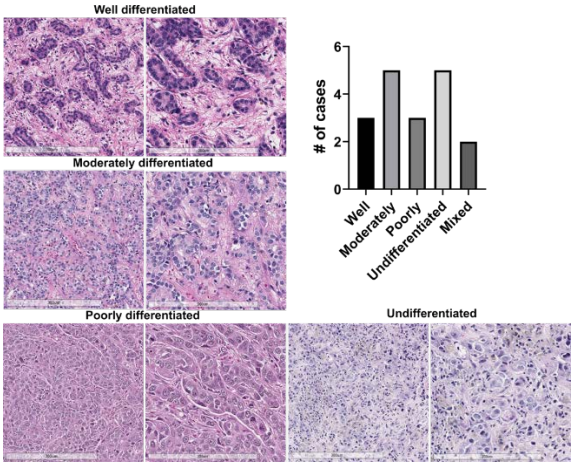

Aim 2 Figure 1. Characterization of differentiation status of BCLM based on H&E histology. H&E low and high mag representative images of well, moderately, poorly and undifferentiated cases. Graph depicts quantitation of data from n=18 cases.

Objective 2- We next characterized these BCLM for growth patterns relative to adjacent normal liver tissue (**Aim 2 Figure 2)**, as is routinely done for colorectal cancer metastatic to liver. In colorectal cancer, liver lesions with desmoplastic growth pattern having the best prognosis. See van Dam et al, British Journal of Cancer 2017 PMID: 28982110 for detailed description of patterns. Of the 18 cases described in Table 2, 10 cases had adjacent normal tissue, permitting growth pattern evaluation-the other cases are included as n/a. Only 2/10 had desmoplastic growth patterns (**Aim 2 Figure 2**).

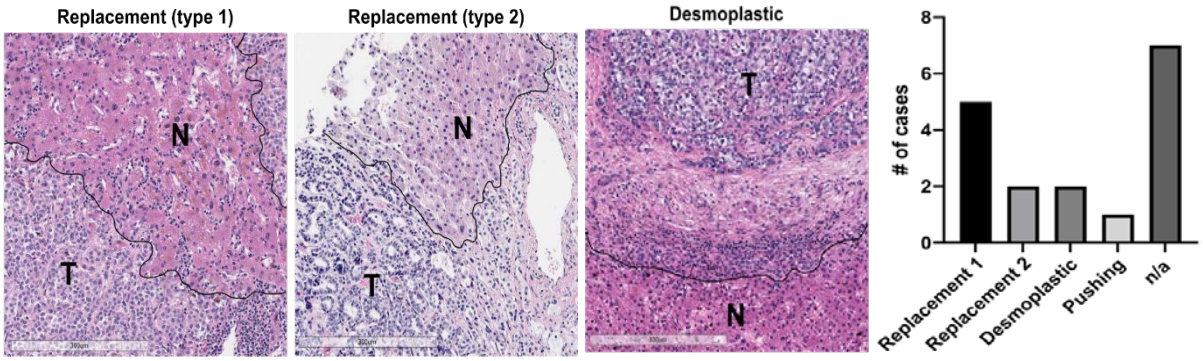

Aim 2 Figure 2. BCLM growth patterns suggest prominence of Replacement pattern with low frequency of Desmoplastic phenotype. H&E representative images of growth patterns and graph showing data quantified.

Objective 3- Using multiplex IHC, broadly interrogate between luminal and basal breast cancer, distinguish tumor cells from hepatocytes and bile ducts, determine tumor ER and Ki 67 expression, proximity of lymphatics, as well as presence of basement membrane protein collagen IV, which identify liver sinusoids. We refer to this panel as the Discovery panel. Using this panel, we are also able to determine what liver anatomical structures the metastases interact with, such as the venous blood supply, bile ducts, and/or hepatic sinusoids. The mIHC Discovery panel and rational are depicted in **Aim 2 Figure 3. .**

Aim 2 Figure 3 Discovery multiplexIHC Panel

Marker	Staining Pattern
Gata3	Luminal breast cells; may mark basal breast cells
CK5	Basal breast cells
CK7	Luminal breast cells, liver bile duct cells
CK18	Hepatocytes, breast cells
Heppar	Hepatocytes
ER	estrogen receptor + cells
Ki67	Proliferative cells
D240	Lymphatics
Aqp1	Aquaporin 1; blood vessel endothelium, bile ducts
Col IV	Basement membrane, adjacent to sinusoids

Breast Tumor
Gata3+/- (luminal origin)
CK7+ (luminal origin)
CK5 +/- (basal origin)
CK18+
Heppar-
Aqp1-

Hepatocytes
Heppar+
CK18+
CK7-
CK5/6-

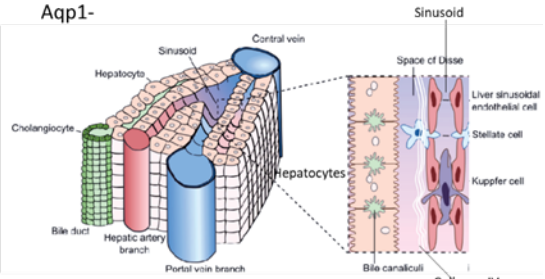

Adapted from Lilienberg 2015

The above 18 cases of liver metastases were evaluated using the Discovery mIHC panel and we found minimal expression of basal marker cytokeratin 5, and more robust expression of luminal cytokeratins 7 and 18, as well as the luminal marker Gata3. See **Aim 2 Figure 4** for image of representative stained case and **Aim 2 Figure 5** for data quantitation. High expression of luminal associated cytokeratin and Gata3 proteins, along with our prior finding of acinar-like structures in the liver metastases, suggest these metastatic tumors in the liver are differentiated, luminal ER+ tumors. We found no evidence of EMT or desmoplasia, except in the treated cases with residual disease. Further, these data show that the metastases are not composed entirely of tumor cells. To that end, we find that basement membrane protein collagen IV composes on average 38% of tumor areas with a range of 17-61% and standard deviation of 12% in our sample. These Col IV data implicate breast cancer growth along sinusoids as the primary site of BCLM.

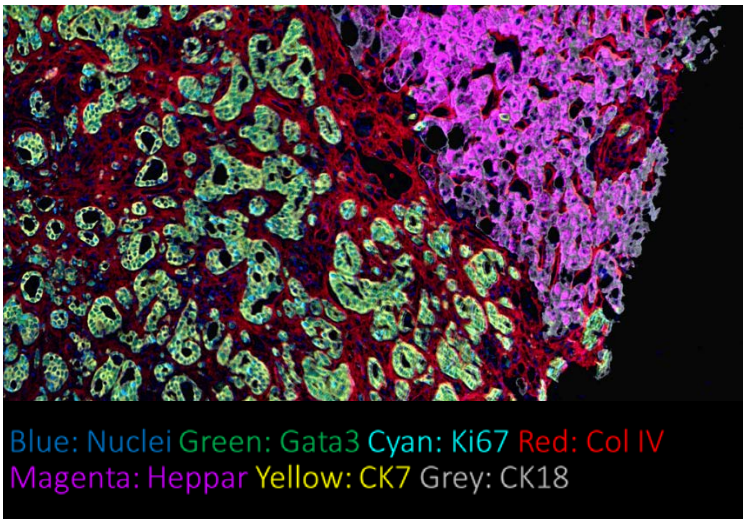

Aim 2 Figure 4. BCLM can display a high level of luminal differentiation. Representative mIHC image from a breast cancer liver metastasis showing ductal-alveolar growth pattern. Green: Gata3 (tumor); Yellow: CK18; Red: Ki67; Cyan: Aqp1 (blood vessels).

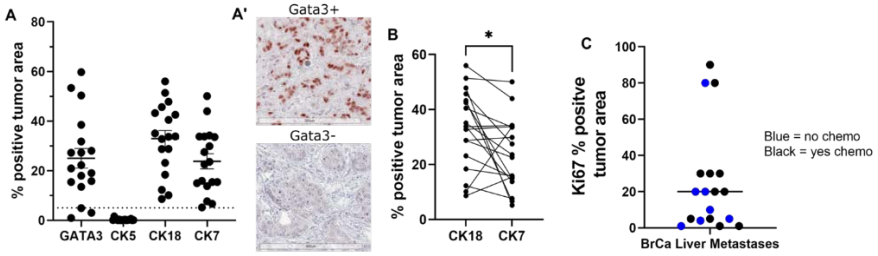

Aim 2 Figure 5. Quantitation of Discovery panel data confirms high expression of luminal markers CK18, CK 7 and Gata 3, and low expression of basal makers CK5. Further Many cases had low ki67BCLM can display a high level of luminal differentiation.

Objective 4- Characterize the ECM composition of BCLM-with the goal of identifying targetable vulnerabilities. Based on rat liver and mammry gland mass-spec based ECM proteomics, we focused on the most abundant ECM proteins shared by the mammary gland and liver, which included tenascin C, insoluble fibronectin, transglutaminase, collagen I, IV, and VI. While these data are not yet fully analyzed, we have found a wide range of expression for ColIV, FN and TNC across cases, with TNC showing the most unique expression patterns with cases split into a low and high TNC expression groups (**Aim 2 Figure 6**). Using an automated FIJI pipeline for quantitating patterns in ECM such as ECM density, branch points and endpoints (Wershof et al, Life Science Alliance 2021)), we find associations between TNC structure and tumor cell proliferation. Tumors with high ki67 associate with TNC that is more branched and at higher density (**Aim 2 Figure 7**).

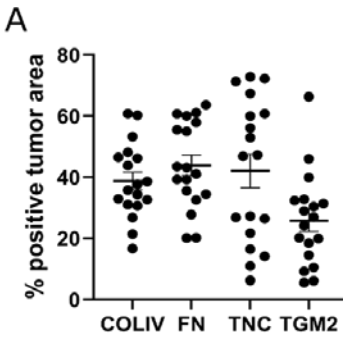

Aim 2 Figure 6-Quantitiaton of ECM proteins in BCLM. Tumors segregate into low and high TNC levels, with implications still unknown.

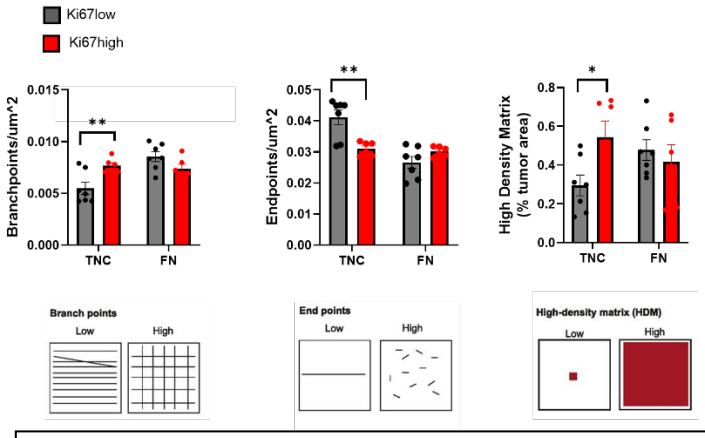

Aim 2 Figure 7-Quantitiaton of ECM structural characteristics in BCLM. Tumors with high Ki67 have higher density TNC and more branchpoints, and fewer end points, suggesting increased TNC deposition and possible turnover.

Aim 2 Significance Statement. Breast cancer confined to the breast is not a lethal disease, however, at time of diagnosis, 20-30% of cases without evidence of overt metastasis have in fact, metastasized. This means then once the primary tumor has been removed from the breast, these women remain at very high risk of future disease progression, not at the primary site, but at secondary sites. Because the breast cancer is already disseminated at time of diagnosis (but undetected at time of diagnosis), it becomes imperative to treat breast cancer in the context of its dissemination, i.e., at the site of metastasis. However, disseminated disease remains exceptionally difficult to treat and control for reasons that remain largely unknown. Here we focused on human breast cancer disseminated to the liver, a highly lethal site of breast cancer metastasis that occurs at higher levels in young women and associates with recent pregnancy. In our relatively small study, we have found that BCLM is frequently luminal, ER+, differentiated and has low ki67. Our data suggest that therapeutic strategies that target slowly proliferating luminal tumors may be efficacious. Our observation that BCLM associated closely with collagen IV may yield new targets aimed at this tumor/ECM interface.

Aim 3) Obtain first-of-kind evidence for weaning-induced liver involution in women via a serial MRI imaging study of livers in healthy women across pregnancy and weaning.

Summary of Significant Results and Key Conclusions for Aim 3 are published: Q Bartlett A, Vesco KK, Purnell JQ, Francisco M, Goddard E, Guan X, DeBarber A, Leo MC, Baetscher E, Rooney W, Naugler W, Guimaraes AR, Catalano P, Xia Z, Schedin P.. Pregnancy and weaning regulate human maternal liver size and function. Proc Natl Acad Sci U S A. 2021 Nov 30;118(48):e2107269118. doi: 10.1073/pnas.2107269118. PMID: 34815335

In studies performed in Aim 3, we obtain first-of-kind evidence for weaning-induced liver involution in women via a serial MRI imaging study of livers in healthy women across pregnancy and weaning. The rationale for this aim was based on our rodent studies showing that during pregnancy, the rodent liver undergoes hepatocyte proliferation and increases in size, followed by weaning-induced involution via hepatocyte cell death and stromal remodeling, creating a pro-metastatic niche. These data suggested a mechanism for increased liver metastasis in breast cancer patients with recent childbirth. At the time we initiated these studies, it was unknown if the human liver changes in size and function during pregnancy and weaning.

Aim 3: Major Activities and Specific Objectives

In this study, abdominal imaging was obtained in healthy women at early and late pregnancy, and post-wean.

- Completed pregnancy visits for n=45 participants
- Completed post-wean study visits for all enrolled participants (n=17 participants).
- Performed correlative analysis of liver volumetric data with clinical parameters to determine what variables, if any, correlate with liver size during pregnancy and post-wean
- Developed an assay with the OHSU Bioanalytical Shared Resource/Pharmacokinetics Core to measure bile acids in mouse tissues. Plasma samples from early and late pregnancy were utilized to quantify plasma bile acids and 7alpha-hydroxy-4-cholesten-3-one using liquid chromatography-tandem mass spectrometry (LC-MS/MS) performed with a 4000 QTRAP hybrid triple quadrupole-linear ion trap mass spectrometer (SCIEX) operating with electrospray ionization (ESI) in the negative mode The mass spectrometer was interfaced to a Shimadzu HPLC system consisting of SIL-20AC XR auto-sampler and LC-20AD XR LC pumps. Analyte separation was achieved using a gradient HPLC method and Luna 2.5u C18(2)-HST 50x2 mm column (Phenomenex) kept at 50°C with a Shimadzu CTO-20AC column oven.
- Identified a strong association between bile acid levels/production and liver growth and involution in mice.
- Obtained correlative bile acid/liver growth data in pregnant women.
- Published results.

Aim 3: Significant Results and Key Conclusions

Forty seven healthy pregnant women completed early (12-16 weeks gestation) and late pregnancy (32-36 weeks gestation) study visits (Aim 3 Fig 1A). Study participants underwent liver magnetic resonance imaging (MRI) (Fig A'), provided blood samples, had insulin sensitivity assessed via hyperinsulinemic-euglycemic clamp, and completed body composition analyses. To assess whether liver size is increased during pregnancy, we measured livers via MRI and found that, on average, liver volumes increased 15% (182 cm3 ± 197 cm3) from early to late pregnancy ($P < 0.001$) (Fig 1B). Average liver size at early pregnancy was 1239 cm3 +/- 220.8 cm3 and at late pregnancy was 1421cm3 +/- 298.6 cm3 (Fig 1B).

Because liver size is attuned to overall body size via the "hepatostat", we next determined whether the increase in liver size from early to late pregnancy correlated with increased body mass of pregnancy. First, we investigated the existence of the "hepatostat" at baseline, using body weight at the early pregnancy visit as a baseline surrogate, as pregnancy-related weight gain is minimal at this time point. Liver volumes at early pregnancy correlated with body weight (Fig 1C),

confirming previous studies in non-pregnant individuals. In contrast, the change in liver volume during pregnancy did not correlate with gestational weight gain (Fig 1D). Further, we found no relationships between pregnancy liver volume change and change in total fat mass (Fig 1E), subcutaneous abdominal, or visceral adipose tissue volumes (Table 1). However, we did observe a change in a woman's fat free mass, which includes liver, fetal tissue, placenta, and plasma did correlate with change in liver size (Fig 1F). This association between change in fat free mass and liver volume is confounded as fat free mass is not an independent variable from liver mass. These data suggest that liver size increase during pregnancy is unlinked to overall body size, i.e., it is not controlled by the "hepatostat" mechanism. Rather, these data may reflect an unrecognized, reproductive state-controlled program regulating liver size during pregnancy.

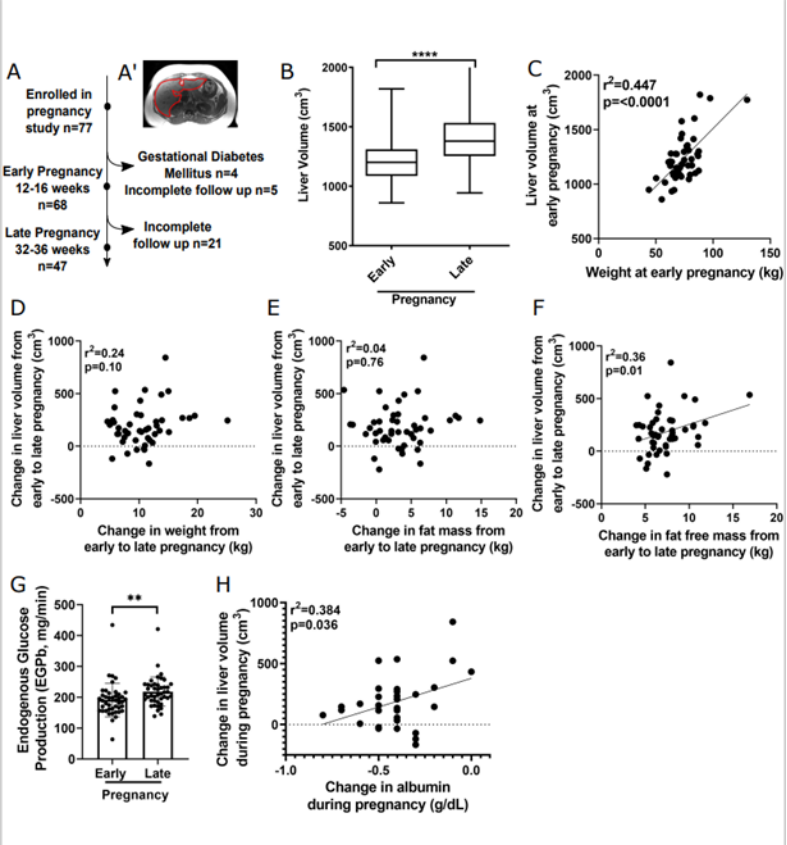

Aim 3 Figure 1 Liver changes during pregnancy: (A) Diagram of the observational study. (A') Liver MRI cross-section. (B) Average liver volume at early and late pregnancy (P: **** < 0.0001 by Two-tailed paired T test). (C) Pearson's correlation of liver volume and BMI at early pregnancy (N = 47). Pearson's correlation of change in liver volume with change in weight (D), fat mass (E), and fat free mass (F). (G) Endogenous glucose production (EGB-b) at early and late pregnancy (P: ** < 0.01 by Two-tailed paired T test). (H) Pearson's correlation of change in liver volume and change in albumin (N = 30).

We next asked if metabolic measures were associated with liver volume change and found no relationship with cholesterol concentrations or with measures of insulin sensitivity, i.e. endogenous glucose production (EGP) and glucose disposal rate (Rd) (Table 1). We also found no relationship between change in liver volume and change in intrahepatic lipid content (Table 1).

In sum, we observed that the increase in human liver volume with late pregnancy occurred independent of weight gain of pregnancy, various other measures of body composition, circulating metabolites, and intrahepatic lipid storage.

We next looked for evidence of weaning-induced liver involution in women, a biology not previously described in humans. Of the 47 women who participated in our pregnancy study, 36% completed a liver MRI >3 months post-wean (median 5.7 months) (Fig 2A). Liver volumes trended toward a decrease in size between late pregnancy and post-wean (Fig 2B), and post-wean liver volumes were similar to early pregnancy, indicative of a return to baseline (Fig 2C). These data provide the first evidence of postpartum liver involution in women.

Table 1. Change in liver volume correlated with measures of body composition and metabolism.

Variable	Mechanism of Collection	Sam	Pearson Correlation Coefficient	P
Body Composition				
Change in Weight	Scale	4	0.260	0
Change in BMI	Scale,	4	0.213	0
Change in Fat Mass	BODPOD	4	0.077	0
Change in Fat Free Mass	BODPOD	4	0.335	0
Change in SAT	MR Imaging	4	0.123	0
Change in VAT	H-MR	4	0.245	0
Change in Intrahepatic	H-MR	4	-0.035*	0
Metabolism				
Change in M Value	Hyperinsulinemic-euglycemic	4	-0.015	0
Change in EGP	Hyperinsuline euglycemic	4	-0.047*	0
Change in Rd	Hyperinsuline euglycemic	4	0.053	0
Change in Fasting Insulin	Blood draw	4	0.095	0
Change in Total	Blood draw	4	0.062	0
Change in Triglycerides	Blood draw	4	0.176	0
Change in LDL	Blood draw	4	-0.119	0
Change in HDL	Blood draw	4	0.103	0
Change in VLDL	Blood draw		-0.103	0

Abbreviations: BMI – body mass index; SAT: subcutaneous adipose tissue; VAT: visceral adipose tissue; EGP: endogenous glucose production; Rd: glucose disposal rate; LDL: low density lipoprotein; HDL: high density lipoprotein; VLDL: very low density lipoprotein; MR: magnetic resonance; H-MR: proton-magnetic resonance
***Denotes Spearman Correlation analysis**

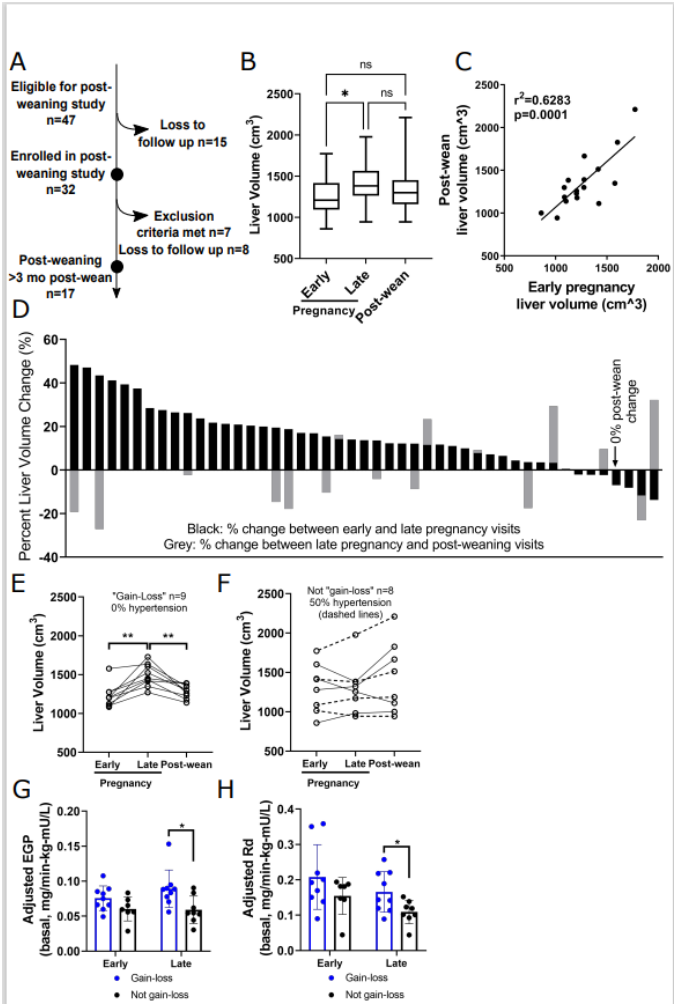

Aim 3 Figure 2 Human liver volumes post-wean: (A) Diagram for post-wean observational study. (B) Liver volume at early, late, and post-wean time points (N=17). (C) Pearson's correlation of liver volumes at early pregnancy and post-wean (n=17). (D) Liver volume change between early and late pregnancy (black bars) and between late pregnancy and post-wean (grey bars) per participant. Primary pattern (E) and secondary patterns (F) of liver volume change with pregnancy and post-wean. Dashed lines show participants with hypertension (Paired T-test). Endogenous glucose production (EGP) (G) and glucose disposal rate, Rd, (H) in women in gain-loss group compared to women in not gain-loss group. Pearson's correlation. P value: * < 0.05, ** < 0.01.

Upon further exploration, we found that none of the women whose liver changes were similar to the normal rodent pattern of "gain-loss" had gestational hypertension, yet 50% of the "not gain-loss" group did (Fig 2F, dashed lines). Further, measures of insulin sensitivity differed between these groups. Specifically, we found the "gain-loss" participants had greater endogenous glucose production at late pregnancy (Fig2G), consistent with published data showing elevated endogenous glucose production in healthy pregnancy. We also found greater glucose disposal rates at late pregnancy in the "gain-loss" group (Fig 2H), consistent with greater insulin sensitivity in the muscle. These data suggest that the "not gain-loss" pattern may be associated with suboptimal gestational metabolic health and gestational hypertension. One question is whether these metabolic parameters impact fetal outcomes. In this cohort, maternal liver size patterns did not correlate with newborn weight, length, or Ponderal index, three common neonatal health measures.

To investigate the mechanistic relationship between reproductive state and liver size, we utilized a rat model. We found liver weight increases during pregnancy were greater than expected due to gestational weight gain alone (Fig 3A). These data suggest rat liver weight during pregnancy is unlinked from the "hepatostat", corroborating our human data (Fig 1D). Next, we confirmed maximum hepatocyte proliferation in the rat livers to occur during pregnancy (Fig 3B), consistent with previous reports. Together, these data suggest a physiological model in which increased liver volume of pregnancy is due to increased hepatocyte proliferation that is activated via an unrecognized, pregnancy-mediated developmental program.

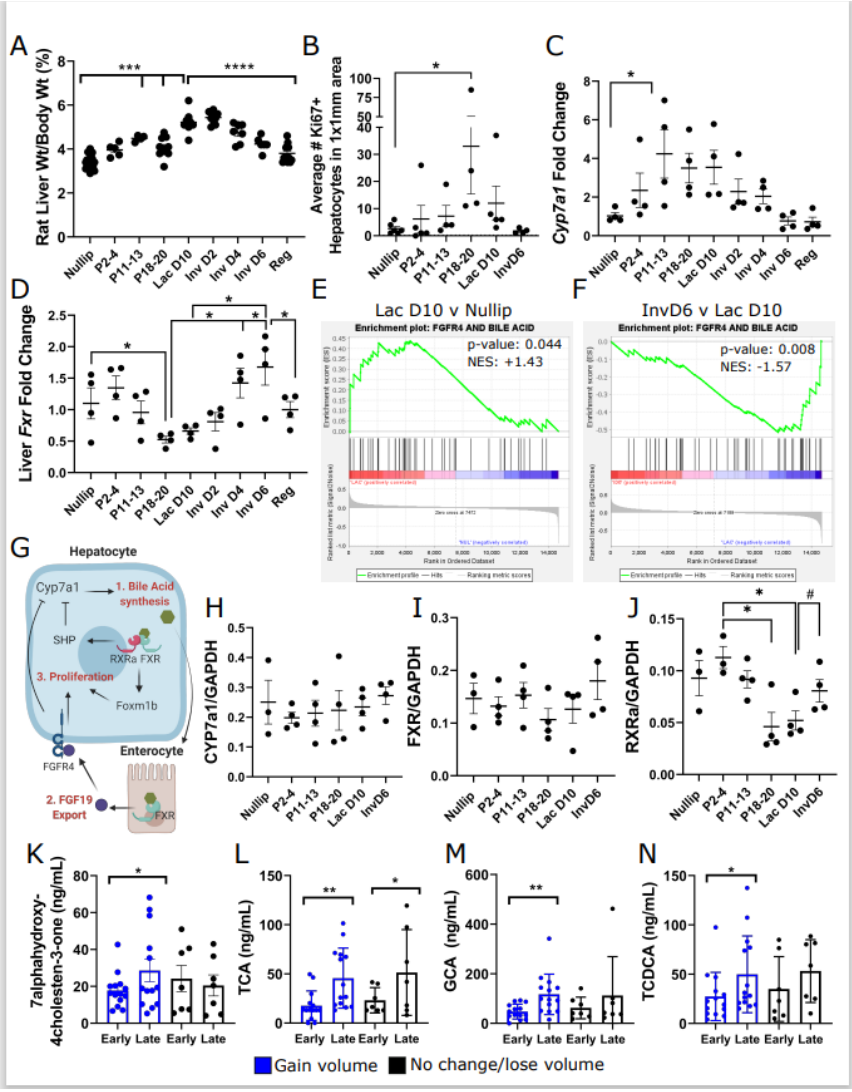

Aim 3 Figure 3 Hepatic bile acid signaling and liver size: (A) Rat liver weight normalized to body weight: Nulliparous (nullip) n=24; early (P2-4) n=5; mid (P11-13) n=4; and late (P18-20) pregnancy n=10; lactation day 10 (Lac D10) n=9; involution (Inv) day 2 n=9; InvD4 n=7; InvD6 n=6; Regressed (Reg) n=14; One-way ANOVA. **(B)** Ki67+ hepatocytes in rat livers, n=3-5/group. **(C)** *Cyp7a1* and **(D)** *FXR* mRNA fold change in liver, n=4 per group; One-way ANOVA. Gene set enrichment analysis plot of FGFR4-bile acid gene pathway for **(E)** lactation day 10 versus nulliparous groups and **(F)** involution day 6 versus lactation day 10 groups. **(G)** Model for pregnancy-enlargement of liver due to hepatocyte proliferation downstream of bile acid signaling. Protein abundance in whole liver of **(H)** CYP7A1, **(I)** FXR, and **(J)** RXRalpha**.** Data are normalized to GAPDH protein abundance; nullip n=3, P2-4, P11-13, P18-20, Lac D10, and InvD6 n=4/group; * p<0.05 by One-way ANOVA; # p<0.05 by student's T test. (**K**) Human 7alphahydroxy-4cholesten-3-one plasma concentrations at early and late pregnancy, separated by liver gain (n=14) and no gain (n=7). Plasma concentrations of bile acids TCA **(L)**, GCA **(M)**, and TCDCA **(N)** Paired T test, P value: * < 0.05, ** <0.01, *** < 0.001, **** < 0.0001.

As a possible mechanism underlying a pregnancy-associated liver growth program, we investigated bile acid metabolism in rodents. Bile acid signaling contributes to liver regeneration following partial hepatectomy and can control liver size independent of body size. Further, bile acids have been shown to regulate hepatocyte proliferation in a pathway dependent on enterocyte-derived fibroblast growth factor 15/19. To investigate if the bile acid pool is modulated by reproductive state, we measured liver *Cyp7a1*, the rate limiting enzyme in bile acid synthesis. We found a 3-4 fold increased expression of *Cyp7a1* with pregnancy, which remained elevated during lactation, followed by a rapid decline with weaning (Fig 3C). Since hepatic FXR signaling acts as a negative regulator of Cyp7a (Fig 3D), we measured hepatic *Fxr*. We found *Fxr* was downregulated during late pregnancy, when *Cyp7a1* was high, and increased with weaning, when *Cyp7a1* was low (Fig 3D). To further investigate the hypothesis that elevated bile acids contribute to hepatocyte proliferation through activation of FGFR4 signaling, we analyzed a RNA-sequencing dataset from mouse liver at various reproductive stages. We performed gene set enrichment analysis using a custom gene set composed of genes in bile acid metabolism and FGFR4 downstream signaling pathways. Consistent with our hypothesis, we found an enrichment for bile acid-FGFR4 signaling pathways in lactation stage mice compared to nulliparous (Fig 3E, SFig3). Additionally, at involution day 6 this bile acid-FGFR4 gene signature was significantly decreased compared to lactation (Fig 3F, SFig3). Further, we identified the upregulation of individual genes involved with bile acid synthesis (*Cyp7a1*, *Cyp8b1*) and proliferation (*Foxm1*) during lactation, which were subsequently

downregulated with involution (supplemental figure 3). Conversely, genes involved with inhibiting bile acid synthesis (*Rxra*, *Shp*) were reduced during lactation and elevated during involution (supplemental figure 3). A model depicting a proposed mechanism by which bile acid-FGFR4 signaling increases hepatocyte proliferation is shown (Fig 3G). Because gene expression and protein concentration are not always linked, we evaluated protein abundance for CYP7A1 and FXR. We were unable to validate reproductive-stage regulation of *Cyp7a1* and *FXR* at the protein level (Fig 3H, I). However, based on our mouse RNA-sequencing data that showed regulation of *RXRa* by reproductive stage (SFig 3), we also measured RXRa protein concentration. RXRa is a known binding partner for FXR that acts as a co-negative regulator of *Cyp7a1* (15, 16). We found that RXRa was significantly reduced at pregnancy days 18-20 and lactation day 10, then was increased at involution day 6 (Fig 3J). The decreased gene expression and protein abundance of RXRa might be sufficient to activate *Cyp7A1* gene expression without a corresponding decrease in FXR protein. In sum, these data associate increased bile acids with the physiologic expansion of the liver during pregnancy—and extend these observations to suggest a role for bile acids in regulating liver size during pregnancy, lactation and weaning.

We then examined associations between liver growth and the bile acid pool in pregnant women by measuring a biomarker of bile acid production, and serum bile acid concentrations at early and late pregnancy. Serum concentrations of 7α-hydroxy-4-cholestene-3-one (7αC4), a readout for cholesterol 7α-hydroxylase (Cyp7a1) enzyme activity, were significantly increased at late compared to early pregnancy only in the women who had an increase in liver volume during pregnancy (Fig 3F). This finding supports the hypothesis that increased bile acid production during pregnancy may be required for liver size increase. Further, among the women whose liver increased in size during pregnancy, we found increases in several primary bile acids and their conjugates (Fig 3G-I). Of note, changes in secondary bile acids, which are metabolic products of gut bacteria, only weakly correlated with liver volume change.. In this human cohort, we did not find associations between concentration of plasma FGF19, an enterocyte product shown to induce hepatocyte proliferation and liver growth in rodents. One potential caveat to our FGF19 analysis is that plasma concentrations of FGF19 may not reflect concentration in the portal vein that links the gut and liver. In sum, these human data are consistent with an increased bile acid pool during pregnancy, which may contribute to the increased liver size observed in pregnancy.

Aim 3 Significance Statement

These data represent the first data demonstrating reproductive control of liver size and function in women, and concur with recent observations in rodents, suggesting a conserved liver biology. The question of whether this newly described liver biology has implications for maternal health during pregnancy or sex-specific risk for liver disease remains to be determined. However, our evidence suggestive of weaning-induced liver involution in women may lead to improved understanding of the high rates of liver metastasis observed in young postpartum breast cancer patients.

4. IMPACT

Summary: We published a manuscript at *Cancers* (https://doi.org/10.3390/cancers13071698), which demonstrates physiologic establishment of a pro-metastatic niche via weaning-induced liver involution. This is finding is impactful because it represents an under-studied and under-appreciated biology – namely that metastases can be promoted by normal physiologic events. This is a divergence from the standard thinking that metastatic niches are formed via primary tumor education.

We published in PNAS (https://doi.org/10.1073/pnas.2107269118), a study of liver volume changes in normal healthy women during pregnancy and post wean. We obtained data demonstrating reproductive control of liver size and function in women, which concurs with our recent observations in rodents, suggesting a conserved liver biology. The question of whether this newly described liver biology has implications for maternal health during pregnancy or sex-specific risk for liver disease remains to be determined. However, our evidence suggestive of

weaning-induced liver involution in women may lead to improved understanding of the high rates of liver metastasis observed in young postpartum breast cancer patients.

Impact: What opportunities for training and professional development has the project provided?

Summary: Two graduate students, 2 undergraduate student summer interns, and 1 technician received extensive technical, study design and rigor, scientific writing and public speaking training as a result of the funding of award WX81XWH-18-0086, as described below.

Alex Quackenbush Bartlett: Q A Bartlett was a PhD candidate who studies were funded by this award. Dr. Bartlett received her PhD in the Spring of 2021. This DoD grant provided the basis of her training and professional development activities. Specifically, Dr. Bartlett has:

- Learned about and implemented IRB and DoD regulatory requirements, including document drafting and revision (Aims 2 & 3)
- Learned about and implemented IACUC regulatory requirements (Aim 1)
- Gained experience in phase 0 clinical trial execution and data analysis (per Aim 3)
- Developed bench skills in multiplex IHC experimental design, staining, and analysis
- Increased proficiency in mouse models, including utilizing antibody-mediated cell depletion strategies and the portal vein injection model of breast cancer metastasis to the liver metastasis
- Honed data presentation skills across monthly presentations either in lab meetings, departmental seminars, poster sessions, or lay public forums
- Developed professional network and awareness of state of the field at 4 different international conferences on metastasis.
- Gained mentoring experience as a preceptor for undergraduate summer research interns, Ms. Churchill and Ms. Fecker, and served as a primary technical trainer for Mr. Klug, an animal husbandry expert in the lab, whose skill set has been expanded by this award to include the liver portal vein breast cancer metastasis model.
- Honed data presentation skills across monthly presentations either in lab meetings, departmental seminars, local and national conferences, poster sessions, and lay public forums
- Developed written communication ability through process of writing two first-author manuscripts

Beth Churchill: Ms. Churchill is an undergraduate summer intern from Michigan State University, who worked with Ms. Quackenbush to carry out multiplex immunohistochemical staining for the animal studies described in Aim 1. As part of her training, Ms. Churchill was able to:

- Engage with primary literature relevant to the project
- Learn to perform multiplex IHC staining and software-based analysis for quantification of multiplex IHC staining
- Gain experience in an established breast cancer research laboratory, including participation in weekly lab meetings and several one-on-one meetings with the principle investigator
- Create a poster describing her research project and present poster at public forum

Adeline Fecker: Ms. Fecker was an undergraduate summer intern from University of Oregon, who worked with Ms. Quackenbush to carry out multiplex immunohistochemical staining for the animal studies described in Aim 1. As part of her training, Ms. Fecker was able to:

- Engage with primary literature relevant to the project
- Learn to perform multiplex IHC staining and software-based analysis for quantification of multiplex IHC staining

- Gain experience in an established breast cancer research laboratory, including participation in weekly lab meetings and several one-on-one meetings with the principle investigator
- Create a poster describing her research project and present poster at public forum

Alex Klug: Mr. Klug is a research associate who has worked with Ms. Quackenbush on all of the animal studies for this project. In this capacity he has learned our novel portal vein model of liver metastasis, as well as multiplex immunohistochemistry.

Michelle Ozaki: Ms. Ozaki is a graduate student who studies were partially funded by this award. As such, this project has provided training and professional development activities for Ms. Ozaki. Specifically, she has:

- Developed bench skills in multiplex IHC experimental design, staining, and analysis
- Trained in portal vein injection model of breast cancer metastasis to the liver
- Engaged in bi-weekly mentor meetings consisting of focused one-on-one work relevant to all three aims of this project
- Honed data presentation skills across monthly presentations either in lab meetings or departmental seminars

Impact: How were the results disseminated to communities of interest?

Summary: Both Dr. Schedin and Ms. Quackenbush have contributed to the broad dissemination of study results to communities of interest. Dr. Schedin has received 22 invitations to present this work during the course of the grant funding, 13 invites to present at national level conferences, and 9 invitations to present a seminar as an invited scholar. Graduate student Alex Q. Bartlett presented work directly related to this grant 8 times over the course of her training, at 5 at national level and 3 regional level conferences, as listed below.

Dr. Pepper Schedin

National Level Conferences

1. Postpartum Tissue Remodeling Drives Breast Cancer Metastasis, Major Symposia: Metastatic Microenvironment Dictates Progression and Therapy Responses, AACR Annual Meeting, Chicago, Illinois, April 15, 2018
2. Education Symposium, Insights & Controversies in Metastasis Biology, Breast cancer's metastatic moment: How postpartum tissue involution facilitates progression, San Antonio Breast Cancer Symposium, San Antonio, Texas, December 4, 2018
3. Young Women's Breast Cancer. What is the role of pregnancy? Susan G. Komen Oregon & SW Washington, 2019 Regional Breast Cancer Issues Conference, Portland, Oregon, March 16, 2019
4. Common Perceptions & Misconceptions of Young Women's Breast Cancer, Education Session: Update on Young Women's Breast Cancer, AACR Annual Meeting 2019, Atlanta, Georgia, March 30, 2019
5. Mucosal Biology and Tissue Involution Cooperate to Drive Breast Cancer Progression, Mammary Gland Biology Gordon Research Conference, Newry Maine, June 11, 2019
6. Postpartum Breast Cancer. Breast Cancer Think Tank 30, Isla Bella Resort, Marathon FL, January 13, 2020
7. Postpartum Breast Cancer. 21st Laura Evans Memorial Breast Cancer Symposium, Sun Valley Idaho, March 6, 2020
8. Prevention of postpartum breast cancer-are we close? Transdisciplinary Cancer Interception, a nature conference, Salt Lake City, Utah, March 9, 2020
9. Young Women's Breast Cancer, a reproductive biology perspective. AACR ED35. Cancer Increases in Younger Populations. AACR Virtual Annual Meeting II, June 23, 2020.

10. Conference Organizer: Session co-chair and program organizer, Session 1: Windows of Opportunity for Early Detection, Cancer Research UK, OHSU Knight Cancer Institute and the Canary Center at Stanford's Early Detection of Cancer Conference, October 6-8, 2020
11. Physiologic Tissue Regression and Breast Cancer Metastasis in Young Women. Theresa's Research Foundation's 8th Annual Metastatic Breast Cancer Conference, University of Utah, Salt Lake City, Utah, September 9, 2021
12. Breast Cancer Early Detection Challenges & Opportunities, Early Detection of Cancer Conference, Virtual, CRUK, the OHSU Knight Cancer Institute and the Canary Center at Stanford, London UK, October 6, 2021
13. Physiologic Tissue Regression and Breast Cancer Metastasis in Young Women. CSHL Cancer Biology and Metastasis Conference, Cold Spring Harbor, NY, Virtual, October 12, 2021

Invited Scholars Seminars

14. Mucosal Biology & Tissue Involution Cooperate to Drive Breast Cancer Metastasis: Cancer Biology Pathways Lecture, Siteman Cancer Center, Washington University, St. Louis, MO, May 22, 2018
15. Keynote, Follow the data; challenging established paradigms in young women's breast cancer. 14th Annual Baylor College of Medicine Breast Center Retreat, Houston, TX, September 6, 2018.
16. Collagen as a Target for NSAID-based Breast Cancer Prevention: A Tribute to Patricia Keely. American Society for Matrix Biology 2018 Biennial Meeting, Las Vegas, NC, October 15, 2018
17. Challenging Established Paradigms in Young Women's Breast Cancer. University of Chicago, School of Medicine, Comprehensive Cancer Center, Chicago, Illinois, October 18, 2018
18. Challenging Established Paradigms in Young Women's Breast Cancer, Louisiana Cancer Research Center, Tulane University School of Medicine, New Orleans, LA, February 11, 2019
19. Challenging Established Paradigms in Young Women's' Breast Cancer, University of Minnesota Medical School, Grand Rounds, Minnesota, MN, May 8, 2019
20. Postpartum Breast Cancer: Population science to bench and bedside and back again. University of Colorado Cancer Center, Cancer Prevention and Control Seminar Series, Anschutz Medical Campus, Aurora, CO, November 13, 2019
21. Invited speaker: Young Women's Breast Cancer: Bench to Population Science and Back Again. Genome Science Institute, Graduate Program in Genetics and Genomics, Boston University, Boston MA, September 23, 2000
22. Invited Speaker: Proximity to Pregnancy Determines Outcomes in Young Women's Breast Cancer. McGill University, Montreal Quebec, February 8, 2021

Dr. Alex Quackenbush Bartlett

National

1. Poster Presenter, Investigating tumor promotion in the postpartum liver metastatic niche. Awarded 3rd place. 17th Biennial Congress of the Metastasis Research Society, Princeton, New Jersey, August 3, 2018.
2. Abstract accepted for poster session, "Does reproductive biology drive liver metastasis in Young Women's Breast Cancer?", AACR Annual Meeting, April 24,2020* cancelled to due Covid-19
3. Poster presentation: Natural killer cells restrict the growth of liver metastases in nude hosts. Society for Immunotherapy of Cancer Annual Meeting, Virtual. November 11-14, 2020.
4. Poster presentation: Evidence for reproductive control of liver size with implications for risk of liver metastases in postpartum breast cancer patients. San Antonio Breast Cancer Symposium, Virtual. December 8-12, 2020.
5. Lightning talk and poster presentation: Immune suppression established by postpartum liver involution promotes liver metastasis. AACR Virtual Special Conference: The Evolving Tumor

Microenvironment in Cancer Progression: Mechanisms and Emerging Therapeutic Opportunities. January 11-12, 2021.

Regional

6. Quackenbush: Poster Presenter, 2018 ARCS (Achievement Rewards for College Scientists) Foundation Oregon Luncheon. Portland, Oregon, October 30, 2018.
7. Oral presentation, "Reproductive-Dependent Biology Drives Liver Metastasis in Young Women's Breast Cancer", Cell, Developmental, and Cancer Biology Annual Retreat, Portland, Oregon September 4, 2019.
8. "Post-wean involution promotes metastasis to the liver via induction of local immune suppression", Cancer Biology Graduate Program Retreat 2020, September 7, 2020.

5. **CHANGES/PROBLEMS:** *The Project Director/Principal Investigator (PD/PI) is reminded that the recipient organization is required to obtain prior written approval from the awarding agency Grants Officer whenever there are significant changes in the project or its direction. If not previously reported in writing, provide the following additional information or state, "Nothing to Report," if applicable:*

- **Changes in approach and reasons for change**

  Our work was slowed by the needs to shut down the lab and reduce clinical research due to COVID19. As of 6-15-2020, we opened at 30% capacity. In 2021, the lab was permitted to operate at 100% capacity as long as social distancing could be maintained. In addition, as lab PI, I was deemed "non-essential" and was required to work remotely, reducing my effectiveness as a mentor. This COVID strategy remained in effect until spring 2022, at which time we resumed normal operations.

  Actual or anticipated problems or delays and actions or plans to resolve them

  - *Describe problems or delays encountered during the reporting period and actions or plans to resolve them.*

    For Aim 2, during COVID19, we needed to explore accessing existing tissue banks to obtain human tissues required to complete this aim, rather than prospectively obtaining liver biopsies of metastatic breast cancer as originally proposed.

- **Changes that had a significant impact on expenditures**

  - *Describe changes during the reporting period that may have had a significant impact on expenditures, for example, delays in hiring staff or favorable developments that enable meeting objectives at less cost than anticipated.*

    Cost of shifting lab based work to exclusively off site/remote work: downtime with restructuring goals, shut down of technical work, loss of access to clinical coordinators-all contributed to reduced output during this granting period.

6. **PRODUCTS:** *List any products resulting from the project during the reporting period. If there is nothing to report under a particular item, state "Nothing to Report."*

- **Publications, conference papers, and presentations**
  Report only the major publication(s) resulting from the work under this award.
  - **Journal publications.**

A. Summary: 2 primary publications based directly on the proposed grant aims, with a lab PhD trainee as first author; 3 primary publications indirectly related to the specific aims of the grant and centrally related to increased metastasis in young women's breast cancer, all led by lab trainees; 3 reviews on metastasis and potential mechanism of liver metastasis in young women's breast cancer, with 1 of the 3 led by a lab trainee; and one commentary in Lancet Oncology, written by worldwide recognized leading experts in the field of young women's breast cancer, designed to bring attention to the under-recognized role of recent pregnancy in metastasis.

B. Publications based directly on the specific aims of the grant

1. Aim 1 studies: Bartlett, A.Q.; Pennock, N.D.; Klug, A.; Schedin, P. Immune Milieu Established by Postpartum Liver Involution Promotes Breast Cancer Liver Metastasis. Cancers 2021, 13, 1698. https://doi.org/10.3390/cancers13071698
2. Aim 3 studies: Bartlett, AQ, Vesco KK, Purnell JQ, Francisco M, Goddard E, Guan X, DeBarber A, Leo MC, Baetscher E, Rooney W, Naugler W, Guimaraes AR, Catalano P, Xia Z, Schedin P: Pregnancy and weaning regulate human maternal liver size and function. Proc Natl Acad Sci U S A 2021, 118. PMID: 34815335

C. Trainee manuscripts based directly on the specific aims of the grant:

1. Betts, CB, Quackenbush, A, Anderson, W, Marshall, N, Schedin P. Mucosal immunity and liver metabolism in the complex condition of lactation insufficiency. Journal of Human Lactation. August 14, 2020. PMID: 32795211 (Review)
2. Bartlett, A.Q.; Pennock, N.D.; Klug, A.; Schedin, P. Immune Milieu Established by Postpartum Liver Involution Promotes Breast Cancer Liver Metastasis. Cancers 2021, 13, 1698. https://doi.org/10.3390/cancers13071698
3. Bartlett, AQ, Vesco KK, Purnell JQ, Francisco M, Goddard E, Guan X, DeBarber A, Leo MC, Baetscher E, Rooney W, Naugler W, Guimaraes AR, Catalano P, Xia Z, Schedin P: Pregnancy and weaning regulate human maternal liver size and function. Proc Natl Acad Sci U S A 2021, 118. PMID: 34815335

D. Publications indirectly based on specific aims of the grant

a. Primary contributions to the literature regarding metastasis in postpartum breast cancer:

1. Sonali Jindal*, Nathan D. Pennock*, Duanchen Sun*, Wesley Horton, Michelle K. Ozaki, Jayasri Narasimhan, Alexandra Q. Bartlett, Sheila Weinmann, Paul E. Goss, Virginia F. Borges, Zheng Xia, and Pepper Schedin. Postpartum breast cancer has a distinct molecular profile that predicts poor outcomes. Nat Commun 12, 6341 (2021). https://doi.org/10.1038/s41467-021-26505-3Shagisultanova E, Gao D,
2. Callihan E, Parris HJ, Risendal B, Hines LM, Slattery ML, Baumgartner K, Schedin P, John EM, Borges VF., Overall survival is the lowest among young women with postpartum breast cancer. Eur J Cancer. 2022 May 4;168:119-127. doi: 10.1016/j.ejca.2022.03.014. PMID: 35525161
3. Guo Q, Sun D, Barrett AS, Jindal S, Pennock ND, Conklin MW, Xia Z, Mitchell E, Samatham R, Mirza N, Jacques S, Weinmann S, Borges VF, Hansen KC, Schedin PJ.,

Mammary collagen is under reproductive control with implications for breast cancer. Matrix Biol. 2022 Jan;105:104-126. doi: 10.1016/j.matbio.2021.10.006. Epub 2021 Nov 25 PMID: 348390

E. Reviews on the role of the postpartum liver in breast cancer metastasis:

1. Betts, CB, Quackenbush, A, Anderson, W, Marshall, N, Schedin P. Mucosal immunity and liver metabolism in the complex condition of lactation insufficiency. Journal of Human Lactation. August 14, 2020. PMID: 32795211
2. Borges VF, Lyons TR, Germain D, Schedin P. Post-partum involution and cancer: an opportunity for targeted breast cancer prevention and treatments? Cancer Res. May 1, 2020. 80(9):1790-1798. Doi: 10.1158/0008/5472.CN-19-3448. PMID: 32075799
3. Hanne Lefrère, Liesbeth Lenaerts, Virginia F Borges, Pepper Schedin, Patrick Neven, and Frédéric Amant, Postpartum breast cancer: mechanisms underlying its worse prognosis, treatment implications, and fertility preservation Int J Gynecol Cancer 2021 Mar;31(3):412-422. doi: 10.1136/ijgc-2020-002072. PMID: 33649008 DOI

F. Editorial/ Commentary on postpartum breast cancer:

1. Amant F, Lefrère H, Borges VF, Cardonick E, Lambertini M, Loibl S, Peccatori F, Partridge A, Schedin P. The definition of pregnancy-associated breast cancer is outdated and should no longer be used. Lancet Oncol. 2021 Jun;22(6):753-754. doi: 10.1016/S1470-2045(21)00183-2, PMID:34087122

7. **PARTICIPANTS & OTHER COLLABORATING ORGANIZATIONS**

- **What individuals have worked on the project?**

Provide the following information for: (1) PDs/PIs; and (2) each person who has worked at least one person month per year on the project during the reporting period, regardless of the source of compensation (a person month equals approximately 160 hours of effort). If information is unchanged from a previous submission, provide the name only and indicate "no change."

YEAR 1

8. Name:	Pepper Schedin
Project Role:	Principal Investigator
Researcher Identifier (e.g. ORCID ID):	0000-0003-4244-987X
Nearest person month worked:	1.68 calendar/no change
Contribution to Project:	Dr. Schedin led all aspects of the project, including scientific focus, experimental design, data analysis, data integrity, budget management, human and animal regulatory aspects, and manuscript writing.
Funding Support:	W81XWH-18-1-0086
Name:	Jonathan Purnell
Project Role:	Co-Investigator
Researcher Identifier (e.g. ORCID ID):	0000-0001-5505-6333
Nearest person month worked:	0.12/no change
Contribution to Project:	Dr. Purnell is co-lead on Aim 3 designed to obtain first-of-kind evidence for weaning-induced liver involution in women via a serial MRI imaging study of livers in healthy women across pregnancy and weaning.
Funding Support:	W81XWH-18-1-0086
Name:	Zahi Mitri

Project Role:	Co-Investigator
Researcher Identifier (e.g. ORCID ID):	0000-0001-8765-7723
Nearest person month worked:	No salary support as of 4/9/2019, as the aim Dr. Mitri is a co-investigator on has yet been initiated. This is because we are awaiting final approval of our IRB documentation from DOD.
Contribution to Project:	Dr. Mitri is a medical oncologist who is involved in Aim 2: to explore the liver metastatic niche in breast cancer patients utilizing tumor and adjacent normal liver tissue obtained from breast cancer patients with liver metastases.
Funding Support:	NA

Name:	Skye Mayo
Project Role:	Co-Investigator
Researcher Identifier (e.g. ORCID ID):	0000-0002-1631-9855
Nearest person month worked:	No salary support as of 4/9/2019, as the aim Dr. Mayo is a co-investigator on has yet been initiated. This is because we are awaiting final approval of our IRB documentation from DOD.
Contribution to Project:	Dr. Mayo is an oncologic surgeon who is involved in Aim 2: to explore the liver metastatic niche in breast cancer patients utilizing tumor and adjacent normal liver tissue obtained from breast cancer patients with liver metastases.
Funding Support:	NA

Name:	Andrea Calhoun
Project Role:	Histotechnician
Researcher Identifier (e.g. ORCID ID):	Does not have an ORCID ID
Nearest person month worked:	3.92 calendar/no change
Contribution to Project:	Ms. Calhoun is responsible for tissue fixation, processing, sectioning and staining related to Aim 1 of our application: Use liver metastasis mouse models to decipher the post-intravasation steps of the metastatic cascade that are supported by the involuting liver.

Funding Support:	W81XWH-18-1-0086
Name:	Sonali Jindal
Project Role:	Pathologist
Researcher Identifier (e.g. ORCID ID):	0000-0002-3911-6815
Nearest person month worked:	0.94 calendar/no change
Contribution to Project:	Dr. Jindal is an MD trained pathologist responsible for oversight of our histology lab, including personnel and the mIHC pipeline, and performs pathologic assessment of all tissues collected from both rodent and human based studies. …
Funding Support:	W81XWH-18-1-0086
Name:	Alex Klug
Project Role:	Animal Husbandry
Researcher Identifier (e.g. ORCID ID):	0000-0003-4958-1961
Nearest person month worked:	3.04 calendar/no change
Contribution to Project:	Mr. Klug is responsible for all animal husbandry associated with Aim 1 of this grant. Mr Klug is also trained in the portal vein injection surgeries, and works as part of a two member team with Ms Quackenbush, to perform all of the surgeries described in Aim 1. Mr Klug is also gaining expertise in mIHC and is contributing to Aim 1 objectives related to mIHC.
Funding Support:	W81XWH-18-1-0086
Name:	Alexandra Quackenbush
Project Role:	Graduate Student
Researcher Identifier (e.g. ORCID ID):	0000-0001-7912-6084
Nearest person month worked:	12.00 calendar/no change
Contribution to Project:	Ms. Quackenbush is deeply involved in all three aims of this grant. She is responsible for all of the preclinical model studies outlined in Aim 1, and in this capacity is

	also responsible for managing Mr. Klug's animal husbandry activities and for his training in the liver metastasis model. For Aim 2, Ms Quackenbush has been instrumental in establishing our IRB approved protocol to obtain research only liver biopsies from women with breast cancer metastatic to the liver. For Aim 3, Ms Quackenbush is lead on data acquisition, coordinating research efforts with KPNW including data transfers, and for manuscript preparation.
Funding Support:	OHSU Knight Cancer Biology Program

YEAR 2	
Name:	Pepper Schedin
Project Role:	PI
Researcher Identifier (e.g. ORCID ID):	0000-0003-4244-987X
Nearest person month worked:	1.67
Contribution to Project:	Dr. Schedin led all aspects of the project, including scientific focus, experimental design, data analysis, data integrity, budget management, human and animal regulatory aspects, and manuscript writing.
Funding Support:	*(Complete only if the funding support is provided from other than this award).*
Name:	Jonathan Purnell
Project Role:	Co-investigator
Researcher Identifier (e.g. ORCID ID):	0000-0001-5505-6333
Nearest person month worked:	0.29
Contribution to Project:	Dr. Purnell is co-lead on Aim 3 designed to obtain first-of-kind evidence for weaning-induced liver involution in women via a serial MRI

	imaging study of livers in healthy women across pregnancy and weaning.
Funding Support:	
Name:	Zahi Mitri
Project Role:	Co-investigator
Researcher Identifier (e.g. ORCID ID):	0000-0001-8765-7723
Nearest person month worked:	0.26
Contribution to Project:	Dr. Mitri is a medical oncologist who is involved in Aim 2: to explore the liver metastatic niche in breast cancer patients utilizing tumor and adjacent normal liver tissue obtained from breast cancer patients with liver metastases.
Funding Support:	
Name:	Skye Mayo
Project Role:	Collaborator
Researcher Identifier (e.g. ORCID ID):	0000-0002-1631-9855
Nearest person month worked:	0.26
Contribution to Project:	Surgeon providing liver biopsies for metastatic BrCa patients, involved in liver biopsy IRB development
Funding Support:	
Name:	Alex Quackenbush
Project Role:	Graduate student
Researcher Identifier (e.g. ORCID ID):	0000-0001-7912-6084

Nearest person month worked:	12
Contribution to Project:	Ms. Quackenbush carried out the animal studies, worked with other team members to develop IRB protocols and other participant documents for human research protocols, organized tissue collection and multiplex IHC protocol development for Aim 2, and has performed liver volume analysis, data interpretation, and manuscript writing for Aim 3.
Funding Support:	
Name:	Alex Klug
Project Role:	Animal husbandry
Researcher Identifier (e.g. ORCID ID):	0000-0003-4958-1961
Nearest person month worked:	7.89
Contribution to Project:	Mr. Klug worked on all animal studies.
Funding Support:	
Name:	Andrea Calhoun
Project Role:	Histotechnician
Researcher Identifier (e.g. ORCID ID):	
Nearest person month worked:	5.19
Contribution to Project:	Multiplex IHC development, staining, and data capture for Aim 2.
Funding Support:	
Name:	Jayasri Narasimhan

Project Role:	Histotechnician
Researcher Identifier (e.g. ORCID ID):	
Nearest person month worked:	7.31
Contribution to Project:	Tissue sectioning and multliplex IHC development, staining, and data capture for Aim 2.
Funding Support:	
Name:	Sonali Jindal
Project Role:	Pathologist
Researcher Identifier (e.g. ORCID ID):	0000-0002-3911-6815
Nearest person month worked:	2.55
Contribution to Project:	Lab oversight on IRB submissions and maintenance. IHC oversight and QA. Evaluation of multiplex IHC results for Aim 2.
Funding Support:	

YEAR 3	
Name:	*Pepper Schedin*
Project Role:	*PI*
Researcher Identifier (e.g. ORCID ID):	*0000-0003-4244-987X*
Nearest person month worked:	*1.68*

Contribution to Project:	*Dr. Schedin led all aspects of the project, including scientific focus, experimental design, data analysis, data integrity, budget management, human and animal regulatory aspects, and manuscript writing.*
Funding Support:	*(Complete only if the funding support is provided from other than this award).*
Name:	*Jonathan Purnell*
Project Role:	*Co-investigator*
Researcher Identifier (e.g. ORCID ID):	*0000-0001-5505-6333*
Nearest person month worked:	*0.26*
Contribution to Project:	*Dr. Purnell is co-lead on Aim 3 designed to obtain first-of-kind evidence for weaning-induced liver involution in women via a serial MRI imaging study of livers in healthy women across pregnancy and weaning.*
Funding Support:	
Name:	*Zahi Mitri*
Project Role:	*Co-investigator*
Researcher Identifier (e.g. ORCID ID):	*0000-0001-8765-7723*
Nearest person month worked:	*0.26*
Contribution to Project:	*Dr. Mitri is a medical oncologist who is involved in Aim 2: to explore the liver metastatic niche in breast cancer patients utilizing tumor and adjacent normal liver tissue obtained from breast cancer patients with liver metastases.*
Funding Support:	

Name:	*Skye Mayo*
Project Role:	*Collaborator*
Researcher Identifier (e.g. ORCID ID):	*0000-0002-1631-9855*
Nearest person month worked:	*0.26*
Contribution to Project:	*Surgeon providing liver biopsies for metastatic BrCa patients, involved in liver biopsy IRB development*
Funding Support:	
Name:	*Alex Quackenbush*
Project Role:	*Graduate student*
Researcher Identifier (e.g. ORCID ID):	*0000-0001-7912-6084*
Nearest person month worked:	*12*
Contribution to Project:	*Ms. Quackenbush carried out the animal studies, worked with other team members to develop IRB protocols and other participant documents for human research protocols, organized tissue collection and multiplex IHC protocol development for Aim 2, and has performed liver volume analysis, data interpretation, and manuscript writing for Aim 3.*
Funding Support:	
Name:	*Andrea Calhoun*
Project Role:	*Histotechnician*

Researcher Identifier (e.g. ORCID ID):	
Nearest person month worked:	*3.70*
Contribution to Project:	*Multiplex IHC development, staining, and data capture for Aim 2.*
Funding Support:	
Name:	*Jayasri Narasimhan*
Project Role:	*Histotechnician*
Researcher Identifier (e.g. ORCID ID):	
Nearest person month worked:	*1.03*
Contribution to Project:	*Tissue sectioning and multliplex IHC development, staining, and data capture for Aim 2.*
Funding Support:	
Name:	*Sonali Jindal*
Project Role:	*Pathologist*
Researcher Identifier (e.g. ORCID ID):	*0000-0002-3911-6815*
Nearest person month worked:	*1.63*
Contribution to Project:	*Lab oversight on IRB submissions and maintenance. IHC oversight and QA. Evaluation of multiplex IHC results for Aim 2.*

Funding Support:	
Name:	*Weston Anderson*
Project Role:	*Scientific editor*
Researcher Identifier (e.g. ORCID ID):	
Nearest person month worked:	*2.23*
Contribution to Project:	*Preparation of manuscripts*
Funding Support:	
Name:	*AeSoon Bensen*
Project Role:	*Research Assistant*
Researcher Identifier (e.g. ORCID ID):	
Nearest person month worked:	*3.00*
Contribution to Project:	*Multiplex immunohistochemistry*
Funding Support:	
Name:	*Elizabeth Mitchell*
Project Role:	*Study team member*
Researcher Identifier (e.g. ORCID ID):	

Nearest person month worked:	*0.96*
Contribution to Project:	*Data analysis for multiplex IHC*
Funding Support:	
Name:	*Michelle Ozaki*
Project Role:	*Graduate student*
Researcher Identifier (e.g. ORCID ID):	
Nearest person month worked:	*0.96*
Contribution to Project:	*Multiplex IHC development and staining*
Funding Support:	

YEAR 4

Participants & Other Collaborating Organizations

What individuals have worked on the project?

Provide the following information for: (1) Project Directors (PDs)/ PIs; and (2) each person who has worked at least one person month per year on the project during the reporting period, regardless of the source of compensation (a person month equals approximately 160 hours of effort).

Name: Pepper Schedin

Project Role: Principle Investigator

Researcher Identifier: ORCID ID 0000-0003-4244-987X

Nearest person month worked: 0.42

Contribution to Project: Dr. Schedin has been responsible for Aim 1 study design and data interpretation, team coordination (weekly meeting with lab team members; monthly meetings with liver biopsy group), oversight of multiplex IHC staining for Aim 2, manuscript preparation for Aim 3, and advancing IRB submissions.

Name: Jonathan Purnell

Project Role: Co-Investigator

Researcher Identifier: ORCID ID 0000-0001-5505-6333

Nearest person month worked: 0.03

Contribution to Project: Advanced liver imaging IRB, participant recruitment Aim 3, liver biology/metabolism expert, pregnancy expert, and liver volumetric analysis plans.

Name: Zahi Mitri

Project Role: Co-Investigator

Researcher Identifier: ORCID ID 0000-0001-8765-7723

Nearest person month worked: 0.06

Contribution to Project: Breast Cancer Oncologist involved in Liver biopsy IRB and patient recruitment to Aim 2.

Name: Skye Mayo

Project Role: Collaborator

Researcher Identifier: ORCID ID 0000-0002-1631-9855

Nearest person month worked: 0.06

Contribution to Project: Surgeon providing liver biopsies for metastatic BrCa patients, involved in liver biopsy IRB development

Name: Michelle Ozaki

Project Role: Graduate Student

Researcher Identifier:

Nearest person month worked: 3.00

Contribution to the Project: Ms. Ozaki has worked on multiplex IHC development for Aim 2 of this project.

Name: Elise DeWilde

Project Role: Research Assistant

Researcher Identifier:

Nearest person month worked: 1.50

Contribution to the Project: Ms. DeWilde has worked on multiplex IHC staining for Aim 2 of this project.

Name: Solange Bassale

Project Role: Research Assistant

Researcher Identifier:

Nearest person month worked: 0.75

Contribution to the Project: Ms. Bassale has contributed statistical analyses to this project.

9. Special Reporting Requirements

Describe the Regulatory Protocol and Activity Status (if applicable).

Describe the Protocol and Activity Status for sections a-c, as applicable, using the format described for each section. If there is nothing significant to report during this reporting period, state "Nothing to Report."

(a) ***Human Use Regulatory Protocols***

TOTAL PROTOCOLS: 2 human subject research protocols are required to complete the Statement of Work

PROTOCOL (1 of 2 total): (For Aim 3)

Protocol [HRPO Assigned Number]: E00004.1a

Title: Liver imaging across pregnancy and weaning to investigate postpartum liver involution

Target required for clinical significance: 20

Target approved for clinical significance: 32

SUBMITTED TO AND APPROVED BY:

Nancy Englar, MHL, CIP
Human Subject Protections Scientist
Human Research Protection Office
USAMRMC Office of Research Protections (ORP)

STATUS: NO CHANGES FROM PREVIOUS QR#6 & STUDY IS COMPLETED

(i) Number of subjects recruited/original planned target: 32/44 (base pool are all participants in the Babybump study)

Number of subjects screened/original planned target: 32/44

Number of patients enrolled/original planned target: 32/44

Number of patients completed/original planned target: 17/44

(ii) Report amendments submitted to the IRB and USAMRMC HRPO for review:

(iii) Adverse event/unanticipated problems involving risks to subjects or others and actions or plans for mitigation:

-nothing to report for entire funding period.

PROTOCOL (2 of 2 total): (For Aim 2)

Protocol [HRPO Assigned Number]: E00004.2A

Title: Exploration of the Liver Metastatic Niche in Breast Cancer (Aim 2)

Target required for clinical significance: not applicable as this is an exploratory aim

Target approved for clinical significance: not applicable as this is an exploratory aim

SUBMITTED TO AND APPROVED BY:Ms. Karen Eaton, MS
General Dynamics Health Solutions
Human Subjects Protection Scientist
Human Research Protection Office
USAMRMC Office of Research Protections (ORP)
Email: karen.m.eaton.ctr@mail.mi

STATUS:

(i) Number of subjects recruited/original planned target: 34/40-56 (range estimate as described in SOW)

Number of subjects screened/original planned target: 34/40-56

Number of patients enrolled/original planned target: 28/40-56

Number of patients completed/original planned target: 28/(40-56)

(ii) Report amendments submitted to the IRB and USAMRMC HRPO for review: nothing to report

(iii) Adverse event/unanticipated problems involving risks to subjects or others and actions or plans for mitigation

-nothing to report.

(b) Use of Human Cadavers for Research Development Test & Evaluation (RDT&E), Education or Training

"Cadaver" is defined as a deceased person or portion thereof, and is synonymous with the terms "human cadaver" and "post-mortem human subject" or "PMHS." The term includes organs, tissues, eyes, bones, arteries or other specimens obtained from an individual upon or after death. The term "cadaver" does not include portions of an individual person, such as organs, tissue or blood, that were removed while the individual was alive (for example, if a living person donated tissue for use in future research protocols, that tissue is not considered a "cadaver" under this policy, regardless of whether the donor is living or deceased at the time of tissue use).

TOTAL ACTIVITIES: **No RDT&E, education or training activities involving human cadavers will be performed to complete the Statement of Work (SOW).**

ACTIVITES: **No RDT&E, education or training activities involving human cadavers will be performed to complete the Statement of Work (SOW).**

(c) Animal Use Regulatory Protocols

TOTAL PROTOCOL(S):

State the total number of animal use protocols required to complete this project (e.g., 2 animal use research protocols will be required to complete the Statement of Work.). If not applicable, write "No animal use research will be performed to complete the Statement of Work."

PROTOCOL(S):

List the identifier and title for all animal use protocols needed to complete the project. Include information about the approved target number for statistical significance, type of submission, type of approval with associated dates, and performance status.

The following format shall be used:

TOTAL PROTOCOL(S): 1 animal use research protocol will be required to complete the Statement of Work.

PROTOCOL (1 of 1 total):

Protocol [ACURO Assigned Number]: BC170206.e001

Title: Rodent Models of Pregnancy Associated Breast Cancer

Target required for statistical significance: 116

Target approved for statistical significance: 176

SUBMITTED TO AND APPROVED BY:

- OHSU IACUC
- Ms. Sheron Westbrook, Animal Program Oversight Specialist Office of Research Protections (ORP)
- Larry J. Shelton Jr., DVM, MPH, DACLAM Colonel, US Army Director, Animal Care and Use

STATUS:

Nothing to report

10. APPENDICES

- Betts, CB, Quackenbush, A, Anderson, W, Marshall, N, Schedin, P. Mucosal immunity and liver metabolism in the complex condition of lactation insufficiency. Journal of Human Lactation, Aug 14, 2020. PMID: 32795211
- Bartlett, A.Q., Pennock, N.D., Klug, A., Schedin, P. Immune Milieu Established by Postpartum Liver Involution Promotes Breast Cancer Liver Metastasis. Cancers 2021, 13, 1698. https://doi.org/10.3390/cancers13071698
- Q Bartlett A, Vesco KK, Purnell JQ, Francisco M, Goddard E, Guan X, DeBarber A, Leo MC, Baetscher E, Rooney W, Naugler W, Guimaraes AR, Catalano P, Xia Z, Schedin P. Pregnancy and weaning regulate human maternal liver size and function. Proc Natl Acad Sci U S A. 2021 Nov 30;118(48):e2107269118. doi: 10.1073/pnas.2107269118. PMID: 34815335

Original Perspective

international lactation consultant association®

Journal of Human Lactation
2020, Vol. 36(4) 582–590

DOI: 10.1177/0890334420947656
journals.sagepub.com/home/jhl
SAGE

Mucosal Immunity and Liver Metabolism in the Complex Condition of Lactation Insufficiency

Courtney B. Betts, PhD[1*], Alexandra Quackenbush, BS[1*], Weston Anderson, BA[1], Nicole E. Marshall, MD[2], and Pepper J. Schedin, PhD[1,3,4]

Abstract

Lactation insufficiency is variously defined and includes the inability to produce milk, not producing enough milk to exclusively meet infant growth requirements, and pathological interruption of lactation (e.g., mastitis). Of women with intent-to-breastfeed, lactation insufficiency has been estimated to affect 38%–44% of newly postpartum women, likely contributing to the nearly 60% of infants that are not breastfed according to the World Health Organization's guidelines. To date, research and clinical practice aimed at improving feeding outcomes have focused on hospital lactation support and education, with laudable results. However, researchers' reports of recent rodent studies concerning fundamental lactation biology have suggested that the underlying pathologies of lactation insufficiency may be more nuanced than is currently appreciated. In this article, we identify mucosal biology of the breast and lactation-specific liver biology as two under-researched aspects of lactation physiology. Specifically, we argue that further scientific inquiry into reproductive state-dependent regulation of immunity in the human breast will reveal insights into novel immune based requirements for healthy lactation. Additionally, our synthesis of the literature supports the hypothesis that the liver is an essential player in lactation—highlighting the potential that pathologies of the liver may also be associated with lactation insufficiency. More research into these biologic underpinnings of lactation is anticipated to provide new avenues to understand and treat lactation insufficiency.

Keywords

breastfeeding, breast immunology, insufficient milk, lactation, lactation disorders, liver metabolism, mastitis, maternal physiology

Background

Exclusive breastfeeding for the first 6 months of life for all infants has been recommended by the World Health Organization (WHO) since at least 2001, as breastfeeding strongly associates with reduced infant morbidity and mortality (Edmond et al., 2006; Lamberti et al., 2011, 2013; World Health Organization & UNICEF, 2019). However, as of 2019, only an estimated 41% of infants, globally, were breastfed according to these guidelines (Sultana et al., 2013). There are many barriers to exclusive breastfeeding (EBF), including lactation insufficiency (Sultana et al., 2013). Lactation insufficiency is variously defined, and ranges from the inability to produce milk, not producing enough milk to meet infant growth requirements (Figure 1A), and unintended pathological interruption of lactation, for example, mastitis (Sultana et al., 2013). Determining the extent of lactation insufficiency is difficult given that the human mammary gland is one of the only organs without a diagnostic test to measure function (Hartmann & Cregan, 2001; Hurst, 2007). Mammary glands are unique in that full glandular development requires the hormones of pregnancy for

[1]Department of Cell, Developmental and Cancer Biology, Oregon Health and Science University, Portland, OR, USA
[2]Obstetrics and Gynecology, School of Medicine, Oregon Health and Science University, Portland, OR, USA
[3]University of Colorado Cancer Center, Aurora, CO, USA
[4]Knight Cancer Institute, Oregon Health and Science University, Portland, OR, USA

*Drs Courtney B. Betts and Alexandra Quackenbush contributed equally to the work.

Date submitted: January 16, 2020; Date accepted: July 14, 2020.

Corresponding Author:
Pepper J. Schedin, PhD, Oregon Health and Science University, 2720 S.W. Moody Avenue, Portland, OR 97201, USA.
Email: Schedin@OHSU.edu

maturation. Lactogenesis occurs in two stages. The first stage is secretory differentiation, which takes place during pregnancy when the initiation of glandular capacity for milk synthesis begins. The second is secretory activation, which occurs after delivery of the placenta and the associated progesterone withdrawal, and results in the onset of copious milk production (Neville & Morton, 2001). Secretory activation is an endocrine-driven process which should occur regardless of milk removal, while the ongoing ability to produce milk is driven by autocrine control. If milk is not removed regularly, local feedback inhibition will lead to mammary gland involution and weaning (Neville & Morton, 2001). The secretory activation phase is also characterized in humans and rodents by increasing lactose concentrations in the milk, putatively via galactose synthesis by mammary epithelial cells (Mohammad et al., 2012). Interference of any of these processes, from insufficient glandular tissue to altered hormonal concentrations to ineffective milk removal, could result in lactation insufficiency.

While many primiparous women struggle with delayed lactogenesis (estimates range from 38% to 44% in recent studies; Nommsen-Rivers et al., 2012), true failure of the onset of lactation remains rare, with only 1.7% of women not experiencing the onset of lactation within the first week following parturition (Nommsen-Rivers et al., 2010). Clinical estimates have found that, for women intending to breastfeed, between 5% and 15% experience either delayed or failed lactogenesis (Hurst, 2007). However, considering the reported disparities between intent to lactate and meeting lactation goals, the actual incidence of lactation insufficiency could be higher.

Psychosocial factors (e.g., stress, misaligned expectations about nursing an infant, lack of significant other support, and lack of adequate lactation education) have all been reported as causes of lactation insufficiency (Lau, 2001; Lau & Simpson, 2004). However, there are numerous physiologic risk factors for lactation insufficiency including maternal age, diabetes, polycystic ovarian syndrome, preterm birth, and inadequate breast development during puberty and pregnancy (Neifert et al., 1985). Additionally, in the clinic, lack of change in breast size during pregnancy is viewed as a risk factor for lactation insufficiency (Hurst, 2007). The hypothesis is that insufficient or stunted glandular development during pregnancy may result in too few mammary epithelial cells to produce an adequate milk supply. The same could be true of stunted mammary development during puberty. However, very little is known about normal mammary gland development on the tissue or cellular level specifically pertaining to milk production, and there is likely natural variation from person to person. As a result, there is scant scientific evidence to either support or reject this "mammary gland development" hypothesis.

Mastitis, another commonly recognized cause of lactation insufficiency, can result in gland damage and/or activation of unplanned involution, both of which would lead to the removal of milk producing cells, thereby reducing milk production. Specifically, bacterial sensing during mastitis via the circulating factor lipopolysaccharide binding protein (LBP) culminates in STAT-3 activation, a known trigger of involution (de Andrés et al., 2018; Jena et al., 2019; Stein et al., 2004; Zeng et al., 2009). Mastitis caused by overt bacterial infection is a well-studied issue among lactating women with effective treatment options, and has been covered in other excellent reviews (Barbosa-Cesnik et al., 2003; Jahanfar et al., 2013).

Another clinically recognized risk factor for lactation insufficiency is obesity. Women with overweight/obesity who intended EBF have lower rates of EBF 6 weeks to 6 months after birth compared to their peers of normal weight (Marshall et al., 2019, 2020). The exact biological mechanism(s) are unknown but may involve obesity-associated systemic metabolic dysregulation that influences the ability to make milk. The study of obesity as a cause of lactation insufficiency is widely recognized but remains an emerging field; it is not the focus of this article.

Considering the exclusions we outline above, this paper is not a systematic review, but rather seeks to synthesize potential biologic mediators not commonly connected to lactation. Recently, researchers conducting rodent studies concerning fundamental lactation biology have suggested that the underlying pathologies of lactation insufficiency may be more nuanced than is currently appreciated. Specifically, new evidence suggested that active mucosal immune programs within the breast, and enhanced function from the liver, might contribute to healthy lactation. The primary literature exploring the role of liver function and immunity in the breast is modest but

Key Messages

- Lactation insufficiency has been estimated to negatively influence 38%–44% of newly postpartum women. However, the physiological underpinnings of lactation insufficiency in humans are still under investigation.
- Results from preclinical models strongly support the hypothesis that active immune programs in the breast during lactation support healthy lactation—indicating autoimmunity as a potential factor in lactation insufficiency for some women.
- Likewise, researchers have reported results from both rodent and human studies supporting a functional role for the liver in milk production—suggesting that metabolic dysregulation and pathologies of the liver may contribute to lactation insufficiency.
- Roles for mammary gland immune function and liver function in healthy lactation and lactation insufficiency are worthy of additional study, with the hope of positively influencing lactation insufficiency management.

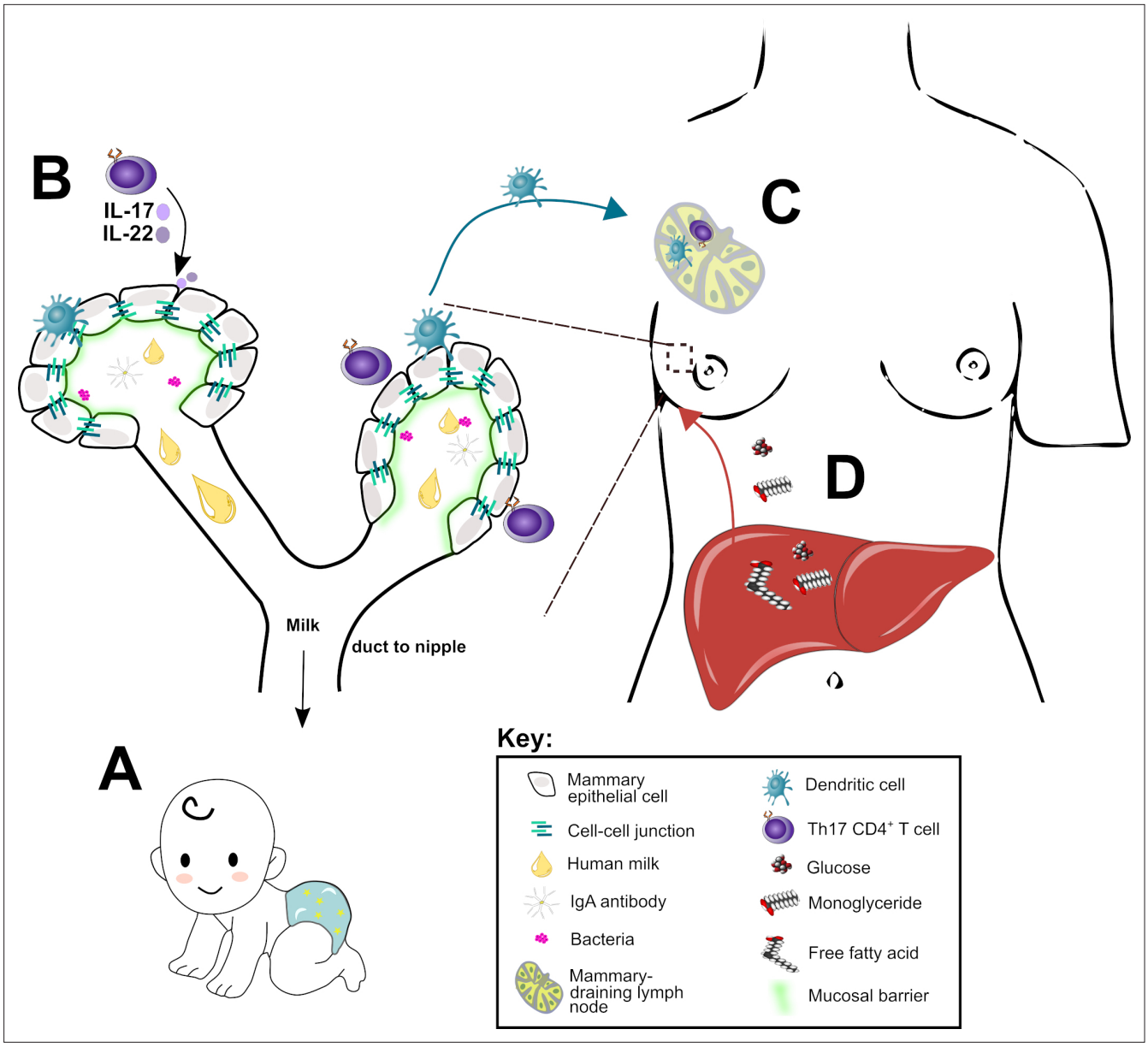

Figure 1. Mucosal Immunity in the Mammary Gland and Liver Metabolism as Potential Contributors to Healthy Lactation.
Note. A: Successful lactation is measured indirectly via infant growth and development. B: Mucosal immunity in the lactating mammary gland including barrier function and tolerogenic dendritic cells. C: Mammary draining lymph node regulates naïve T cell priming during lactation. D: Liver-mammary gland link during lactation for metabolic coordination and exchange of milk raw materials.

intriguing. Here, we present data supportive of the hypothesis that lactation is influenced by liver function and immunity, with the goal of illuminating future avenues for quantitatively assessing lactation function.

The Study of Mastitis Reveals Insight Into Mammary Gland Mucosal Immunity

Mucosal immunity is classically defined in organs with exposure to the outside world (e.g., the lungs and gastrointestinal tract). Modulation of mucosal immunity functions by reducing tissue-damaging responses due to persistent foreign antigen (Gill et al., 2010). Within the field of mammary gland biology, the mammary gland is not widely regarded as a mucosal organ that is exposed to persistent foreign antigen. However, the complex condition of clinical mastitis offers some insights into mucosal-like biological processes within the breast that may ensure lactation success. Mastitis occurs in 10%–27% of breastfeeding women (Ingman et al., 2014; Sordillo & Streicher, 2002); it is

commonly associated with a form of lactation insufficiency driven by interrupted lactation (Wöckel et al., 2008). The etiology of mastitis is thought to be largely due to overt bacterial infections (Boakes et al., 2018). Notably, skin-resident *staphylococcus epidermidis* is the most common bacterial species found in milk cultures of women with clinical symptoms of mastitis, suggesting entrance of externally-located bacteria into the mammary gland (Marín et al., 2017). Also, animal models of bacterial mastitis commonly rely upon the administration of bacteria into the teat canal (Glynn et al., 2014; Ingman et al., 2015). Taken together, these results suggest that translocation of bacteria from the skin into the mammary duct, and then into the mammary tissue can result in pathogenic mastitis in animal models, and thus may account for mastitis in women. However, bacteria also are present in healthy mammary tissue and in the milk of healthy women (Figure 1B), which suggests that bacteria can be a normal component of the mammary gland environment (Ballard & Morrow, 2013; Kvist et al., 2008; Urbaniak et al., 2014). Interestingly, researchers have shown that the breast microbiome is complex and can be influenced by diet, indicating that the mere presence of bacteria in the breast alone is not sufficient to explain the etiology of mastitis (Fernández et al., 2016; Jiménez et al., 2008; Shively et al., 2018).

During lactation, the normal mammary gland may be protected from bacterial translocation into underlying breast tissue by a highly impermeable epithelial barrier that is actively immune monitored (Figure 1B, cell-cell junctions; Betts et al., 2018; Nguyen et al., 2001; Owens et al., 2013; Stelwagen et al., 1999). Evidence that this protection is mediated in part by immunological programs is suggested by extensive studies in the gut, which show that highly orchestrated chemical and cellular barriers are essential for staving off infection from exogenous bacteria (Moens & Veldhoen, 2012; Okumura & Takeda, 2017). Based on these gut studies, we propose one origin of breast mastitis is through loss of epithelial cell barrier function and immune surveillance, resulting in aberrant bacterial translocation into the breast. However, the presence of a mucosal immunologic barrier has not been systematically investigated or demonstrated in the human breast. One could argue for the existence of a barrier function in the healthy lactating breast given the relative infrequency of mastitis compared to the number of nursing events that could introduce aberrant bacteria to the breast. Further, overt bacterial infection does not account for all cases of mastitis (Boakes et al., 2018; Kvist et al., 2008); thus, a full understanding of both microbe-dependent and independent inflammatory processes during lactation is required to fully understand mastitis.

Betts et al. (2018) is the first study of its kind to systematically assess the mammary gland for mucosal immunological hallmarks. This research team found that the adult murine mammary gland exhibits numerous mucosal hallmarks that are highly enriched during lactation, including a predominance of Th17 $CD4^+$ T cells (Figure 1B), which play important roles in mucosal barrier function (Betts et al., 2018). The role for Th17 $CD4^+$ T cells has been exquisitely described in the gut mucosa, where these cells produce IL-17, a cytokine that directly regulates epithelium impermeability by enhancing inter-cellular tight junctions (Kinugasa et al., 2000; Lee et al., 2015; Reynolds et al., 2012). Specifically, in models of intestinal injury IL-17 positively regulates the localization of the tight junction protein occludin, leading to decreased inter-cellular permeability, as measured by increased electrical resistance and protection from pathological bacterial colonization (Reynolds et al., 2012). Similar findings have corroborated the role of IL-17 cytokines in gut epithelial cell tight junction integrity in both homeostatic and acute injury contexts (Kinugasa et al., 2000; Reynolds et al., 2012). Further, IL-17 and IL-22 produced by Th17 $CD4^+$ T cells in the gut stimulate receptors on mucosal epithelial cells, leading to enhanced secretion of the antimicrobial β-defensin 2 (Huang et al., 2007; Kao et al., 2004). In addition, the Th17 $CD4^+$ T cell produces IL-22 (Figure 1B), which acts on intestinal epithelial cells to induce the production of the Reg family of antimicrobial proteins, including RegIIIγ (Zheng et al., 2008). Enhanced mRNA expression of antimicrobial mucins 1, 3, and 10 during lactation suggest that similar Th17 mucosal function is active in the lactational mammary gland (Betts et al., 2018).

Another component of mucosal immune programs that may be active in the mammary gland is immune tolerance. Immune tolerance is enhanced in the mammary gland during lactation in comparison to other reproductive states (Betts et al., 2018). Mucosal tissues are at risk of over-reacting to foreign antigens leading to pathologic inflammation, a risk mitigated by active immune tolerance programs (Steele et al., 2012). To address whether the mammary gland displays immune tolerance, a novel DO11.10 mouse model of naïve T cell priming was utilized. It was found that naïve systemic $CD4^+$ T cells became activated in the mammary gland draining lymph node when their specific antigen was introduced into the mammary gland of the nulliparous host (Betts et al., 2018). Conversely, T cell activation was not observed when antigen was injected into the lactating mammary gland. This relative lack of naïve T cell activation during lactation associated with increased numbers of tolerogenic antigen presenting dendritic cells (Figure 1B and C), specifically dendritic cells with reduced MHC-II and co-stimulatory molecule expression (CD80, CD86; Betts et al., 2018). Also, mammary gland dendritic cells during lactation showed reduced antigen presentation capability when assessed functionally. Altogether, this body of work is consistent with mucosal immune tolerance being active in the lactating gland, supporting the idea that mucosal immune tolerance plays a role in lactation success.

If mucosal immune tolerance is essential for lactation, then disruption of this tolerance mechanism is anticipated to contribute to lactation insufficiency. Recently, researchers have provided support for this nascent hypothesis. In

particular, a form of non-pathogen mastitis called idiopathic granulomatous has sparked interest in the immune requirements for successful lactation. In women, idiopathic granulomatous mastitis is a local inflammatory reaction that does not respond to antibiotics but does respond to steroids (Kim et al., 2003). This has led to the postulation of idiopathic granulomatous mastitis as an autoimmune disease of the lactating breast (Azlina et al., 2003; Katz et al., 2007). To investigate the possibility of autoimmunity in the mammary gland leading to lactation insufficiency, Kesaraju and colleagues (2012) utilized a unique rodent model that elicited immunity to a lactation-specific milk protein. The expected outcome was that autoimmunity to a milk protein would result in autoimmune inflammation, damage to secretory mammary epithelium, and reduced milk production. In this model, mature SWR/J female mice were immunized prior to mating with the milk protein alpha lactalbumin, a protein necessary for lactose production. Following immunization, females were randomized to a lactating or nulliparous study arm. Mammary tissue inflammation consistent with autoimmunity, that is Th1 skewed T cells that produced the inflammatory cytokine IFNγ, was only observed in the lactation group. Mammary tissue inflammation was not observed in non-immunized or immunized but nulliparous mice. Further, the immunized lactation group mice failed to sustain their pups, leading to pup alopecia and runting (Kesaraju et al., 2012). These outcomes supported an important conclusion: Autoimmunity to a lactation specific antigen is possible and leads to lactation insufficiency. This evidence suggested that mucosal immune tolerance, to functionally oppose potential autoimmunity, is a critical component of lactation success in rodents. The presence and requirement of mucosal immune programs in rodent models of lactation provide impetus to investigate the role of breast mucosal biology in supporting lactation in women.

Evidence of a Liver–Mammary Gland Functional Unit During Lactation and Weaning

To meet the nutritional needs of a nursing infant it is understood that the liver and the mammary gland both support lactation by increasing metabolic output (Tigas et al., 2002). As a result, it has been hypothesized that during lactation the mammary gland and the liver contribute to lactation success by working as a functional unit. Therefore, understanding the role of the liver in milk production, including through the normal regulatory pathways of liver glucose production (Tigas et al., 2002), may yield insight into lactation insufficiency of unknown origin. It is well accepted that mammary epithelial cells are the major producers of mature milk, including lipids, in part through the up-regulation of gene expression in the mammary gland related to fatty acid synthesis (Rudolph et al., 2007). Nonetheless, it is also known that the majority of fatty acids needed for milk production are obtained through diet via absorption, bile emulsification, and the break down to free fatty acids and monoglycerides, which occurs in the small intestine (Rudolph et al., 2007). In this capacity, the liver, which has a role in lipid homeostasis through adsorption of circulating lipids, has been viewed as an intermediate storehouse for fatty acids prior to transit to the mammary gland. However, recent evidence has suggested an even more important role for the liver in milk production, one that requires the liver to undergo a reproductive state change that has not previously been described.

Early evidence for reproductive state alterations in the liver included the demonstration of increased biosynthetic capability during lactation. For example, in sows, on the day prior to birth, higher circulating urea and creatinine concentrations—both made by the liver—positively correlated with colostrum yield, the first product of lactation (Loisel et al., 2014). Additionally, both fatty acid oxidation and glucose production in the rodent liver significantly increase during lactation, ostensibly to meet the elevated glucose needs of milk production (Goddard et al., 2017; Rawson et al., 2012). The liver produces glucose through glycogenolysis and gluconeogenesis (Tigas et al., 2002). Intriguingly, gluconeogenesis pathways are more active in the liver than in the mammary gland during lactation (Figure 1D), suggesting that the liver is a primary source of glucose for milk production (Rudolph et al., 2007). Consistent with this finding, protein and lactose concentrations in milk correlate strongly with hepatic glucose metabolism in dairy cows (Grum et al., 2002; Weber et al., 2013). In further support of the liver playing an active role in lactation, researchers recently have reported the lactating rodent liver is metabolically distinct from pre-pregnant and post-weaning stages, with increasing anabolic metabolism (Goddard et al., 2017). These data support the hypothesis that during lactation the liver plays a key role in the production of milk, alongside the mammary gland, with the liver as the predominate site of glucose synthesis. How glucose production in the liver is regulated during lactation remains an open question. One potential explanation is that the liver increases nutrient output in response to low nutrient blood levels, which are lowered due to increased uptake by the lactating mammary gland. However, in multiple small studies with lactating women, researchers reported neither lactation nor feeding at the breast to result in hypoglycemia (Bentley-Lewis et al., 2007; Colatrella et al., 2012), raising an intriguing alternative hypothesis to account for the increased metabolic output during lactation. Specifically, the liver may increase metabolic output in response to developmentally regulated cues from the mammary gland.

Additionally, similar architectural and physical changes occur in the mammary gland and liver during lactation, which could be interpreted as evidence for coordinated lactational programs in these two organs. For example, quantitative extracellular matrix proteomics demonstrates that the liver changes its matrix composition during lactation, as

does the mammary gland (Goddard et al., 2016). In addition, the physical size of the mammary gland and liver are regulated in tandem during pregnancy and lactation in the rodent (Dai et al., 2011; Hollister et al., 1987). Furthermore, in rodents, liver size decreases to its pre-pregnant size concurrent with weaning rather than at parturition, demonstrating that liver size is dissociated from the overall body weight of the dam at the pregnancy to lactation switch (Goddard et al., 2017). Additional data that are consistent with the regulated coordination of the liver and the mammary gland have been observed upon weaning. The process that results in the reduction in liver size post-wean shares all the hallmarks of weaning-induced mammary gland involution, including programmed cell death of the hepatocytes, immune cell influx, extracellular matrix remodeling, and catabolic metabolism consistent with tissue loss. In further support of a liver–mammary gland functional link, a recent study by Hyatt et al. (2019) found evidence of a causal relationship between lactation and liver size increase. These authors found that parous rats which were permitted to lactate had significantly greater liver mass compared to parous rats not permitted to lactate (Hyatt et al., 2019). We argue that these data and the synchronous growth during pregnancy, maintenance during lactation, and weaning-induced involution processes in the mammary gland and liver provide strong support for a mammary gland–liver functional unit that is established to meet the metabolic demands of lactation. However, whether this functional link is regulated in response to the developmental programs of pregnancy and lactation, or indirectly regulated due to increased metabolic demands of lactation, remains to be determined.

Summary and Future Directions

Lactation insufficiency is a serious clinical problem that will likely require interdisciplinary research to fully delineate. Here, we identify mucosal biology of the breast and liver biology as two under-researched aspects of lactation that may provide new avenues to understand the etiology of lactation insufficiency—especially for cases not corrected with education, support, or antibiotics.

We argue that further scientific inquiry into reproductive state-dependent regulation of immunity in the breast will likely reveal immunological requirements for healthy lactation. Specifically, autoimmunity to milk proteins might be one mechanism underlying lactation insufficiency. However, active immune regulation in the lactating mammary gland has so far only been demonstrated in animal models, including evidence of autoimmunity influencing milk production (Kesaraju et al., 2012; Schwartz & Strauchen, 1990). Research into mucosal breast biology in healthy women may yield insight into the initiation of autoimmune disorders within the breast and lead to new strategies for the prevention of some types of lactation insufficiency. Moreover, the demonstration of immune suppression in the breast as a requisite for healthy lactation in women could contribute to the development of new standards of care in the detection and treatment of lactation insufficiency. Specifically, the development of clinical diagnostic tests to detect auto-antibodies to milk components in lactating women would broaden the tool kit available to clinicians treating mastitis of unknown origin.

Additionally, the hypothesis that the liver is an essential player in lactation because of its enhanced glucose production, metabolic processing of lipids, and shuttling of these vital milk components to the mammary gland, has an evidence-base. An outstanding question is whether various liver pathologies may impede successful lactation, including fatty liver disease, hepatitis C, and cirrhosis. One untested hypothesis is that fatty liver disease of any etiology may reduce the liver's capacity to support lactation, limiting lipid or glucose transport to the mammary gland, and reducing milk supply. These questions could be addressed by epidemiological studies of reproductive-age women with liver conditions, as well as prospective studies in lactating women.

Altogether, this commentary highlights the potential influence that investigating the physiological underpinnings of healthy lactation could have on improving lactation success, and thus infant health. While lactation insufficiency has obvious implications for the infant, there may be unappreciated consequences for maternal health. For example, the "reset hypothesis" proposes that lactation is critical for the metabolic health of a new mother by decreasing insulin resistance, a potentially powerful biology in reducing the development of diabetes (Stuebe & Rich-Edwards, 2009). Also, a lactation duration of 6 months or longer has been associated with reduced incidence of non-alcoholic fatty liver disease and breast cancer (Ajmera et al., 2019; Palmer et al., 2014). Therefore, lactation represents a significant opportunity to potentially make inroads in the treatment of multiple health problems that disproportionately affect women, including breast cancer, liver disease, autoimmune disorders and, of course, lactation insufficiency. Studying the role of immunity and the liver in supporting lactation may lead to important discoveries in all these fields.

Declaration of Conflicting Interests

The author declared no potential conflicts of interest with respect to the research, authorship, and/or publication of this article.

Funding

The author(s) disclosed receipt of the following financial support for the research, authorship, and/or publication of this article: F31 CA196052/CA/NCI NIH HHS/United States to CB, R01 CA169175/CA/NCI NIH HHS/United States to PS; K23HD069520-01A1 NIH/HHS/NICHHD to NM; U.S. Department of Defense CDMRP BC170206 to PS.

ORCID iD

Pepper J. Schedin, PhD https://orcid.org/0000-0003-4244-987X

References

Ajmera, V. H., Terrault, N. A., VanWagner, L. B., Sarkar, M., Lewis, C. E., Carr, J. J., & Gunderson, E. P. (2019). Longer lactation duration is associated with decreased prevalence of non-alcoholic fatty liver disease in women. *Journal of Hepatology*, *70*(1), 126–132. doi:10.1016/j.jhep.2018.09.013

Azlina, A. F., Ariza, Z., Arni, T., & Hisham, A. N. (2003). Chronic granulomatous mastitis: Diagnostic and therapeutic considerations. *World Journal of Surgery*, *27*(5), 515–518. doi:10.1007/s00268-003-6806-1

Ballard, O., & Morrow, A. L. (2013). Human milk composition: Nutrients and bioactive factors. *Pediatric Clinics of North America*, *60*(1), 49–74. doi:10.1016/j.pcl.2012.10.002

Barbosa-Cesnik, C., Schwartz, K., & Foxman, B. (2003). Lactation mastitis. *JAMA*, *289*(13), 1609–1612. doi:10.1001/jama.289.13.1609

Bentley-Lewis, R., Goldfine, A. B., Green, D. E., & Seely, E. W. (2007). Lactation after normal pregnancy is not associated with blood glucose fluctuations. *Diabetes Care*, *30*(11), 2792–2793. doi:10.2337/dc07-1243

Betts, C. B., Pennock, N. D., Caruso, B. P., Ruffell, B., Borges, V. F., & Schedin, P. (2018). Mucosal immunity in the female murine mammary gland. *The Journal of Immunology*, *201*(2), 734–746. doi:10.4049/jimmunol.1800023

Boakes, E., Woods, A., Johnson, N., & Kadoglou, N. (2018). Breast infection: A review of diagnosis and management practices. *European Journal of Breast Health*, *14*(3), 136–143. doi:10.5152/ejbh.2018.3871

Colatrella, A., Framarino, M., Toscano, V., Bongiovanni, M., Festa, C., Mattei, L., Merola, G., Bitterman, O., Maravalle, M., & Napoli, A. (2012). Continuous glucose monitoring during breastfeeding in women with recent gestational diabetes mellitus. *Diabetes Technology & Therapeutics*, *14*(7), 576–582. doi:10.1089/dia.2011.0266

Dai, G., Bustamante, J. J., Zou, Y., Myronovych, A., Bao, Q., Kumar, S., & Soares, M. J. (2011). Maternal hepatic growth response to pregnancy in the mouse. *Experimental Biology and Medicine*, *236*(11), 1322–1332. doi:10.1258/ebm.2011.011076

de Andrés, J., Jiménez, E., Espinosa-Martos, I., Rodríguez, J. M., & García-Conesa, M.-T. (2018). An exploratory search for potential molecular targets responsive to the probiotic *Lactobacillus salivarius* PS2 in women with mastitis: Gene expression profiling vs. interindividual variability. *Frontiers in Microbiology*, *9*, 2166. doi:10.3389/fmicb.2018.02166

Edmond, K. M., Zandoh, C., Quigley, M. A., Amenga-Etego, S., Owusu-Agyei, S., & Kirkwood, B. R. (2006). Delayed breastfeeding initiation increases risk of neonatal mortality. *Pediatrics*, *117*(3), e380–386. doi:10.1542/peds.2005-1496

Fernández, L., Cárdenas, N., Arroyo, R., Manzano, S., Jiménez, E., Martín, V., & Rodríguez, J. M. (2016). Prevention of infectious mastitis by oral administration of lactobacillus salivarius pS2 during late pregnancy. *Clinical Infectious Diseases*, *62*(5), 568–573. doi:10.1093/cid/civ974

Gill, N., Wlodarska, M., & Finlay, B. B. (2010). The future of mucosal immunology: Studying an integrated system-wide organ. *Nature Immunology*, *11*(7), 558–560. doi:10.1038/ni0710-558

Glynn, D. J., Hutchinson, M. R., & Ingman, W. V. (2014). Toll-like receptor 4 regulates lipopolysaccharide-induced inflammation and lactation insufficiency in a mouse model of mastitis. *Biology of Reproduction*, *90*(5), 91. doi:10.1095/biolreprod.114.117663

Goddard, E. T., Hill, R. C., Barrett, A., Betts, C., Guo, Q., Maller, O., Borges, V. F., Hansen, K. C., & Schedin, P. (2016). Quantitative extracellular matrix proteomics to study mammary and liver tissue microenvironments. *International Journal of Biochemistry & Cell Biologybiology*, *81*(Pt A), 223–232. doi:10.1016/j.biocel.2016.10.014

Goddard, E. T., Hill, R. C., Nemkov, T., D'Alessandro, A., Hansen, K. C., Maller, O., Mongoue-Tchokote, S., Mori, M., Partridge, A. H., Borges, V. F., & Schedin, P. (2017). The rodent liver undergoes weaning-induced involution and supports breast cancer metastasis. *Cancer Discovery*, *7*(2), 177–187. doi:10.1158/2159-8290.CD-16-0822

Grum, D. E., Drackley, J. K., & Clark, J. H. (2002). Fatty acid metabolism in liver of dairy cows fed supplemental fat and nicotinic acid during an entire lactation. *Journal of Dairy Science*, *85*(11), 3026–3034. doi:10.3168/jds.S0022-0302(02)74388-9

Hartmann, P., & Cregan, M. (2001). Lactogenesis and the effects of insulin-dependent diabetes mellitus and prematurity. *The Journal of Nutrition*, *131*(11), 3016S–3020. doi:10.1093/jn/131.11.3016S

Hollister, A., Okubara, P., Watson, J. G., & Chaykin, S. (1987). Reproduction in mice: Liver enlargement in mice during pregnancy and lactation. *Life Science*, *40*(1), 11–18. doi:10.1016/0024-3205(87)90246-3

Huang, F., Kao, C.-Y., Wachi, S., Thai, P., Ryu, J., & Wu, R. (2007). Requirement for both JAK-mediated PI3K signaling and ACT1/TRAF6/TAK1-dependent NF-kappaB activation by IL-17A in enhancing cytokine expression in human airway epithelial cells. *Journal of Immunology*, *179*(10), 6504–6513. doi:10.4049/jimmunol.179.10.6504

Hurst, N. M. (2007). Recognizing and treating delayed or failed lactogenesis II. *Journal of Midwifery & Women's Health*, *52*(6), 588–594. doi:10.1016/j.jmwh.2007.05.005

Hyatt, H. W., Zhang, Y., Hood, W. R., & Kavazis, A. N. (2019). Changes in metabolism, mitochondrial function, and oxidative stress between female rats under nonreproductive and 3 reproductive conditions. *Reproductive Science*, *26*(1), 114–127. doi:10.1177/1933719118766264

Ingman, W. V., Glynn, D. J., & Hutchinson, M. R. (2014). Inflammatory mediators in mastitis and lactation insufficiency. *Journal of Mammary Gland Biology and Neoplasia*, *19*(2), 161–167. doi:10.1007/s10911-014-9325-9

Ingman, W. V., Glynn, D. J., & Hutchinson, M. R. (2015). Mouse models of mastitis—How physiological are they? *International Breastfeeding Journal*, *10*, 12. doi:10.1186/s13006-015-0038-5

Jahanfar, S., Ng, C. J., & Teng, C. L. (2013). Antibiotics for mastitis in breastfeeding women. *Cochrane Database of Systematic Reviews*, *4*(2). doi:10.1002/14651858.CD005458.pub3

Jena, M. K., Jaswal, S., Kumar, S., & Mohanty, A. K. (2019). Molecular mechanism of mammary gland involution: An update. *Developmental Biology*, *445*(2), 145–155. doi:10.1016/j.ydbio.2018.11.002

Jiménez, E., Fernández, L., Maldonado, A., Martín, R., Olivares, M., Xaus, J., & Rodríguez, J. M. (2008). Oral administration of Lactobacillus strains isolated from breast milk as an alternative for the treatment of infectious mastitis during lactation. *Applied and Environmental Microbiology*, *74*(15), 4650–4655. doi:10.1128/AEM.02599-07

Kao, C.-Y., Chen, Y., Thai, P., Wachi, S., Huang, F., Kim, C., Harper, R. W., & Wu, R. (2004). Il-17 markedly up-regulates beta-defensin-2 expression in human airway epithelium via JAK and NF-kappaB signaling pathways. *The Journal of Immunology*, *173*(5), 3482–3491. doi:10.4049/jimmunol.173.5.3482

Katz, U., Molad, Y., Ablin, J., Ben-David, D., Paran, D., Gutman, M., & Langevitz, P. (2007). Chronic idiopathic granulomatous mastitis. *Annals of the New York Academy of Sciences*, *1108*, 603–608. doi:10.1196/annals.1422.063

Kesaraju, P., Jaini, R., Johnson, J. M., Altuntas, C. Z., Gruden, J. J., Sakalar, C., & Tuohy, V. K. (2012). Experimental autoimmune breast failure: A model for lactation insufficiency, postnatal nutritional deprivation, and prophylactic breast cancer vaccination. *American Journal of Pathology*, *181*(3), 775–784. doi:10.1016/j.ajpath.2012.05.025

Kim, J., Tymms, K. E., & Buckingham, J. M. (2003). Methotrexate in the management of granulomatous mastitis. *ANZ Journal of Surgery*, *73*(4), 247–249. doi:10.1046/j.1445-1433.2002.02564.x

Kinugasa, T., Sakaguchi, T., Gu, X., & Reinecker, H. C. (2000). Claudins regulate the intestinal barrier in response to immune mediators. *Gastroenterology*, *118*(6), 1001–1011. doi:10.1016/s0016-5085(00)70351-9

Kvist, L. J., Larsson, B. W., Hall-Lord, M. L., Steen, A., & Schalén, C. (2008). The role of bacteria in lactational mastitis and some considerations of the use of antibiotic treatment. *International Breastfeeding Journal*, *3*, 6. doi:10.1186/1746-4358-3-6

Lamberti, L. M., Fischer Walker, C. L., Noiman, A., Victora, C., & Black, R. E. (2011). Breastfeeding and the risk for diarrhea morbidity and mortality. *BMC Public Health*, *11*(Suppl 3), S15. doi:10.1186/1471-2458-11-S3-S15

Lamberti, L. M., Zakarija-Grković, I., Fischer Walker, C. L., Theodoratou, E., Nair, H., Campbell, H., & Black, R. E. (2013). Breastfeeding for reducing the risk of pneumonia morbidity and mortality in children under two: A systematic literature review and meta-analysis. *BMC Public Health*, *13*(Suppl 3), S18. doi:10.1186/1471-2458-13-S3-S18

Lau, C. (2001). Effects of stress on lactation. *Pediatric Clinics of North America*, *48*(1), 221–234. doi:10.1016/S0031-3955(05)70296-0

Lau, C., & Simpson, C. (2004). Animal models for the study of the effect of prolonged stress on lactation in rats. *Physiology & Behavior*, *82*(2–3), 193–197. doi:10.1016/j.physbeh.2004.05.004

Lee, J. S., Tato, C. M., Joyce-Shaikh, B., Gulen, M. F., Gulan, F., Cayatte, C., Chen, Y., Blumenschein, W. M., Judo, M., Ayanoglu, G., McClanahan, T. K., Li, X., & Cua, D. J. (2015). Interleukin-23-independent IL-17 production regulates intestinal epithelial permeability. *Immunity*, *43*(4), 727–738. doi:10.1016/j.immuni.2015.09.003

Loisel, F., Farmer, C., Ramaekers, P., & Quesnel, H. (2014). Colostrum yield and piglet growth during lactation are related to gilt metabolic and hepatic status prepartum. *Journal of Animal Science*, *92*(7), 2931–2941. doi:10.2527/jas.2013-7472

Marshall, N. E., Lallande, L. F., Schedin, P. J., Thornburg, K. L., & Purnell, J. Q. (2020). Exclusive breastfeeding rates at 6 weeks postpartum as a function of preconception body mass index are not impacted by postpartum obstetrical practices or routines. *Breastfeeding Medicine*, *15*(7), 458–464. doi:10.1089/bfm.2020.0006

Marshall, N. E., Lau, B., Purnell, J. Q., & Thornburg, K. L. (2019). Impact of maternal obesity and breastfeeding intention on lactation intensity and duration. *Maternal & Child Nutrition*, *15*(2), e12732. doi:10.1111/mcn.12732

Marín, M., Arroyo, R., Espinosa-Martos, I., Fernández, L., & Rodríguez, J. M. (2017). Identification of emerging human mastitis pathogens by MALDI-TOF and assessment of their antibiotic resistance patterns. *Frontiers in Microbiology*, *8*, 1258. doi:10.3389/fmicb.2017.01258

Moens, E., & Veldhoen, M. (2012). Epithelial barrier biology: Good fences make good neighbours. *Immunology*, *135*(1), 1–8. doi:10.1111/j.1365-2567.2011.03506.x

Mohammad, M. A., Hadsell, D. L., & Haymond, M. W. (2012). Gene regulation of UDP-galactose synthesis and transport: potential rate-limiting processes in initiation of milk production in humans. *American Journal of Physiology-Endocrinology and Metabolism*, *303*(3), E365–E376. doi:10.1152/ajpendo.00175.2012

Neifert, M. R., Seacat, J. M., & Jobe, W. E. (1985). Lactation failure due to insufficient glandular development of the breast. *Pediatrics*, *76*(5), 823–828.

Neville, M. C., & Morton, J. (2001). Physiology and endocrine changes underlying human lactogenesis II. *The Journal of Nutrition*, *131*(11), 3005S–3008. doi:10.1093/jn/131.11.3005S

Nguyen, D. A., Parlow, A. F., & Neville, M. C. (2001). Hormonal regulation of tight junction closure in the mouse mammary epithelium during the transition from pregnancy to lactation. *Journal of Endocrinology*, *170*(2), 347–356. doi:10.1677/joe.0.1700347

Nommsen-Rivers, L. A., Chantry, C. J., Peerson, J. M., Cohen, R. J., & Dewey, K. G. (2010). Delayed onset of lactogenesis among first-time mothers is related to maternal obesity and factors

associated with ineffective breastfeeding. *The American Journal of Clinical Nutrition*, *92*(3), 574–584. doi:10.3945/ajcn.2010.29192

Nommsen-Rivers, L. A., Dolan, L. M., & Huang, B. (2012). Timing of stage II lactogenesis is predicted by antenatal metabolic health in a cohort of primiparas. *Breastfeeding Medicine*, *7*(1), 43–49. doi:10.1089/bfm.2011.0007

Okumura, R., & Takeda, K. (2017). Roles of intestinal epithelial cells in the maintenance of gut homeostasis. *Experimental & Molecular Medicine*, *49*(5), e338. doi:10.1038/emm.2017.20

Owens, M. B., Hill, A. D., & Hopkins, A. M. (2013). Ductal barriers in mammary epithelium. *Tissue Barriers*, *1*(4), e25933. doi:10.4161/tisb.25933

Palmer, J. R., Viscidi, E., Troester, M. A., Hong, C.-C., Schedin, P., Bethea, T. N., Bandera, E. V., Borges, V., McKinnon, C., Haiman, C. A., Lunetta, K., Kolonel, L. N., Rosenberg, L., Olshan, A. F., & Ambrosone, C. B. (2014). Parity, lactation, and breast cancer subtypes in African American women: results from the AMBER Consortium. *Journal of the National Cancer Institute*, *106*(10). doi:10.1093/jnci/dju237

Rawson, P., Stockum, C., Peng, L., Manivannan, B., Lehnert, K., Ward, H. E., Berry, S. D., Davis, S. R., Snell, R. G., McLauchlan, D., & Jordan, T. W. (2012). Metabolic proteomics of the liver and mammary gland during lactation. *Journal of Proteomics*, *75*(14), 4429–4435. doi:10.1016/j.jprot.2012.04.019

Reynolds, J. M., Martinez, G. J., Nallaparaju, K. C., Chang, S. H., Wang, Y.-H., & Dong, C. (2012). Cutting edge: Regulation of intestinal inflammation and barrier function by IL-17C. *Journal of Immunology*, *189*(9), 4226–4230. doi:10.4049/jimmunol.1103014

Rudolph, M. C., McManaman, J. L., Phang, T., Russell, T., Kominsky, D. J., Serkova, N. J., Stein, T., Anderson, S. M., & Neville, M. C. (2007). Metabolic regulation in the lactating mammary gland: A lipid synthesizing machine. *Physiological Genomics*, *28*(3), 323–336. doi:10.1152/physiolgenomics.00020.2006

Schwartz, I. S., & Strauchen, J. A. (1990). Lymphocytic mastopathy. An autoimmune disease of the breast? *American Journal of Clinical Pathology*, *93*(6), 725–730. doi:10.1093/ajcp/93.6.725

Shively, C. A., Register, T. C., Appt, S. E., Clarkson, T. B., Uberseder, B., Clear, K. Y. J., Wilson, A. S., Chiba, A., Tooze, J. A., & Cook, K. L. (2018). Consumption of Mediterranean versus Western diet leads to distinct mammary gland microbiome populations. *Cell Reports*, *25*(1), e43, 47–56. doi:10.1016/j.celrep.2018.08.078

Sordillo, L. M., & Streicher, K. L. (2002). Mammary gland immunity and mastitis susceptibility. *Journal of Mammary Gland Biology and Neoplasia*, *7*(2), 135–146. doi:10.1023/A:1020347818725

Steele, L., Mayer, L., & Berin, M. C. (2012). Mucosal immunology of tolerance and allergy in the gastrointestinal tract. *Immunologic Research*, *54*(1-3), 75–82. doi:10.1007/s12026-012-8308-4

Stein, T., Morris, J. S., Davies, C. R., Weber-Hall, S. J., Duffy, M.-A., Heath, V. J., Bell, A. K., Ferrier, R. K., Sandilands, G. P., & Gusterson, B. A. (2004). Involution of the mouse mammary gland is associated with an immune cascade and an acute-phase response, involving LBP, CD14 and STAT3. *Breast Cancer Research*, *6*(2), R75–91. doi:10.1186/bcr753

Stelwagen, K., McFadden, H. A., & Demmer, J. (1999). Prolactin, alone or in combination with glucocorticoids, enhances tight junction formation and expression of the tight junction protein occludin in mammary cells. *Molecular and Cellular Endocrinology*, *156*(1–2), 55–61. doi:10.1016/S0303-7207(99)00145-8

Stuebe, A. M., & Rich-Edwards, J. W. (2009). The reset hypothesis: Lactation and maternal metabolism. *American Journal of Perinatology*, *26*(1), 81–88. doi:10.1055/s-0028-1103034

Sultana, A., Rahman, K. U. R., & Manjula, S. (2013). Clinical update and treatment of lactation insufficiency. *Medical Journal of Islamic World Academy of Sciences*, *21*(1), 19–28. doi:10.12816/0000207

Tigas, S., Sunehag, A., & Haymond, M. W. (2002). Metabolic adaptation to feeding and fasting during lactation in humans. *The Journal of Clinical Endocrinology & Metabolism*, *87*(1), 302–307. doi:10.1210/jcem.87.1.8178

Urbaniak, C., Cummins, J., Brackstone, M., Macklaim, J. M., Gloor, G. B., Baban, C. K., Scott, L., O'Hanlon, D. M., Burton, J. P., Francis, K. P., Tangney, M., & Reid, G. (2014). Microbiota of human breast tissue. *Applied and Environmental Microbiology*, *80*(10), 3007–3014. doi:10.1128/AEM.00242-14

Weber, C., Hametner, C., Tuchscherer, A., Losand, B., Kanitz, E., Otten, W., Sauerwein, H., Bruckmaier, R. M., Becker, F., Kanitz, W., & Hammon, H. M. (2013). Hepatic gene expression involved in glucose and lipid metabolism in transition cows: Effects of fat mobilization during early lactation in relation to milk performance and metabolic changes. *Journal of Dairy Science*, *96*(9), 5670–5681. doi:10.3168/jds.2012-6277

Wöckel, A., Abou-Dakn, M., Beggel, A., & Arck, P. (2008). Inflammatory breast diseases during lactation: Health effects on the newborn-a literature review. *Mediators of Inflammation*, *2008*, 1–7. doi:10.1155/2008/298760

World Health Organization & UNICEF. (2019). Increasing commitment to breastfeeding through funding and improved policies and programmes: Global breastfeeding scorecard 2019. 4. https://www.who.int/nutrition/publications/infantfeeding/global-bf-scorecard-2019/en/

Zeng, R., Bequette, B. J., Vinyard, B. T., & Bannerman, D. D. (2009). Determination of milk and blood concentrations of lipopolysaccharide-binding protein in cows with naturally acquired subclinical and clinical mastitis. *Journal of Dairy Science*, *92*(3), 980–989. doi:10.3168/jds.2008-1636

Zheng, Y., Valdez, P. A., Danilenko, D. M., Hu, Y., Sa, S. M., Gong, Q., Abbas, A. R., Modrusan, Z., Ghilardi, N., de Sauvage, F. J., & Ouyang, W. (2008). Interleukin-22 mediates early host defense against attaching and effacing bacterial pathogens. *Nature Medicine*, *14*(3), 282–289. doi:10.1038/nm1720

cancers

MDPI

Article

Immune Milieu Established by Postpartum Liver Involution Promotes Breast Cancer Liver Metastasis

Alexandra Q. Bartlett [1], Nathan D. Pennock [1], Alex Klug [1] and Pepper Schedin [1,2,3,*]

[1] Department of Cell, Developmental, and Cancer Biology, Oregon Health & Science University, Portland, OR 97239, USA; quackena@ohsu.edu (A.Q.B.); pennock@ohsu.edu (N.D.P.); klug@OHSU.edu (A.K.)
[2] Knight Cancer Institute, Oregon Health & Science University, Portland, OR 97201, USA
[3] Young Women's Breast Cancer Translational Program, University of Colorado Anschutz Medical Campus, Aurora, CO 80045, USA
* Correspondence: schedin@ohsu.edu

Simple Summary: Cancer becomes lethal when it metastasizes to secondary sites, and for breast cancer metastasis to the liver is a serious clinical problem. Liver metastasis is promoted, in part, by changes to the liver environment, resulting in the formation of a metastatic niche that supports circulating tumor cells. Understanding how the liver niche support breast cancer cells may lead to development of treatments for patients with metastatic breast cancer. Here, we report that the developmentally regulated process of weaning-induced liver involution increases liver metastasis in cancer cells with otherwise low metastatic potential. Increased metastasis associates with unique immunological properties in the involuting liver, including reduced ability to activate T cells required for tumor cell clearance. These data establish physiologic liver involution as a model to understand the liver metastatic niche and suggest future research into whether the immune milieu identified in the involuting liver could be targeted to treat metastases more generally.

Abstract: In rodents, we identified a physiologic process within the normal liver that creates a pre-metastatic niche. This physiology is weaning-induced liver involution, characterized by hepatocyte cell death, immune influx, and extracellular matrix remodeling. Here, using weaning-induced liver involution as a model of a physiologically regulated pro-metastatic niche, we investigate how liver involution supports breast cancer metastasis. Liver metastases were induced in BALB/c immune competent hosts by portal vein injection of D2OR (low metastatic) or D2A1 (high metastatic) mouse mammary tumor cells. Tumor incidence and multiplicity increased in involution hosts with no evidence of a proliferation advantage. D2OR tumor cell extravasation, seeding, and early survival were not enhanced in the involuting group compared to the nulliparous group. Rather, the involution metastatic advantage was observed at 14 days post tumor cell injection. This metastatic advantage associated with induction of immune tolerance in the involution host liver, reproductive state dependent intra-tumoral immune composition, and CD8-dependent suppression of metastases in nulliparous hosts. Our findings suggest that the normal postpartum liver is in an immune suppressed state, which can provide a pro-metastatic advantage to circulating breast cancer cells. Potential relevance to women is suggested as a postpartum diagnosis of breast cancer is an independent predictor of liver metastasis.

Keywords: metastatic niche; liver metastasis; breast cancer; liver involution

Citation: Bartlett, A.Q.; Pennock, N.D.; Klug, A.; Schedin, P. Immune Milieu Established by Postpartum Liver Involution Promotes Breast Cancer Liver Metastasis. *Cancers* **2021**, *13*, 1698. https://doi.org/10.3390/cancers13071698

Academic Editors: Lingzhi Wang and Qiang Jeremy Wen

Received: 28 February 2021
Accepted: 2 April 2021
Published: 3 April 2021

1. Introduction

Breast cancer deaths are almost exclusively due to spread of the cancer to distant organs, i.e., metastasis, and young women with breast cancer are at a higher risk of dying from metastasis than older women [1,2]. The dominant paradigm to explain the increased deaths in younger women is that their tumors have intrinsic properties that increase metastatic capability. In support of this hypothesis, young women are at increased risk of

being diagnosed with poor prognostic HER2+ and triple negative (ER-PR-HER2-) breast cancers [2,3]. However, research shows that young breast cancer patients have worse outcomes compared to older peers regardless of cancer subtype [4]. This suggests that tumor extrinsic factors, such as the microenvironment at the secondary site, might also contribute to increased metastasis observed in young women. Recently, efforts to investigate secondary environments permissive of metastatic growth have gained momentum as an approach to better understand and target metastasis [5–8].

Sites within secondary organs that support tumor cell survival and proliferation are called "metastatic niches" [6]. Stages of the metastatic process that the niche support include tumor cell adherence to organ-specific endothelium, extravasation, survival, immune avoidance, and outgrowth [9]. These pro-metastatic effects are mediated by niche components including insoluble extracellular matrix (ECM) proteins, soluble proteins, and stromal cells such as fibroblasts, endothelial cells, and immune cells. The evolution of an organ into a pro-metastatic niche has been attributed to tumor education, whereby a primary tumor exerts systemic effects that remodel the distant site to a more permissive state [7,10–14]. However, a largely unexplored hypothesis that may further our understanding of breast cancer metastasis in young women is the idea that physiologic remodeling of secondary sites can form a pro-metastatic niche. To date, how normal physiology impacts a possible metastatic niche is not well-studied, in part due to lack of suitable model systems.

One example of a normal, physiologic process that creates a pro-metastatic niche is weaning-induced liver involution. In rodents, it has been reported that the liver approximately doubles in size during pregnancy and retains elevated size throughout lactation, putatively to accommodate the increased metabolic demands of pregnancy and lactation [15–18]. Liver involution returns the pregnancy and lactation-enlarged liver to a pre-pregnant state via a process that includes hepatocyte programmed cell death, catabolic metabolism, ECM remodeling, and immune cell influx [18]. Of note, during liver involution pro-metastatic ECM proteins, i.e., collagen and tenascin C, are deposited and the abundance of immature monocytes and macrophages is elevated [18]. Weaning-induced liver involution promoted breast cancer liver metastasis in a model where tumor cells were delivered to the liver via portal vein injection [18]. This observation of increased liver metastasis in postpartum mice, a so-called "involution advantage", suggests that physiologic liver involution induces a metastatic niche. Of clinical relevance, liver metastases are common in younger breast cancer patients [19]. Further, one recent study demonstrated that young postpartum breast cancer patients are more likely to develop liver metastasis than age matched, as well as tumor stage and subtype matched, never-pregnant patients [18]. Here, we use weaning-induced liver involution as a model of a physiologic process that induces a metastatic niche, and investigate potential mechanisms by which the involution liver supports metastasis.

We report new evidence that reproductive stage of the liver differentially impacts tumor multiplicity and morphology, including mesenchymal and desmoplastic phenotypes. Further, we found that the normal process of liver involution establishes an adaptive immune suppressed environment, and that the involution metastatic advantage can be recapitulated with depletion of cytotoxic CD8 T cells. These data are evidence for reproductive stage dependent physiologic remodeling of the liver metastatic niche with implications for niche-targeted interventions.

2. Results

To model the clinical observation that young women with good prognostic breast cancers can progress to metastatic liver disease [20], we used a syngeneic BALB/c mouse model where mammary tumor cells of low metastatic ability, D2.OR cells [21,22], are delivered directly to the liver via the portal vein [23]. This allowed us to interrogate how liver involution may impact multiple steps of the metastatic process, including tumor cell extravasation into the liver, initial survival in the liver parenchyma, formation of micrometastases, and expansion into overt liver metastases. We first evaluated the formation

of overt tumors at 6 weeks post-injection, and found a >2-fold increased incidence of liver metastases in mice injected at involution (InvD2) compared to mice injected at nulliparous (Figure 1a). Tumor multiplicity was also increased in the involution group (Figure 1b). We next asked if involution provides a growth advantage to these metastatic lesions. We found no differences between nulliparous and involution groups in tumor size (Figure 1c), tumor proliferation as measured by Ki67 (Figure 1d,e), nor death as measured by gH2AX or cleaved caspase 3 (Figure 1f–i). These data are consistent with the involution metastatic niche promoting tumor establishment rather than growth. Similar results of increased multiplicity in the absence of tumor size or proliferation advantage were observed in the involution group with D2A1 cells, a line with known high metastatic potential [21], suggesting similar mechanisms of promotion in two distinct cancer cell lines with different intrinsic metastatic capabilities (Figure S1).

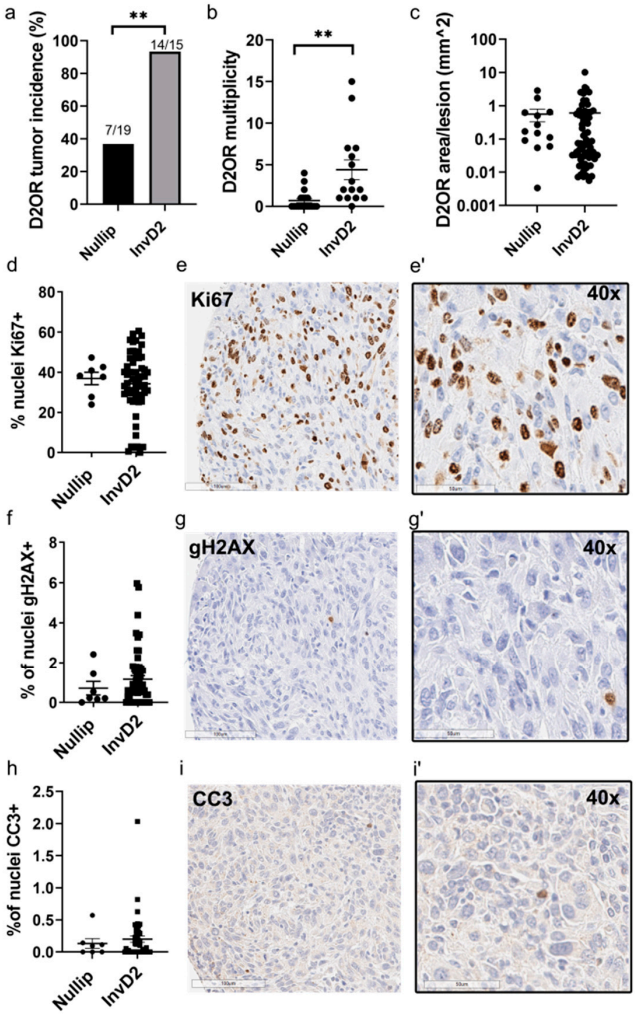

Figure 1. Increased metastasis in involution hosts does not associate with enhanced tumor growth. (**a**) Incidence of D2OR liver metastases in nulliparous (nullip, $n = 19$) and involution day 2 (InvD2, $n = 15$) mice, $n = 3$ independent studies; Two-sided Fisher's exact test; (**b**) Number of metastases (i.e., multiplicity) per mouse in nullip ($n = 19$) and InvD2 ($n = 15$) groups; Two-tailed T test; (**c**) Area per tumor in nullip ($n = 13$ tumors) and InvD2 ($n = 66$ tumors) hosts; IHC quantification of percent of tumor nuclei positive for (**d**) Ki67 in nullip ($n = 7$ tumors) and InvD2 ($n = 57$ tumors); (**f**) γH2AX in nullip ($n = 7$ tumors) and InvD2 ($n = 58$ tumors), and (**h**) cleaved caspase 3 (CC3) in nullip ($n = 7$) and InvD2 ($n = 48$); Representative IHC images at low and high magnification of Ki67 (**e**,**e'**), γH2AX (**g**,**g'**), and CC3 (**i**,**i'**) stains. ** $p < 0.01$.

Clinically, metastases to the liver are categorized into distinct histologies, which have implications for disease outcome [24]. Utilizing histological criteria previously reported in humans, we evaluated tumor cell phenotypes as epithelial, mesenchymal, or metaplastic (i.e., heterogeneous tumors composed of both epithelial and mesenchymal regions with irregular nuclear morphology). We also characterized five previously defined human liver metastasis growth patterns: pushing, replacement, desmoplastic, portal/sinusoidal, and mixed patterns [24]. Representative images of the D2.OR mammary tumor cells growing within mouse livers are shown (Figure 2a1–a5). These murine liver metastases were heterogeneous and highly reminiscent of the tumor heterogeneity observed in human liver metastases. We found that reproductive state influenced both tumor cell morphology and growth pattern (Figure 2b,c). Specifically, tumors that evolved in the nulliparous host liver were more likely to be epithelial in morphology and have a pushing growth pattern. In contrast, tumors from the involution host liver showed greater diversity with increased mesenchymal cell morphology and heterogeneity in growth patterns including desmoplastic and portal/sinusoidal patterns. This observed conservation in liver metastases histology between mice and humans suggests increased human relevance of our breast cancer liver metastasis model. Further, these data represent the novel finding that tumor histology within the liver is shaped by reproductive state of the host, and are consistent with the hypothesis that the liver microenvironment can dictate tumor histology independent of intrinsic tumor cell biology.

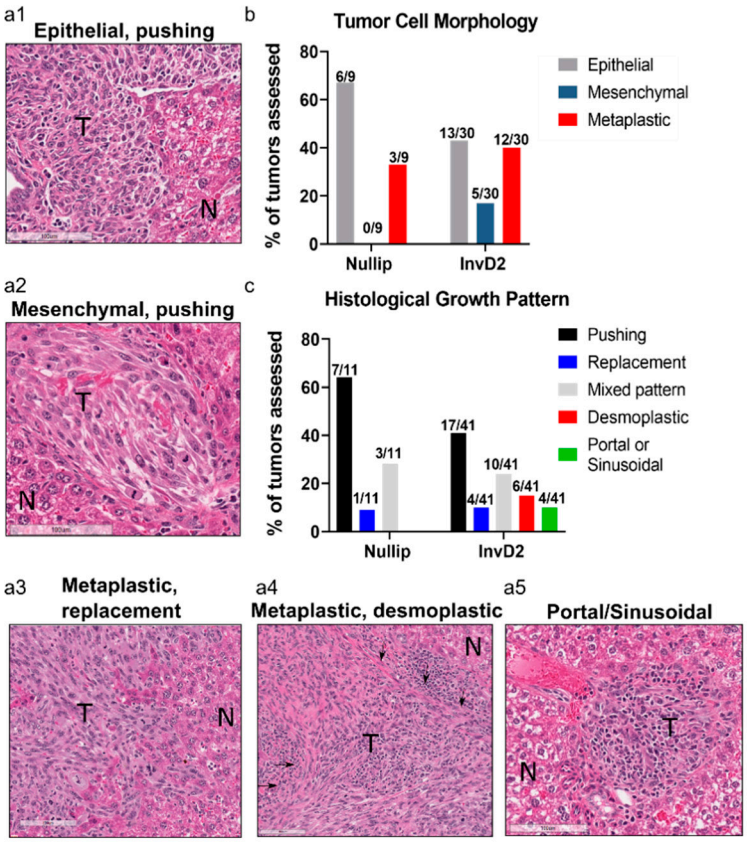

Figure 2. Histology of murine mammary liver metastases resembles human disease and shows increased histological heterogeneity in involution hosts. Representative hematoxylin and eosin stained images from D2.OR tumors classified as (**a1**) epithelial, pushing, (**a2**) mesenchymal, pushing, (**a3**) metaplastic, replacement, (**a4**) metaplastic, desmoplastic with desmoplastic areas noted by black arrows, and (**a5**) portal/sinusoidal pattern. Tumors are denoted by "T" and adjacent normal liver by "N"; (**b**) Quantitation of D2.OR tumor cell morphology and (**c**) histological growth pattern by host reproductive stage.

Because our data supports tumor cell establishment rather than growth as the metastatic advantage in the involuting liver, we predicted that there would be an increased abundance of tumor cells at early time points post-injection in involution hosts. Such data could be indicative of increased tumor cell extravasation and/or initial survival/proliferation advantage in the involuting liver environment. As a tool to visualized tumor cells before they grow into microscopically detectable lesions, we used GFP-tagged D2.OR tumor cells. Because GFP is a foreign protein, we utilized GFP-tolerant mice for these experiments, which were a gift from Lalage Wakefield (National Cancer Institute) [25]. Independent of reproductive state, by 90 min after tumor cell injection, we observed an even distribution of tumor cells throughout the liver, demonstrating uniform tumor cell dispersion (Figure 3a, arrows indicate tumor cells). We found no reproductive stage differences in tumor cell abundance at 90 min or one-day post-injection (Figure 3b), suggesting that the metastatic advantage in involution hosts is not due to differential tumor cell extravasation or initial survival. Unexpectedly, at three-days post-injection there was greater tumor cell abundance in the nulliparous host liver (Figure 3b), indicative that the liver microenvironments are indeed different between nulliparous and involution hosts. In sum, these data do not support the hypothesis that the metastatic advantage in the involution liver is due to increased tumor cell seeding and/or survival at early time points.

We observed two distinct tumor cell patterns at these early time points: single tumor cells (Figure 3c) and tumor cell clusters (Figure 3d). When we delineated these patterns by reproductive group, there was an increase in single cells found in the involution host, as early as one-day post-injection (Figure 3e). An increase in tumor cell clusters in the nulliparous group was also evident as early as one-day post-injection (Figure 3f); however, there was no evidence of a growth advantage in either reproductive group, as measured by tumor area per cluster (Figure 3g). Since tumor cell clusters are consistent with a more epithelial-like state and single tumor cells with a more mesenchymal-like state [26], these early time point data may shed light on our six-week endpoint findings, where mesenchymal-dominant tumors were only observed in the involution group (Figure 2b). In sum, tumor cell morphology may be established early after tumor cell injection.

Although overt metastases are increased in the involution host liver at five to six weeks post-injection (Figure 1, Figure S1), we found no evidence for increased tumor signal in the involution group within three-days of tumor cell injection (Figure 3b). Therefore, we extended the study timeline to 14 days and found increased tumor cell signal as measured by area per lesion, multiplicity, and tumor burden in the livers of involution hosts (Figure 3h–j). Given that immune recognition and adaptive immune activation is known to take 7–10 days to develop after antigen exposure in viral systems [27], this 14 day timeframe of the involution metastatic advantage is consistent with an altered immune environment that impacts adaptive immune recognition of tumor cells.

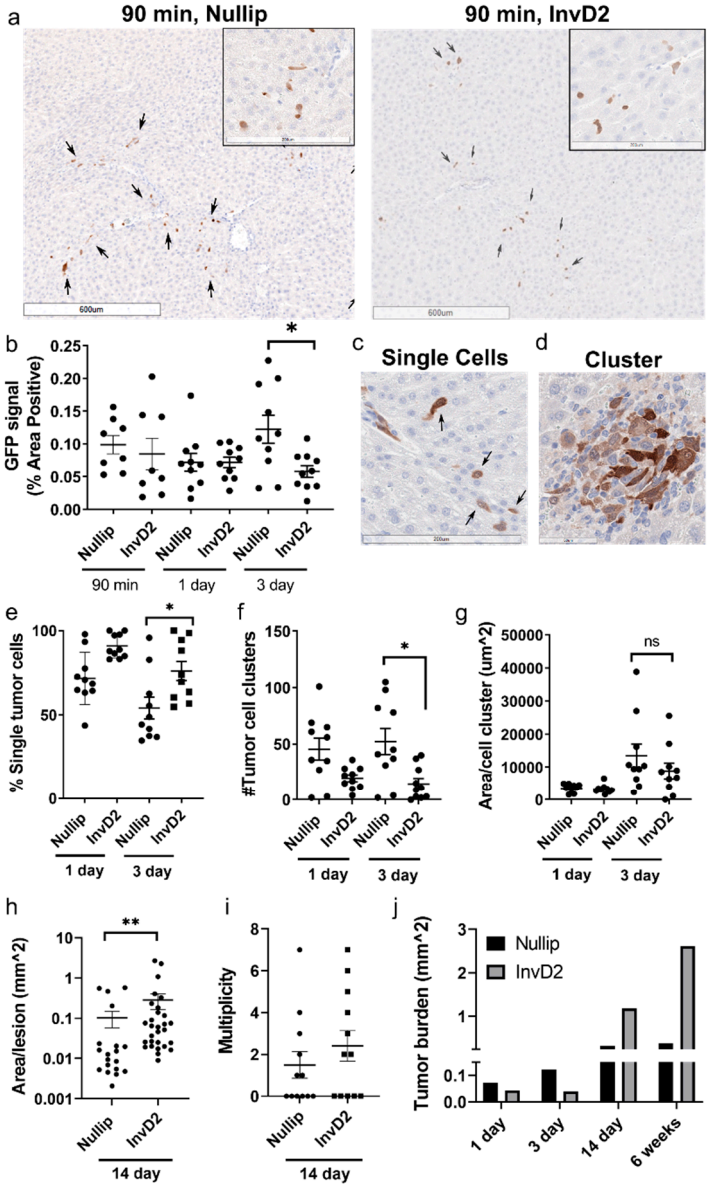

Figure 3. Involution metastatic advantage is observed by 2 weeks post-injection but not at earlier time points. (**a**) Representative low and high magnification IHC images of liver FFPE sections stained to identify GFP-tagged D2.OR cells, arrows indicate tumor cells; (**b**) IHC quantification of GFP+ tumor cells in liver FFPE sections from mice euthanized 90 min (n = 4 mice/group), 1 day (n = 5 mice/group), and 3 days (n = 5 mice/group) after intraportal injection of 500,000 D2.OR-GFP tumor cells per liver. Two sections >200 µm apart were assessed per mouse to quantify independent tumor cells; One-way ANOVA; Representative high magnification images showing GFP+ tumor cells as (**c**) single cells (1 day time point) or, (**d**) clusters, defined as >3 tumor cells, i.e., micro-metastases, (3 day time point); Quantification of GFP+ (**e**) single tumor cells as a percent of total tumor cell signal, (**f**) number of tumor cell clusters, and (**g**) size of tumor cell clusters at 1 and 3 days post-injection; One-way ANOVA; IHC quantification of GFP+ (**h**) tumor area and (**i**) multiplicity from mice euthanized 14 days after intraportal injection of 500,000 D2.OR-GFP tumor cells; Two-tailed Mann–Whitney test; (**j**) timeline of tumor burden in nullip (black) and invD2 (grey) mouse groups showing switch from early (3 day) advantage in nullip to later (≥14 days) advantage in involution. * $p < 0.05$, ** $p < 0.01$.

We observed two distinct tumor cell patterns at these early time points: single tumor cells (Figure 3C) and tumor cell clusters (Figure 3D). When we delineated these patterns by reproductive group, there was an increase in single cells found in the involution host, as early as one day post-injection (Figure 3E). An increase in tumor cell clusters in the

Given our prediction that immune cells are involved in the involution metastatic advantage, we sought to profile the intra-tumor immune milieu. We interrogated tumor-bearing livers from nulliparous and involuting stage mice 14 days after intraportal injection

of D2.OR-GFP tumor cells, the earliest time point where the involution advantage was observed. CD45 staining revealed high levels of tumor infiltrating immune cells, but no differences between groups (Nullip: 12%, InvD2: 14%). Since immune cell abundance did not differ, we next asked whether the activation state of intra-tumoral CD4 or CD8 T cells differed by reproductive group, which could account for differential anti-tumor immune function. We stained for nine common leukocyte lineage and functional state markers (CD45, CD3, CD4, FoxP3, Ki67, PD1, Tox1, CD11b, and F480) using multiplex immunohistochemical (mIHC) methods. Representative pseudo-colored images of select biomarkers, including CK18 marking hepatocytes and some tumor cells, are shown (Figure 4a). Using image cytometry, we quantified various T cell and myeloid subsets as percentage of total CD45+ immune cells (Figure 4b) and performed hierarchical clustering by case (Figure 4c). We found that the profile of tumor immune infiltrate separated cases by reproductive stage of the host, with only one case each clustering outside of its reproductive group (Figure 4c). Of note, we found no relationship between tumor size and immune cell infiltrates (Figure S2), suggestive that tumor size alone does not dictate immune cell infiltrate in this model. In sum, these data support the idea that reproductive stage of the host shapes the composition of the intra-tumoral immune milieu with implications for anti-tumor immunity.

The mIHC analyses further revealed that overall, all of the metastatic tumors are "hot" as defined by high CD3+ cell infiltration (Figure 4a). The majority of CD3+ cells did not show signs of activation, such as the expression of Ki67 or PD1. There were two out of seven involution cases with CD3+ cells that expressed Ki67, PD1, and Tox1, potentially indicating immune activation with exhausted features [28,29]. We next investigated the intra-tumoral ratio of CD4+ to CD8+ T cells, since higher CD4:CD8 ratios associate with increased functional CD8+ T cell responses and better disease outcomes [30–32]. For these studies we define CD4 T cells as CD45+CD3+CD4+, and identify putative CD8 T cells as CD45+CD3+CD4−, herein referred to as CD8. We found higher CD4:CD8 ratios in tumors from nulliparous mice compared to tumors in involution mice (37:1 vs. 8:1). Finally, while CD3+ and CD3+CD4+ T cells were enriched in tumors from nulliparous hosts, CD45+CD3− (putative myeloid lineage cells) and F480+ cells (mature macrophages) were greater in tumors from involution hosts. Taken together, these data raise the possibility that the immune milieu of involution group tumors is characterized by low CD4 and high myeloid populations, which could result in impaired anti-tumor cytotoxic immunity.

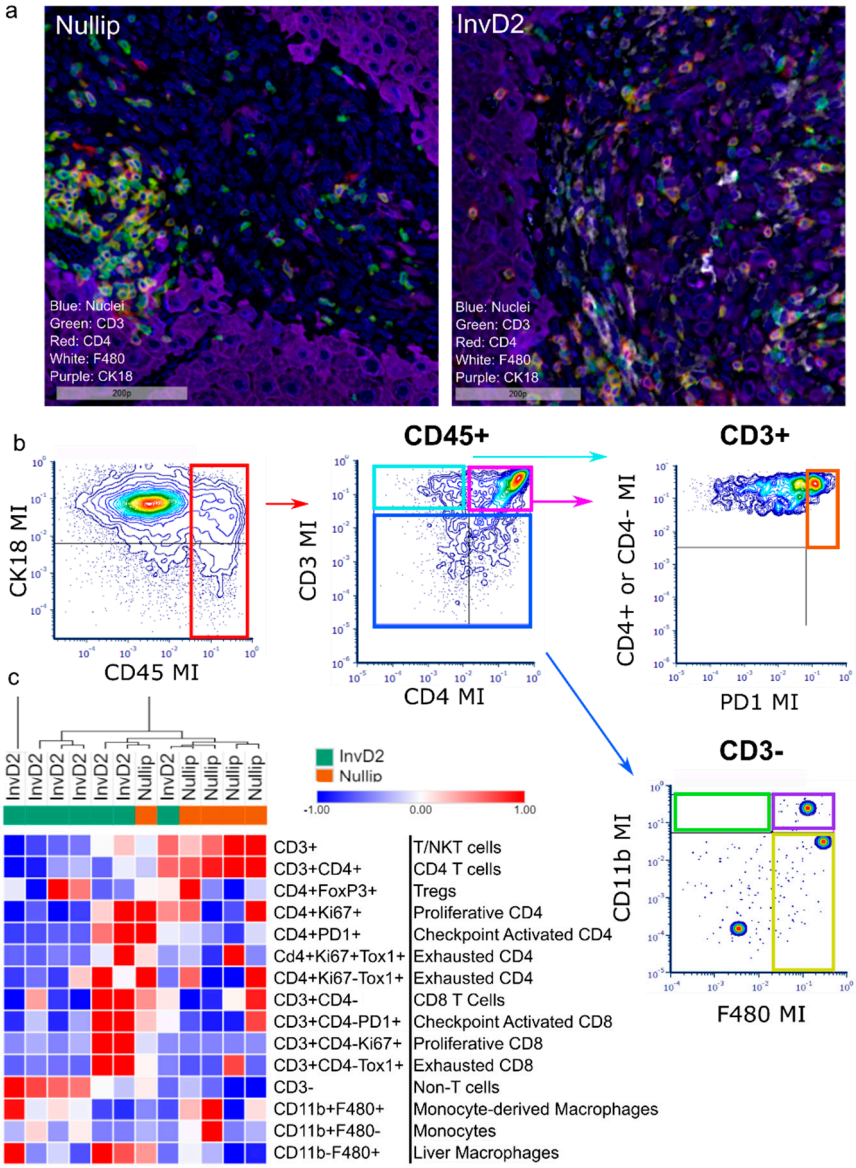

Figure 4. Immune milieu of liver metastases differs by host reproductive state. (**a**) Representative pseudo-colored multiplex IHC images of liver metastases in nullip and InvD2 mice euthanized 14 days after intraportal tumor cell injection showing select biomarkers: nuclei (blue), CD3 (green), CD4 (red), F480 (white), and CK18 (purple); (**b**) Representative image cytometry gating schema, showing the identification of CD45+, CD3+/−, CD4+/−, and PD1+ populations; (**c**) Hierarchical-clustered heat-map of intra-tumoral immune cell populations (%CD45+) identified by image cytometry of multiplex IHC staining for 9 biomarkers (CD45, CD3, CD4, FoxP3, Ki67, PD1, Tox1, CD11b, and F480). Tumor data are reported as average per mouse.

A defining attribute of tumors in the involution group is that they evolved under unique micro-environmental conditions. Liver involution involves programmed cell death of hepatocytes and wound-healing like processes [18], which in other contexts are known to elicit suppression of cytotoxic adaptive immune response [33,34]. This is because phagocytosis of dying cells induces tolerogenic antigen presenting cell functions, which limit autoimmune reactions to the dying cell [33,34]. Based on these prior studies, we hypothesized that the liver metastatic niche during involution may be characterized by immune tolerance, which inadvertently permits tumor cell evasion. To address this hypothesis, we phenotypically assessed CD4+ T cells by flow cytometry at nulliparous, involution day 2, and involution day 6 with the prediction that T cell polarization would be dependent on

reproductive state. We quantitated CD4+ T cells for expression of Th1, Th17, or regulatory (Treg) transcription factors, as well as PD1 (Figure 5a, Figure S3). Each reproductive stage showed a large population of RORgT+ T cells, which we classify as Th17-skewed; however, by involution day 6 (InvD6) this Th17 population had reduced prominence. At InvD6 we also found increased Tbet, PD1, and FoxP3+ CD4 T cells (Figure 5a), data consistent with inflammation (Tbet, Th1), T cell activation (PD1) and induction of a regulatory state (FoxP3+, Treg) in the normal, involuting liver.

One feature of immune tolerance is the inability of adaptive immune cells to proliferate in response to their cognate antigen, which can be robustly assessed in functional assays. To this end, we used an in vivo CD4+ T cell activation assay where we adoptively transferred ovalbumin antigen-specific CD4+ T cells (Do11.10, Figure S4) systemically and subsequently injected their cognate antigen (OVA) into the liver via intrahepatic injection (Figure 5b). Five days after ova or phosphate buffer saline (PBS) control injection, ova-specific T cells were assessed by flow cytometry in both the liver and spleen as a measure of T cell activation. Representative flow cytometry plots are shown (Figure 5c,d, Figure S5). Firstly, we found that the nulliparous host liver responds to ova antigen with a 2-fold increase in ova-specific T cells compared to PBS controls (Figure 5e). Conversely, in the involution group there was no increase in ova-specific T cells after exposure to ova antigen compared to PBS, providing functional evidence for immune tolerance. Similar results were observed in the spleen (Figure 5f). These data raise the possibility that deficient adaptive immunity contributes to increased liver metastasis in the involution host, while intact adaptive immunity is partially responsible for limiting liver metastasis in nulliparous hosts.

If an adaptive immune response to tumor cells in nulliparous hosts contributes to reduced liver metastasis, then we expect depletion of CD8+ T cells to increase metastasis and possibly recapitulate the metastatic advantage observed in the involution group. In our portal vein liver metastasis model, nulliparous mice were either CD8+ T cell-depleted via intraperitoneal injection of anti-CD8 antibody (BioXcell clone 2.43, Lebanon, NH, USA) or treated with isotype control. Antibody dosing began two days prior to tumor cell injection (0.2 mg initial dose) and continued every four days for the course of the experiment (0.1 mg maintenance dose). This antibody dosing scheme was designed to minimize antibody concentration and effectively deplete CD8+ T cells in the liver, in order to mitigate possible off-target antibody effects (Figure S6). Depletion of CD8+ T cells (CD45+CD3+CD8+CD4−) in the liver was confirmed at study endpoint by flow cytometry with no discernable effect on CD4+ T cells (CD45+CD3+CD4+CD8−) (Figure 6a,b). Incidence and multiplicity of liver metastasis six weeks after injection increased in anti-CD8 treated nulliparous animals compared to isotype control (Figure 6c,d). Of note, multiplicity in the anti-CD8 treated nulliparous group was commensurate with multiplicity in the isotype treated involution group. These data are consistent with differential CD8+ T cell activation during involution contributing to the increase in metastatic outgrowth and multiplicity observed in the involution group.

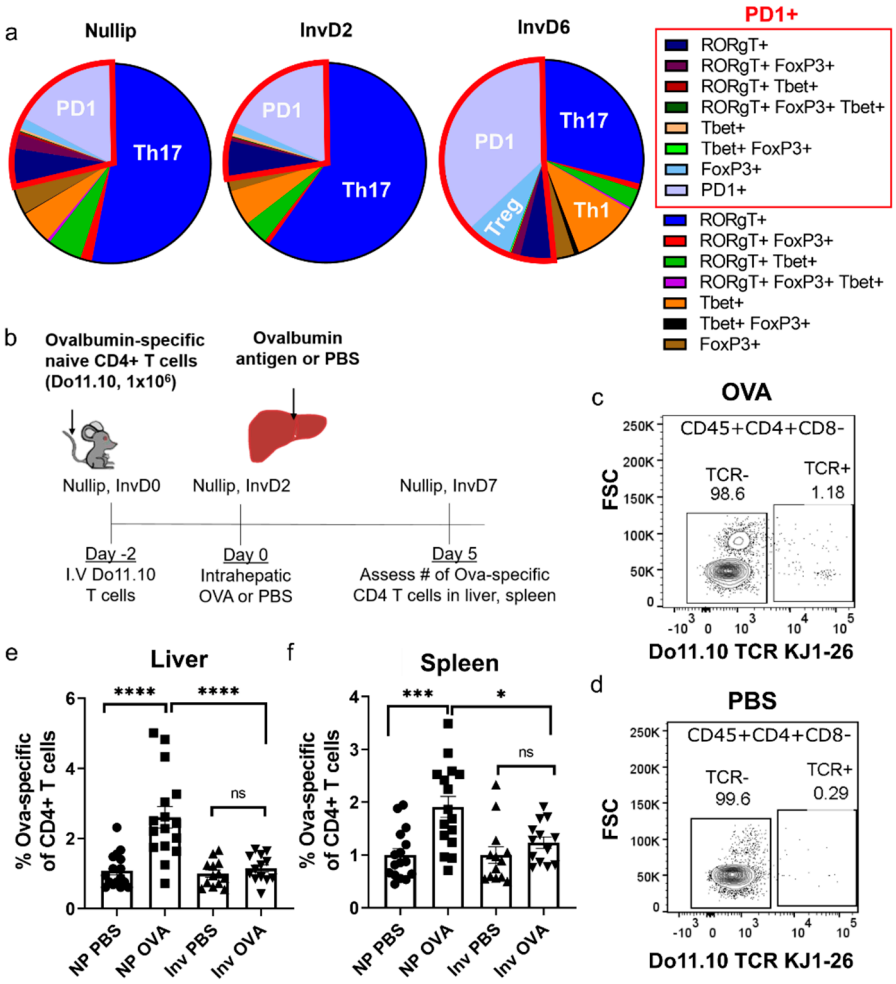

Figure 5. CD4+ T cell polarization is reproductive stage dependent with implications for antigen-specific activation. (**a**) Flow cytometry phenotyping of CD45+ CD4+ T cells from livers of mice at nullip, InvD2, and InvD6 reproductive stages (nullip $n = 8$, InvD2 $n = 5$, InvD6 $n = 6$). Only CD45+ CD4+ T cells that expressed at least one of the four phenotyping markers RORgT, Tbet, PD1, or FoxP3 are shown (see Figure S3 for total CD45+CD4+ T cell polarization); (**b**) Experimental schema for the in vivo T cell activation assay (Figure S4 shows transferred CD4+ Do11.10 cells); Representative flow cytometry plots showing expression of ova-specific Do11.10 T cell receptor (TCR) in CD45+ CD4+ CD8- cells from mice intra-hepatically injected with (**c**) ovalbumin (OVA) antigen or (**d**) PBS; Flow cytometry quantification of ova-specific CD4+ T cells (Do11.10 TCR+) as %CD4+ in (**e**) whole liver or (**f**) spleen across 2 independent experiments (nullip PBS $n = 16$, nullip OVA n=15, InvD2 PBS $n = 13$, InvD2 OVA $n = 13$). Data normalized to PBS average for reproductive group, One-way ANOVA. * $p < 0.05$, *** $p < 0.001$, **** $p < 0.0001$.

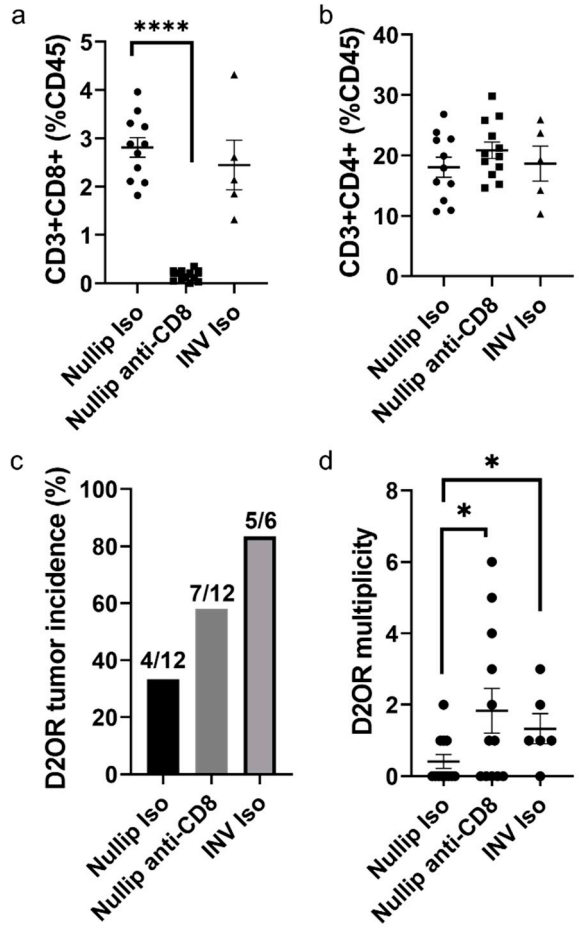

Figure 6. Depletion of CD8+ T cells in the nulliparous host recapitulates the involution metastatic advantage. Flow cytometry quantification of (**a**) CD8 and (**b**) CD4 T cells from livers of mice at endpoint of 6 week metastases study where mice were treated with CD8-depleting or isotype control antibody demonstrating effective CD3+CD8+ T cell depletion; (**c**) Incidence and (**d**) multiplicity of D2.OR liver metastases 6 weeks after intrasplenic injection of 50,000 D2.OR tumor cells with and without CD8 depletion in nulliparous hosts. Nullip Iso $n = 12$, Nullip anti-CD8 $n = 12$, INV Iso $n = 6$. One-way ANOVA: $^{*}p < 0.05$, $^{****}p < 0.0001$.

3. Discussion

Metastasis has historically been considered an intrinsic property of the cancer cell [35–38], which is in part enabled by a cancer cell's ability to reshape distant sites into favorable environments [6,7,10,14]. In line with this thinking, tumor-induced remodeling of the liver microenvironment has been well described [39,40]. Such tumor education of the liver pre-metastatic niche includes macrophage and fibroblast activation that results in pro-metastatic inflammatory signaling and ECM protein deposition [11–13]. However, recently it has been posited that pro-metastatic liver niche remodeling could occur independent of a primary tumor, including processes such as liver repair and regeneration following injury [18,41]. Here, we provide further evidence of a physiologic process, weaning-induced liver involution, which induces a liver pre-metastatic niche.

Previously, it was demonstrated that liver metastases were promoted in postpartum mice using the fast-growing, metastatic-competent D2A1 mouse mammary tumor cell line [18]. In the present study, we find that the postpartum liver also supports metastasis of D2.OR mammary tumor cells, a cell line with lower growth rate and demonstrated low metastatic potential [21,22]. An advantage of using a cell line with slow growth is that it may permit evolution of tumor cell-microenvironment interactions that are more reminiscent of what occurs in human disease.

Liver metastases can be categorized by growth pattern in relation to adjacent normal hepatocytes using a method developed for colorectal cancer liver metastases [24]. Three main growth patterns have been identified: desmoplastic, pushing, and replacement. Patients whose metastases had a dominant desmoplastic pattern were found to have longer overall and recurrence free survival compared to those with a dominant replacement growth pattern [24,42]. In our study, we classified mouse mammary cancer liver metastases according to these guidelines. We found potential relevance to human disease, as the heterogeneous histological growth patterns reported in human liver metastases were observed. Use of this histological growth classification for liver metastases is not common in breast cancer. However, a recent study of 58 breast cancer patients found that the replacement pattern was dominant, and as in colorectal cancer liver metastasis, the desmoplastic pattern associated with longer overall survival [43]. Although we found approximately 14% of tumors with desmoplastic growth pattern in murine involution hosts and none in nulliparous hosts, our study was not designed to evaluate survival so we cannot determine survival differences between tumor histologic patterns. While a key strength of our breast cancer liver metastasis model is the observation of a range of tumor histological patterns in the liver, how reproductive state influences these patterns and outcomes will require further investigation.

Tumor cell morphological properties such as cytoplasmic volume, roundness, and elongation have been implicated in metastatic potential [44,45]. These studies viewed tumor cell morphology as a cell-autonomous property, yet the microenvironment may also shape morphology [46,47]. Here, we observed distinct tumor cell morphological patterns based on host reproductive stage. Single, solitary tumor cells were more prevalent in the involution group. The high percent of single tumor cells in the involution host could be indicative of a more mesenchymal phenotype since they lack cell-cell adhesion with other tumor cells and show elongated morphology. In contrast, tumor cell clusters, indicative of tumor epithelial cell interactions, were increased in nulliparous host livers. Further, we have reason to believe the involution liver could preferentially support tumor cell epithelial-to-mesenchymal transition (EMT). The involution liver has significantly elevated TGFβ and ECM proteins tenascin-C and fibronectin, which are all known to mediate EMT [18,48–50]. Promotion of tumor cell EMT by the involution microenvironment is intriguing, given the connection between mesenchymal state and metastatic promotion [50], including evasion of the immune system [51–54]. Our work does not directly test the potential of tumor clusters versus single cells in the liver environment to form overt metastases. However, our data are consistent with an advantage to the solitary tumor cells since there are more metastatic events in the involution group at study endpoint. Additional studies are needed to explore the relationship between the presence of early single tumor cells and metastatic success in this model.

We show in both D2.OR and D2A1 models that liver metastatic advantage involves increased metastasis incidence and multiplicity in involution hosts, which appears to occur without a tumor cell proliferation advantage. Seeing no proliferation advantage, we predicted that the involution microenvironment increases a tumor cell's chance of successfully forming a metastasis, and used the metastatic cascade as framework to investigate this possibility [9,10]. The metastatic cascade describes how a tumor cell escapes the primary site and arrives at a secondary organ, then must lodge, extravasate, survive, form micrometastasis, and grow in order to become a metastatic tumor [9,10]. Prior work has shown that late stages (i.e., after arrival at the secondary organ) are rate-limiting for metastatic success [55,56].

We initially hypothesized that the involution advantage would be evident early, at the tumor cell extravasation, survival, and/or proliferation steps, due to the known, pro-metastatic ECM remodeling that occurs in the liver post wean [18]. The rodent involuting liver is enriched for collagen I, fibronectin, and tenascin-C [18,57], ECM proteins demonstrated to promote establishment of tumor cells in the niche [58–62]. However, we found no evidence for involution-specific ECM proteins contributing to these early, metastatic events.

Specifically, no differences in tumor cell abundance were observed between groups at days one and three post portal vein injection, time points when tumor cells become established in the niche. Rather, the involution metastatic advantage was observed at 14 days after tumor cell injection. This timeframe is consistent with the involuting liver promoting a later step in the metastatic cascade, at the transition from a micro- to an overt metastatic lesion.

Suppression of anti-tumor immunity is one potential mechanism by which the involuting liver promotes tumor growth from micro- to overt metastasis. Others have shown that the liver pre-metastatic niche is characterized by alteration to innate immune composition, including elevated neutrophils, bone marrow-derived myeloid cells, and M2-polarized macrophages [40,63]. Adaptive immune cells, including CD4+ Th17 polarized and T regulatory (Treg) cells, have also been shown to play a functional role in promoting liver metastasis [64,65]. These innate and adaptive immune cell populations support metastasis in part by limiting anti-tumor immunity via active suppression of the cytotoxic T cell response [66]. In previous work from our lab, we showed that the involution liver has increased abundance of neutrophils, immature monocytes, and macrophages compared to the nulliparous liver [18]. Here we build on that dataset to show that CD4+ Th17 polarized T cells are abundant in the murine liver regardless of reproductive state. Furthermore, CD4+ T cell polarization is modulated by reproductive state with the normal, involuting liver being characterized by Th1-skewed inflammation, upregulation of the checkpoint molecule PD1, and increased abundance of Tregs. This immune composition data demonstrate that the involution liver has most of the immune characteristics attributed to a tumor-educated pre-metastatic niche [63]. Further, utilizing a functional in vivo T cell activation assay, we identify immune tolerance as a new attribute of weaning-induced liver involution, similar to what was recently described in the mammary gland during weaning-induced involution [67].

We propose that the stimulus for tolerance mechanisms is the hepatocyte programmed cell death that occurs post-wean to return the pregnancy and lactation-enlarged liver to its pre-pregnant size [18]. Such programmed cell death is considered "immunologically silent" [33,34]. This immune-tolerization is achieved in part via signaling from the apoptotic cell to the antigen presenting cell (APC), which results in reduction of the co-stimulatory signals on the APC typically required for T cell activation [67,68]. An additional, unexplored possibility is that the unique ECM composition of the involuting liver contributes to regulation of the immune milieu. It is known that collagen, fibronectin, and tenascin-C can regulate immune cell trafficking and function [69], including recruitment of immature monocytes [13] and suppression of T cell activation [70]. These published reports provide further rationale for the matrisome of the involuting liver contributing to impaired anti-tumor immunity, although such a possibility requires future study. In sum, these studies of normal involuting liver provide evidence for both T cell inflammation and tolerance, with implications for tumors emerging in this environment.

Clinically, tumors that are classified as "hot" (i.e., those with robust T cell infiltration) are associated with better prognosis, most likely due to anti-tumor effects of CD3+ T cells [71,72]. In our murine model of breast cancer liver metastasis, we find that the majority of tumors were CD3+ "hot", indicating that T cells were able to enter tumors in both nulliparous and involution hosts. While robust intra-tumoral CD3+ infiltration is typically a positive biomarker for disease prognosis, in our mouse model the majority of tumors in involution hosts and ~1/3 of tumors in nulliparous hosts grew into large metastatic lesions. This paradox could indicate that the effector status of CD3+ cells is differentially compromised by reproductive state, a premise supported by the observation that nulliparous and involution tumors delineated by immune profiling. Specifically, tumors that evolved in involution host livers had lower CD4:CD8 ratios, increased myeloid infiltration, and increased exhaustion markers including PD1 and Tox1 [28,29]. Our finding that depletion of CD8+ T cells in the nulliparous host recapitulates the involution metastatic advantage provides further rationale for the hypothesis that ineffective anti-tumor immunity contributes to the involution metastatic advantage. Whether liver metastases in

young women's breast cancer show similar pro-tumor patterns of tumor immune infiltrates remains to be determined.

The results presented here may have significance for a recently appreciated type of aggressive, young women's breast cancer called postpartum breast cancer (PPBC) [73–75]. A diagnosis of breast cancer within five years of a recent pregnancy is an independent predictor of liver metastasis, which suggests that the postpartum liver may be uniquely susceptible to metastasis as we demonstrate in the rodent models [18]. In support of this hypothesis, we recently found that the size of the human liver is regulated by reproductive state and provided the first data suggesting that weaning-induced liver involution may occur in women [76]. Since we report in the rodent model a relationship between immune composition in the normal involution liver and resulting tumor immune infiltrate, such a paradigm may also exist in human breast cancer liver metastasis. If so, the rodent studies provide evidence that PPBC liver metastasis may involve immune modulation and be responsive to immune checkpoint therapies. While checkpoint blockade immunotherapy must be tested in preclinical models, our findings could help direct much-needed new treatments for breast cancer liver metastases in young women.

4. Materials and Methods

4.1. Animal Husbandry

Oregon Health & Science University (OHSU) Institutional Animal Care and Use Committees approved (TR01_IP00000967, approved on 13 April 2020) all animal procedures. Age-matched (10–12 weeks) female BALB/c mice (Charles River Laboratories, Wilmington, MA, USA) were housed and bred as described [77]. Briefly, for involution group animals pup number was normalized across dams to assure equal lactation and pups were weaned between 9-11 days after birth. At study endpoints, mice were euthanized across groups either by CO2 asphyxiation or while under anesthesia by exsanguination via portal vein perfusion with PBS. Whole livers and/or spleens were removed, washed 3× in 1× PBS, and processed for subsequent assays as described.

4.2. Cell Culture

D2.OR, D2.OR-GFP, and D2A1 mouse mammary tumor cells were kindly provided by Ann Chambers (University of Western Ontario, London, Ontario, Canada) and cultured as previously described [21]. For tumor cell injection preparation, cells were washed and suspended in cold 1× PBS. Cells were tested in January 2018, were confirmed murine pathogen and Mycoplasma free, and the origin of cells was validated (Idexx Bioresearch, Columbia, MO, USA). Cells used in these studies were within 3 passages of tested vials.

4.3. Liver Metastases Studies

Liver metastases were induced by intra-portal vein injection of D2OR, D2OR-GFP, and D2A1 mouse mammary tumor cells, as previously described [23]. Tumor cells were suspended in 10 µL 1×PBS with various number of cells: 50,000 D2.OR for 6 week endpoint and CD8 T cell depletion studies; 5,000 D2A1 for 5 week endpoint study; 500,000 D2.OR-GFP for 90 min, 1, 3, and 14 day endpoint studies. Tumor cells were injected into either involution group mice 2 days after weaning, involution day 2 (InvD2), or age-matched nulliparous mice. For D2A1 and D2.OR studies, BALB/c mice were used. For D2.OR-GFP studies, "Glowing Head" BALB/c mice (Gnrhr-luc/EGFP) were used as these mice are tolerant to the GFP protein, which were a gift from Lalage Wakefield (National Cancer Institute, USA) [25]. Whole liver was formalin-fixed and paraffin embedded (FFPE) for histological analyses. Liver metastases were assessed following euthanasia at 5 and 6 week time points by visual assessment of the liver and by hematoxylin and eosin staining of FFPE liver sections. For the D2.OR-GFP 90 min, 1, 3, and 14 day endpoint studies, immunohistochemistry (IHC) for GFP+ tumor cells was used for assessment. To assess for solitary tumor cells and micrometastases, two distinct depths of liver tissue $\geq$200 µm apart were sectioned per mouse for subsequent IHC analyses.

4.4. CD8 Depletion Experiment

Antibody concentration (BioXcell; clone 2.43) for CD8+ T cell depletion in the liver and spleen was determined by testing two initial dose concentrations (0.2 mg, 0.4 mg) and two maintenance dose concentrations (0.1 mg, 0.2 mg). Antibody was delivered in 200 µL sterile PBS via intraperitoneal injection, with initial dose given at day 0 and maintenance doses given at day 4 and day 8. 72 h post last maintenance dose mice were euthanized and liver and spleen collected for flow cytometry assessment. For subsequent tumor experiments the lowest concentrations combination that was effective at depleting CD8+ T cells was used: 0.2 mg initial dose and 0.1 mg maintenance dose (Figure S4). Mice were randomized, in a rolling study design, to receive either isotype control (BioXcell; BE0090) or CD8 depleting antibody (BioXcell; clone 2.43). In tumor studies, initial antibody dose was given 2 days prior to tumor cell injection and maintenance doses were given every 4 days for the 6 week course of the experiment. Data are presented as percent of CD45+ cells.

4.5. Histological Analyses

Liver FFPE tissue sections representing all liver lobes were stained with hematoxylin and eosin to evaluate for presence of tumors, tumor size, tumor multiplicity, and tumor morphology. Morphology was characterized as epithelial-dominant, mesenchymal-dominant, or metaplastic, defined as tumors with irregular nuclei and a mix of epithelial and mesenchymal components. Histological growth pattern was characterized as established for scoring liver metastases in colorectal cancer into pushing, replacement, desmoplastic, mixed pattern, and portal/sinusoidal patterns [24]. Assessments were completed by two evaluators blinded to study design.

4.6. Immunohistochemistry

Single-stain IHC detection was performed as described [78]. Briefly, tissues were deparaffinized, rehydrated, and heat-mediated antigen retrieval was performed with EDTA for 5 min at 125 °C. The following primary antibodies were applied for 1 h at room temperature: Ki67 (1:400, Neo-markers #RM-9106-S), phospho-γH2AX (1:400, Cell Signaling #9718), Cleaved caspase 3 (CC3, 1:150, Cell Signaling #9664). Green fluorescent protein was applied overnight at 4 °C (GFP, 1:400 Abcam #ab13970). Secondary antibodies were applied for 30 min at room temperature: anti-rabbit (RTU, Agilent #K400) for Ki67, phospho-γH2AX, and CC3. For GFP, anti-chicken secondary was applied for 1 h at room temperature (1:1000, LSBio, LS-C61278). DAB chromogen (Agilent, K346889-2) with hematoxylin counter stain (Agilent, S330130-2) was used to visualize positive stain. Stained sections were scanned using the Aperio AT2 slide scanner (Leica Biosystems, Wetzlar, Germany). Signal quantification was performed by Aperio ImageScope v12.1.0.5029 as described previously [79]. For quantitation, all mice and tumors found in the stained tissue section were included for every analysis, unless staining was unsuccessful as defined as loss of tissue from slide and/or failure for positive controls to stain. All analyses were done by investigators blinded to study group. Data are presented as percent area positive unless otherwise noted in the figure legend.

Multiplex IHC staining was performed as previously described with modification [80]. Tissues were deparaffinized, rehydrated, and heat-mediated antigen retrieval was performed with EDTA for 5 min at 125 °C. Hematoxylin staining was performed on all tissues prior to antibody cycles, and tissues were scanned using the Aperio AT2 slide scanner (Leica Biosystems). Table 1 lists the antibodies and conditions used. Secondary antibodies were applied for 30 min: anti-rabbit (Histofine 414341F) and anti-rat (Histofine, 414311F). After each antibody cycle, tissues were scanned using the Aperio AT2 slide scanner (Leica Biosystems). Following scanning, 3-Amino-9-Ethylcarbazole (AEC) chromogen was removed with 1 × 70% and 1 × 100% alcohol wash for 2 min each. Primary and secondary antibodies were removed using 20% SDS-glycine pH 2 at 70 °C for 30–60 min. Secondary only and isotype controls were utilized to confirm antibody stripping after each cycle. This cycle was repeated for each primary antibody listed in Table 1. Each tissue slide included a

positive control tissue microarray (TMA) to confirm primary antibody staining for each cycle. The TMA was comprised of mouse spleen, lymph node, and liver tissue from mice subjected to inflammatory stimuli.

Table 1. Multiplex IHC Antibodies and Conditions.

Primary Antibody	Manufacturer	Catalog #	Lot#	Concentration	Incubation	Secondary Antibody
CD4	Cell Signaling	ab25229	Lot:4	1:50	O/N 4 °C	anti-Rb
CD45	BDPharminigen	550539	Lot: 4141820 & 9301732	1:50	60 min	anti-Rt
Ki67	Cell Signaling	12202	Lot: 6 (11/20)	1:800	60 min	anti-Rb
FoxP3	eBioscience	14-5773-82	Lot:E023634 + 2172602	1:100	60 min	anti-Rt
CD3	Abcam	ab16669	Lot: GR291605-1	1:100	60 min	Anti-Rb
Tox1	Abcam	ab237009	Lot: GR3241900-3	1:300	60 min	anti-Rt
PD1	Cell Signaling	84651	Lot: 4 (11/20)	1:200	60 min	anti-Rb
CD11b	Abcam	ab133357	EPR1344	1:30k	60 min	anti-Rb
F480	Cell Signaling	70076S	Lot:	1:500	60 min	anti-Rb
CK18	Abcam	ab181597	Lot: GR321105-11	1:1000	60 min	anti-Rb

4.7. Multiplex IHC, Image Processing and Data Analysis

After staining, scanned images from each cycle were analyzed using an image processing pipeline previously described with minor modification [80]. Image alignment and extraction were performed using the SURF algorithm in the Computer Vision Toolbox of Matlab version R2018b (The MathWorks, Inc, Natick, MA, USA). Single cell segmentation and color deconvolution were performed in FIJI, and mean intensity quantification was performed in Cell Profiler version 3.5.1. Image cytometry was performed using FCS Express 6 Image Cytometry RUO (De Novo Software, Glendale, CA, USA). Data are presented as a percentage of CD45+ cells per tumor, averaged by mouse.

4.8. Flow Cytometry

For flow cytometric quantification of liver CD4+ T cell polarization, left and caudate liver lobes were dissected following CO2 euthanasia and rinsed in 1× PBS to wash exterior blood. Liver lobes were minced and digested in 1 mg/mL collagenase I, 0.5 mg/mL hyaluronidase, and 0.5 mg/mL DNase at 37 °C for 30 min while rotating, and filtered through a 100 µm filter. Red blood cells were lysed using 1× RBC lysis buffer (eBioscience). Cell pellets were washed with 1× PBS, resuspended, and cells counted in trypan blue using a hemocytometer. 1×10^6 cells per sample in 100 µL PBS or FACS buffer were blocked with CD16/32 (eBioscience, 1:100) for 30 min, stained for cell surface markers (Live/Dead, Aqua; CD45, 30-F11, PerCP; CD11b M1/70 BV711; CD4 RM4-5, BV786; PD-1 29F.1A12 PE-Cy7) for 30 min at room temperature, stained for intracellular proteins (Tbet 4B10, BV421; RORγT AFKJS-9, PE; FoxP3 FJK-16s, APC) overnight at 4C, and fixed with 4% paraformaldehyde (BD Biosciences, San Jose, CA, USA) for 20 min. Samples were ran on the LSRFortessa (BD Biosciences; Oregon Health and Science University) and analyzed as described below. Data in Figure 5 are presented as % of CD4+ cells that expressed at least one of the following: Tbet, RORγT, FoxP3, or PD1. Data in supplemental Figure S3 are presented as percent of total CD4+ cells.

For adoptive transfer experiment, whole liver and spleen were used for flow cytometric quantification of Do11.10 CD4+ T cells. Here a different digestion protocol with the addition of a Percoll gradient was used in order to enrich for immune cells. Whole livers were cut into small pieces and digested with 0.5 mg/mL collagenase 1 and 0.5 mg/mL DNase in RPMI1640 at 37 °C for 30 min, rotating. Tissue digests were filtered through a 100 µm filter and washed in RPMI1640. Samples were fractionated in a 33% Percoll solution with centrifugation at 800× *g* for 30 min at room temperature with no brake. Supernatant was collected and red blood cells were lysed using 1× RBC lysis buffer (eBioscience).

Samples were washed and resuspended in RPMI1640 and counted in trypan blue using a hemocytometer. The entire liver sample was advanced to flow cytometry staining. For spleen digestion, spleens were processed through a 70 µm filter. Red blood cells were lysed using 1× RBC lysis (eBiosciences). Samples were washed and resuspended in PBS, counted in trypan blue, and 1×10^6 cells per sample in 100 µL were stained for flow cytometry. The following antibodies were used: Live Dead (Aqua), CD4 (RM4-5, BV786), CD45 (30-F11, PerCP), Do11.10 TCR (KJ1-26, PE-Cy7), CD8 (53-6.7, APCe780). Samples were ran on the LSRFortessa (BD Biosciences; Oregon Health & Science University) and analyzed as described below. Data are presented as % of CD4+ cells.

For the CD8 depletion experiment, the median lobe was digested as in the adoptive transfer experiment and used to confirm CD8 depletion. However, if there was a tumor visually apparent in the median lobe at time of euthanasia, the caudate lobe was used to confirm CD8 depletion. The following antibodies were used: CD49b (DX5, BV421), CD3 (17A2, BV785), CD4 (RM4-5, FITC), CD8b (H35-17.2, PE-Cy7), CD45 (30-F11, APC), and Live/Dead (NearIR). Due to restrictions imposed by Covid-19, samples for the CD8 depletion study were ran on the Fortessa X50 (BD Biosciences; Fred Hutch, Seattle, WA, USA). One sample from the INV iso group had insufficient cellularity and was excluded from analysis. Data are presented as % of CD45+ cells.

All samples were analyzed using FlowJo v10 software (Becton, Dickinson & Company Franklin Lakes, NJ, USA). Unstained, single color, and fluorescent-minus-one staining controls were utilized for every experiment.

4.9. Adoptive Transfer In Vivo T Cell Activation Assay

T cell activation was assessed with an in vivo activation assay as described with minor modification [63]. Briefly, CD4+ splenocytes were isolated from Do11.10 transgenic female mice (Jackson Laboratories Stock #003303) and enriched to >95% CD4+ T cells (Figure S4) using a CD4+ negative selection kit (MACS miltenyi) under non-stimulating conditions (putative naïve T cells). Subsequently, 1×10^6 isolated T cells in 100 µL 1× PBS were adoptively transferred via tail vein with insulin syringe into syngeneic BALB/c involution Day 0 or nulliparous age-matched hosts. Two days later either ovalbumin protein antigen (10 µg in 10 µL, Worthington) or 10 µL 1× PBS was injected into the left lobe of the liver via intrahepatic injection. Five days post antigen or PBS injection, whole liver and spleens were harvested, digested and stained for flow cytometry to detect Do11.10 T cells, as described above. A known quantity of absolute counting beads were added to samples (C36950 Invitrogen) and flow cytometry performed. Do11.10 TCR+ CD4+ T cell counts in liver and spleens were calculated by normalizing to the known abundance of counting beads. Data are presented as % of CD4+ cells.

4.10. Statistical Analysis and Hierarchical Clustering

Statistical analyses were performed using GraphPad Prism v.8 or v.9 software (GraphPad Software, San Diego, CA, USA). All data are expressed as mean ± standard error of the mean (SEM) unless otherwise noted. Statistical significance was determined using the following statistical tests with specific test fully described in the figure legends: Two-sided Fisher's exact test, Two-tailed *T* test, One-way ANOVA with multiple comparisons, and Two-tailed Mann-Whitney test. Hierarchical clustering of multiplex IHC data was performed with the Morpheus web-based tool (https://software.broadinstitute.org/morpheus, accessed date: 27 January 2021), as described previously [81].

5. Conclusions

Here we provide the first evidence for reproductive state dependent CD4+ T cell activation in the normal murine liver, including induction of tolerance during weaning-induced liver involution. Further, we show that the immune milieu of mammary tumors evolving within the involuting liver microenvironment are durably altered in a manner consistent with tumor promotion. Our data supports the hypothesis that ineffective anti-

tumor immunity within the involuting liver contributes to increased breast cancer liver metastasis. Taken together, our data provide a compelling argument for host reproductive factors being determinative for liver metastasis in the postpartum period with specific implications for young women's breast cancer. Further, weaning-induced liver involution may serve as a robust model to investigate initiation and treatment of liver metastasis with potential utility for liver metastases overall.

Supplementary Materials: The following are available online at https://www.mdpi.com/article/10.3390/cancers13071698/s1, Figure S1: Increased D2A1 metastasis in involution hosts does not associate with enhanced tumor growth, Figure S2: Tumor immune infiltrate does not correlate with tumor size, Figure S3: CD4+ T cell polarization is reproductive stage dependent, Figure S4: Representative flow cytometry plots demonstrate enrichment of CD4+ cells from whole spleen for adoptive transfer in vivo T cell activation experiment, Figure S5: Representative flow cytometry gating for adoptive transfer in vivo T cell activation experiment, Figure S6: Evidence that lowest initial and maintenance dose concentrations of CD8-depleting antibody effectively depletes CD8+ T cells in the liver and spleen.

Author Contributions: Conceptualization, A.Q.B. and P.S.; methodology, A.Q.B., N.D.P., and P.S.; validation, A.Q.B. and P.S.; formal analysis, A.Q.B.; investigation, A.Q.B., A.K., and N.D.P.; writing—original draft preparation, A.Q.B.; writing—review and editing, A.Q.B. and P.S.; visualization, A.Q.B.; supervision, P.S.; project administration, P.S.; funding acquisition, P.S. All authors have read and agreed to the published version of the manuscript.

Funding: This research was funded by the following grants to PS: Department of Defense grant #BC170206, Department of Defense grant #BC191620, Eccles Foundation, and funds from the Knight Cancer Institute (KCI). This work was also supported by the KCI Cancer Center Support Grant P30CA69533. AQB was partially supported by the following: Ruth L Kirschstein T32 "PERT" Training Grant, Achievement Rewards for College Scientists (ARCS) Foundation, and the OHSU Cancer Biology Graduate Program Student Stipend Award.

Institutional Review Board Statement: The study was conducted according to the guidelines of the Declaration of Helsinki, and approved by the Institutional Animal Care and Use Committees at Oregon Health & Science University (TR01_IP00000967, approved on 13 April 2020).

Informed Consent Statement: Not applicable.

Data Availability Statement: The data presented in this study are available in this article and in the supplemental material.

Acknowledgments: The authors want to thank Andrea Calhoun for superior histologic support in the multiplex IHC studies, Nina Fletcher for IHC staining of D2A1 metastases, and Erica Goddard for going above and beyond reasonable expectation to run flow cytometry samples for the CD8 depletion study during the Covid-19 lab shutdowns. The authors are grateful to Weston Anderson for outstanding assistance with manuscript writing, editing, and preparation.

Conflicts of Interest: The authors declare no conflict of interest.

References

1. Anders, C.K.; Johnson, R.; Litton, J.; Phillips, M.; Bleyer, A. Breast cancer before age 40 years. *Semin. Oncol.* **2009**, *36*, 237–249. [CrossRef] [PubMed]
2. Gnerlich, J.L.; Deshpande, A.D.; Jeffe, D.B.; Sweet, A.; White, N.; Margenthaler, J.A. Elevated breast cancer mortality in women younger than age 40 years compared with older women is attributed to poorer survival in early-stage disease. *J. Am. Coll. Surg.* **2009**, *208*, 341–347. [CrossRef] [PubMed]
3. Anders, C.K.; Hsu, D.S.; Broadwater, G.; Acharya, C.R.; Foekens, J.A.; Zhang, Y.; Wang, Y.; Marcom, P.K.; Marks, J.R.; Febbo, P.G.; et al. Young age at diagnosis correlates with worse prognosis and defines a subset of breast cancers with shared patterns of gene expression. *J. Clin. Oncol.* **2008**, *26*, 3324–3330. [CrossRef]
4. Partridge, A.H.; Hughes, M.E.; Warner, E.T.; Ottesen, R.A.; Wong, Y.N.; Edge, S.B.; Theriault, R.L.; Blayney, D.W.; Niland, J.C.; Winer, E.P.; et al. Subtype-Dependent Relationship Between Young Age at Diagnosis and Breast Cancer Survival. *J. Clin. Oncol.* **2016**, *34*, 3308–3314. [CrossRef] [PubMed]
5. Ursini-Siegel, J.; Siegel, P.M. The influence of the pre-metastatic niche on breast cancer metastasis. *Cancer Lett.* **2016**, *380*, 281–288. [CrossRef]

6. Kaplan, R.N.; Riba, R.D.; Zacharoulis, S.; Bramley, A.H.; Vincent, L.; Costa, C.; MacDonald, D.D.; Jin, D.K.; Shido, K.; Kerns, S.A.; et al. VEGFR1-positive haematopoietic bone marrow progenitors initiate the pre-metastatic niche. *Nature* **2005**, *438*, 820–827. [CrossRef]
7. Peinado, H.; Zhang, H.; Matei, I.R.; Costa-Silva, B.; Hoshino, A.; Rodrigues, G.; Psaila, B.; Kaplan, R.N.; Bromberg, J.F.; Kang, Y.; et al. Pre-metastatic niches: Organ-specific homes for metastases. *Nat. Rev. Cancer* **2017**, *17*, 302–317. [CrossRef]
8. Psaila, B.; Lyden, D. The metastatic niche: Adapting the foreign soil. *Nat. Rev. Cancer* **2009**, *9*, 285–293. [CrossRef] [PubMed]
9. Fidler, I.J. The pathogenesis of cancer metastasis: The 'seed and soil' hypothesis revisited. *Nat. Rev. Cancer* **2003**, *3*, 453–458. [CrossRef]
10. Valastyan, S.; Weinberg, R.A. Tumor metastasis: Molecular insights and evolving paradigms. *Cell* **2011**, *147*, 275–292. [CrossRef]
11. Costa-Silva, B.; Aiello, N.M.; Ocean, A.J.; Singh, S.; Zhang, H.; Thakur, B.K.; Becker, A.; Hoshino, A.; Mark, M.T.; Molina, H.; et al. Pancreatic cancer exosomes initiate pre-metastatic niche formation in the liver. *Nat. Cell Biol.* **2015**, *17*, 816–826. [CrossRef] [PubMed]
12. Nielsen, S.R.; Quaranta, V.; Linford, A.; Emeagi, P.; Rainer, C.; Santos, A.; Ireland, L.; Sakai, T.; Sakai, K.; Kim, Y.S.; et al. Macrophage-secreted granulin supports pancreatic cancer metastasis by inducing liver fibrosis. *Nat. Cell Biol.* **2016**, *18*, 549–560. [CrossRef] [PubMed]
13. Lee, J.W.; Stone, M.L.; Porrett, P.M.; Thomas, S.K.; Komar, C.A.; Li, J.H.; Delman, D.; Graham, K.; Gladney, W.L.; Hua, X.; et al. Hepatocytes direct the formation of a pro-metastatic niche in the liver. *Nature* **2019**, *567*, 249–252. [CrossRef]
14. Kok, S.Y.; Oshima, H.; Takahashi, K.; Nakayama, M.; Murakami, K.; Ueda, H.R.; Miyazono, K.; Oshima, M. Malignant subclone drives metastasis of genetically and phenotypically heterogenous cell clusters through fibrotic niche generation. *Nat. Commun.* **2021**, *12*, 863. [CrossRef]
15. Dai, G.; Bustamante, J.J.; Zou, Y.; Myronovych, A.; Bao, Q.; Kumar, S.; Soares, M.J. Maternal hepatic growth response to pregnancy in the mouse. *Exp. Biol. Med. (Maywood)* **2011**, *236*, 1322–1332. [CrossRef] [PubMed]
16. Hollister, A.; Okubara, P.; Watson, J.G.; Chaykin, S. Reproduction in mice: Liver enlargement in mice during pregnancy and lactation. *Life Sci.* **1987**, *40*, 11–18. [CrossRef]
17. Hyatt, H.W.; Zhang, Y.; Hood, W.R.; Kavazis, A.N. Changes in Metabolism, Mitochondrial Function, and Oxidative Stress Between Female Rats Under Nonreproductive and 3 Reproductive Conditions. *Reprod. Sci.* **2019**, *26*, 114–127. [CrossRef]
18. Goddard, E.T.; Hill, R.C.; Nemkov, T.; D'Alessandro, A.; Hansen, K.C.; Maller, O.; Mongoue-Tchokote, S.; Mori, M.; Partridge, A.H.; Borges, V.F.; et al. The Rodent Liver Undergoes Weaning-Induced Involution and Supports Breast Cancer Metastasis. *Cancer Discov.* **2017**, *7*, 177–187. [CrossRef]
19. Cummings, M.C.; Simpson, P.T.; Reid, L.E.; Jayanthan, J.; Skerman, J.; Song, S.; McCart Reed, A.E.; Kutasovic, J.R.; Morey, A.L.; Marquart, L.; et al. Metastatic progression of breast cancer: Insights from 50 years of autopsies. *J. Pathol.* **2014**, *232*, 23–31. [CrossRef]
20. Goddard, E.T.; Bassale, S.; Schedin, T.; Jindal, S.; Johnston, J.; Cabral, E.; Latour, E.; Lyons, T.R.; Mori, M.; Schedin, P.J.; et al. Association Between Postpartum Breast Cancer Diagnosis and Metastasis and the Clinical Features Underlying Risk. *JAMA Netw. Open* **2019**, *2*, e186997. [CrossRef] [PubMed]
21. Morris, V.L.; Tuck, A.B.; Wilson, S.M.; Percy, D.; Chambers, A.F. Tumor progression and metastasis in murine D2 hyperplastic alveolar nodule mammary tumor cell lines. *Clin. Exp. Metastasis* **1993**, *11*, 103–112. [CrossRef]
22. Morris, V.L.; Koop, S.; MacDonald, I.C.; Schmidt, E.E.; Grattan, M.; Percy, D.; Chambers, A.F.; Groom, A.C. Mammary carcinoma cell lines of high and low metastatic potential differ not in extravasation but in subsequent migration and growth. *Clin. Exp. Metastasis* **1994**, *12*, 357–367. [CrossRef]
23. Goddard, E.T.; Fischer, J.; Schedin, P. A Portal Vein Injection Model to Study Liver Metastasis of Breast Cancer. *J. Vis. Exp.* **2016**. [CrossRef]
24. Van Dam, P.J.; Van der Stok, E.P.; Teuwen, L.A.; Van den Eynden, G.G.; Illemann, M.; Frentzas, S.; Majeed, A.W.; Eefsen, R.L.; Coebergh van den Braak, R.R.J.; Lazaris, A.; et al. International consensus guidelines for scoring the histopathological growth patterns of liver metastasis. *Br. J. Cancer* **2017**, *117*, 1427–1441. [CrossRef]
25. Day, C.P.; Carter, J.; Weaver Ohler, Z.; Bonomi, C.; El Meskini, R.; Martin, P.; Graff-Cherry, C.; Feigenbaum, L.; Tuting, T.; Van Dyke, T.; et al. "Glowing head" mice: A genetic tool enabling reliable preclinical image-based evaluation of cancers in immunocompetent allografts. *PLoS ONE* **2014**, *9*, e0109956. [CrossRef]
26. Kalluri, R.; Weinberg, R.A. The basics of epithelial-mesenchymal transition. *J. Clin. Investig.* **2009**, *119*, 1420–1428. [CrossRef] [PubMed]
27. Kaech, S.M.; Wherry, E.J.; Ahmed, R. Effector and memory T-cell differentiation: Implications for vaccine development. *Nat. Rev. Immunol.* **2002**, *2*, 251–262. [CrossRef] [PubMed]
28. Blank, C.; Mackensen, A. Contribution of the PD-L1/PD-1 pathway to T-cell exhaustion: An update on implications for chronic infections and tumor evasion. *Cancer Immunol. Immunother.* **2007**, *56*, 739–745. [CrossRef] [PubMed]
29. Khan, O.; Giles, J.R.; McDonald, S.; Manne, S.; Ngiow, S.F.; Patel, K.P.; Werner, M.T.; Huang, A.C.; Alexander, K.A.; Wu, J.E.; et al. TOX transcriptionally and epigenetically programs CD8(+) T cell exhaustion. *Nature* **2019**, *571*, 211–218. [CrossRef] [PubMed]
30. Borst, J.; Ahrends, T.; Babala, N.; Melief, C.J.M.; Kastenmuller, W. CD4(+) T cell help in cancer immunology and immunotherapy. *Nat. Rev. Immunol.* **2018**, *18*, 635–647. [CrossRef] [PubMed]

31. Sheu, B.C.; Hsu, S.M.; Ho, H.N.; Lin, R.H.; Torng, P.L.; Huang, S.C. Reversed CD4/CD8 ratios of tumor-infiltrating lymphocytes are correlated with the progression of human cervical carcinoma. *Cancer* **1999**, *86*, 1537–1543. [CrossRef]
32. Shah, W.; Yan, X.; Jing, L.; Zhou, Y.; Chen, H.; Wang, Y. A reversed CD4/CD8 ratio of tumor-infiltrating lymphocytes and a high percentage of CD4(+)FOXP3(+) regulatory T cells are significantly associated with clinical outcome in squamous cell carcinoma of the cervix. *Cell. Mol. Immunol.* **2011**, *8*, 59–66. [CrossRef] [PubMed]
33. Steinman, R.M.; Turley, S.; Mellman, I.; Inaba, K. The induction of tolerance by dendritic cells that have captured apoptotic cells. *J. Exp. Med.* **2000**, *191*, 411–416. [CrossRef] [PubMed]
34. Erwig, L.P.; Henson, P.M. Immunological consequences of apoptotic cell phagocytosis. *Am. J. Pathol.* **2007**, *171*, 2–8. [CrossRef]
35. Jacob, L.S.; Vanharanta, S.; Obenauf, A.C.; Pirun, M.; Viale, A.; Socci, N.D.; Massague, J. Metastatic Competence Can Emerge with Selection of Preexisting Oncogenic Alleles without a Need of New Mutations. *Cancer Res.* **2015**, *75*, 3713–3719. [CrossRef] [PubMed]
36. Nguyen, D.X.; Massague, J. Genetic determinants of cancer metastasis. *Nat. Rev. Genet.* **2007**, *8*, 341–352. [CrossRef]
37. Pereira, B.; Chin, S.F.; Rueda, O.M.; Vollan, H.K.; Provenzano, E.; Bardwell, H.A.; Pugh, M.; Jones, L.; Russell, R.; Sammut, S.J.; et al. The somatic mutation profiles of 2,433 breast cancers refines their genomic and transcriptomic landscapes. *Nat. Commun.* **2016**, *7*, 11479. [CrossRef]
38. Ursini-Siegel, J.; Schade, B.; Cardiff, R.D.; Muller, W.J. Insights from transgenic mouse models of ERBB2-induced breast cancer. *Nat. Rev. Cancer* **2007**, *7*, 389–397. [CrossRef]
39. Kruger, A. Premetastatic niche formation in the liver: Emerging mechanisms and mouse models. *J. Mol. Med.* **2015**, *93*, 1193–1201. [CrossRef]
40. Van den Eynden, G.G.; Majeed, A.W.; Illemann, M.; Vermeulen, P.B.; Bird, N.C.; Hoyer-Hansen, G.; Eefsen, R.L.; Reynolds, A.R.; Brodt, P. The multifaceted role of the microenvironment in liver metastasis: Biology and clinical implications. *Cancer Res.* **2013**, *73*, 2031–2043. [CrossRef]
41. Lee, J.W.; Beatty, G.L. Inflammatory networks cultivate cancer cell metastasis to the liver. *Cell Cycle* **2020**, *19*, 642–651. [CrossRef] [PubMed]
42. Eefsen, R.L.; Vermeulen, P.B.; Christensen, I.J.; Laerum, O.D.; Mogensen, M.B.; Rolff, H.C.; Van den Eynden, G.G.; Hoyer-Hansen, G.; Osterlind, K.; Vainer, B.; et al. Growth pattern of colorectal liver metastasis as a marker of recurrence risk. *Clin. Exp. Metastasis* **2015**, *32*, 369–381. [CrossRef] [PubMed]
43. Bohlok, A.; Botzenhart, L.; Lucidi, V.; Noel, J.C.; Demetter, P.; Larsimont, D.; Donckier, V.; Vermeulen, P.B. Histological growth pattern as a potential prognostic factor in patients operated for breast cancer liver metastases. *J. Clin. Oncol.* **2019**, *37*, e12576. [CrossRef]
44. Wu, P.H.; Phillip, J.M.; Khatau, S.B.; Chen, W.C.; Stirman, J.; Rosseel, S.; Tschudi, K.; Van Patten, J.; Wong, M.; Gupta, S.; et al. Evolution of cellular morpho-phenotypes in cancer metastasis. *Sci. Rep.* **2015**, *5*, 18437. [CrossRef] [PubMed]
45. Lyons, S.M.; Alizadeh, E.; Mannheimer, J.; Schuamberg, K.; Castle, J.; Schroder, B.; Turk, P.; Thamm, D.; Prasad, A. Changes in cell shape are correlated with metastatic potential in murine and human osteosarcomas. *Biol. Open* **2016**, *5*, 289–299. [CrossRef]
46. Anderson, A.R.; Weaver, A.M.; Cummings, P.T.; Quaranta, V. Tumor morphology and phenotypic evolution driven by selective pressure from the microenvironment. *Cell* **2006**, *127*, 905–915. [CrossRef]
47. Hanahan, D.; Coussens, L.M. Accessories to the crime: Functions of cells recruited to the tumor microenvironment. *Cancer Cell* **2012**, *21*, 309–322. [CrossRef]
48. Nagaharu, K.; Zhang, X.; Yoshida, T.; Katoh, D.; Hanamura, N.; Kozuka, Y.; Ogawa, T.; Shiraishi, T.; Imanaka-Yoshida, K. Tenascin C induces epithelial-mesenchymal transition-like change accompanied by SRC activation and focal adhesion kinase phosphorylation in human breast cancer cells. *Am. J. Pathol.* **2011**, *178*, 754–763. [CrossRef]
49. Park, J.; Schwarzbauer, J.E. Mammary epithelial cell interactions with fibronectin stimulate epithelial-mesenchymal transition. *Oncogene* **2014**, *33*, 1649–1657. [CrossRef]
50. Polyak, K.; Weinberg, R.A. Transitions between epithelial and mesenchymal states: Acquisition of malignant and stem cell traits. *Nat. Rev. Cancer* **2009**, *9*, 265–273. [CrossRef]
51. Akalay, I.; Janji, B.; Hasmim, M.; Noman, M.Z.; Thiery, J.P.; Mami-Chouaib, F.; Chouaib, S. EMT impairs breast carcinoma cell susceptibility to CTL-mediated lysis through autophagy induction. *Autophagy* **2013**, *9*, 1104–1106. [CrossRef]
52. Kudo-Saito, C.; Shirako, H.; Takeuchi, T.; Kawakami, Y. Cancer metastasis is accelerated through immunosuppression during Snail-induced EMT of cancer cells. *Cancer Cell* **2009**, *15*, 195–206. [CrossRef]
53. Soundararajan, R.; Fradette, J.J.; Konen, J.M.; Moulder, S.; Zhang, X.; Gibbons, D.L.; Varadarajan, N.; Wistuba, I.I.; Tripathy, D.; Bernatchez, C.; et al. Targeting the Interplay between Epithelial-to-Mesenchymal-Transition and the Immune System for Effective Immunotherapy. *Cancers* **2019**, *11*, 714. [CrossRef]
54. Dongre, A.; Rashidian, M.; Eaton, E.N.; Reinhardt, F.; Thiru, P.; Zagorulya, M.; Nepal, S.; Banaz, T.; Martner, A.; Spranger, S.; et al. Direct and Indirect Regulators of Epithelial-Mesenchymal Transition (EMT)-mediated Immunosuppression in Breast Carcinomas. *Cancer Discov.* **2020**. [CrossRef]
55. Kienast, Y.; Von Baumgarten, L.; Fuhrmann, M.; Klinkert, W.E.; Goldbrunner, R.; Herms, J.; Winkler, F. Real-time imaging reveals the single steps of brain metastasis formation. *Nat. Med.* **2010**, *16*, 116–122. [CrossRef]

56. Luzzi, K.J.; MacDonald, I.C.; Schmidt, E.E.; Kerkvliet, N.; Morris, V.L.; Chambers, A.F.; Groom, A.C. Multistep nature of metastatic inefficiency: Dormancy of solitary cells after successful extravasation and limited survival of early micrometastases. *Am. J. Pathol.* **1998**, *153*, 865–873. [CrossRef]
57. Goddard, E.T.; Hill, R.C.; Barrett, A.; Betts, C.; Guo, Q.; Maller, O.; Borges, V.F.; Hansen, K.C.; Schedin, P. Quantitative extracellular matrix proteomics to study mammary and liver tissue microenvironments. *Int. J. Biochem. Cell Biol.* **2016**, *81*, 223–232. [CrossRef] [PubMed]
58. Barkan, D.; El Touny, L.H.; Michalowski, A.M.; Smith, J.A.; Chu, I.; Davis, A.S.; Webster, J.D.; Hoover, S.; Simpson, R.M.; Gauldie, J.; et al. Metastatic growth from dormant cells induced by a col-I-enriched fibrotic environment. *Cancer Res.* **2010**, *70*, 5706–5716. [CrossRef] [PubMed]
59. Hoye, A.M.; Erler, J.T. Structural ECM components in the premetastatic and metastatic niche. *Am. J. Physiol. Cell Physiol.* **2016**, *310*, C955–C967. [CrossRef]
60. Kai, F.; Drain, A.P.; Weaver, V.M. The Extracellular Matrix Modulates the Metastatic Journey. *Dev. Cell* **2019**, *49*, 332–346. [CrossRef]
61. Oskarsson, T.; Acharyya, S.; Zhang, X.H.; Vanharanta, S.; Tavazoie, S.F.; Morris, P.G.; Downey, R.J.; Manova-Todorova, K.; Brogi, E.; Massague, J. Breast cancer cells produce tenascin C as a metastatic niche component to colonize the lungs. *Nat. Med.* **2011**, *17*, 867–874. [CrossRef] [PubMed]
62. Winkler, J.; Abisoye-Ogunniyan, A.; Metcalf, K.J.; Werb, Z. Concepts of extracellular matrix remodelling in tumour progression and metastasis. *Nat. Commun.* **2020**, *11*, 5120. [CrossRef] [PubMed]
63. Brodt, P. Role of the Microenvironment in Liver Metastasis: From Pre- to Prometastatic Niches. *Clin. Cancer Res.* **2016**, *22*, 5971–5982. [CrossRef] [PubMed]
64. Coffelt, S.B.; Kersten, K.; Doornebal, C.W.; Weiden, J.; Vrijland, K.; Hau, C.S.; Verstegen, N.J.M.; Ciampricotti, M.; Hawinkels, L.; Jonkers, J.; et al. IL-17-producing gammadelta T cells and neutrophils conspire to promote breast cancer metastasis. *Nature* **2015**, *522*, 345–348. [CrossRef] [PubMed]
65. Lee, J.C.; Mehdizadeh, S.; Smith, J.; Young, A.; Mufazalov, I.A.; Mowery, C.T.; Daud, A.; Bluestone, J.A. Regulatory T cell control of systemic immunity and immunotherapy response in liver metastasis. *Sci. Immunol.* **2020**, *5*, eaba0759. [CrossRef]
66. Kitamura, T.; Qian, B.Z.; Pollard, J.W. Immune cell promotion of metastasis. *Nat. Rev. Immunol.* **2015**, *15*, 73–86. [CrossRef] [PubMed]
67. Betts, C.B.; Pennock, N.D.; Caruso, B.P.; Ruffell, B.; Borges, V.F.; Schedin, P. Mucosal Immunity in the Female Murine Mammary Gland. *J. Immunol.* **2018**, *201*, 734–746. [CrossRef]
68. Noelia, A.G.; Bensinger, S.J.; Hong, C.; Beceiro, S.; Bradley, M.N.; Zelcer, N.; Deniz, J.; Ramirez, C.; Diaz, M.; Gallardo, G.; et al. Apoptotic cells promote their own clearance and immune tolerance through activation of the nuclear receptor LXR. *Immunity* **2009**, *31*, 245–258. [CrossRef]
69. Gordon-Weeks, A.; Yuzhalin, A.E. Cancer Extracellular Matrix Proteins Regulate Tumour Immunity. *Cancers* **2020**, *12*, 3331. [CrossRef]
70. Jachetti, E.; Caputo, S.; Mazzoleni, S.; Brambillasca, C.S.; Parigi, S.M.; Grioni, M.; Piras, I.S.; Restuccia, U.; Calcinotto, A.; Freschi, M.; et al. Tenascin-C Protects Cancer Stem-like Cells from Immune Surveillance by Arresting T-cell Activation. *Cancer Res.* **2015**, *75*, 2095–2108. [CrossRef]
71. Galon, J.; Costes, A.; Sanchez-Cabo, F.; Kirilovsky, A.; Mlecnik, B.; Lagorce-Pages, C.; Tosolini, M.; Camus, M.; Berger, A.; Wind, P.; et al. Type, density, and location of immune cells within human colorectal tumors predict clinical outcome. *Science* **2006**, *313*, 1960–1964. [CrossRef]
72. Zhang, L.; Conejo-Garcia, J.R.; Katsaros, D.; Gimotty, P.A.; Massobrio, M.; Regnani, G.; Makrigiannakis, A.; Gray, H.; Schlienger, K.; Liebman, M.N.; et al. Intratumoral T cells, recurrence, and survival in epithelial ovarian cancer. *N. Engl. J. Med.* **2003**, *348*, 203–213. [CrossRef]
73. Callihan, E.B.; Gao, D.; Jindal, S.; Lyons, T.R.; Manthey, E.; Edgerton, S.; Urquhart, A.; Schedin, P.; Borges, V.F. Postpartum diagnosis demonstrates a high risk for metastasis and merits an expanded definition of pregnancy-associated breast cancer. *Breast. Cancer Res. Treat.* **2013**, *138*, 549–559. [CrossRef] [PubMed]
74. Azim, H.A., Jr.; Santoro, L.; Russell-Edu, W.; Pentheroudakis, G.; Pavlidis, N.; Peccatori, F.A. Prognosis of pregnancy-associated breast cancer: A meta-analysis of 30 studies. *Cancer Treat. Rev.* **2012**, *38*, 834–842. [CrossRef]
75. Shao, C.; Yu, Z.; Xiao, J.; Liu, L.; Hong, F.; Zhang, Y.; Jia, H. Prognosis of pregnancy-associated breast cancer: A meta-analysis. *BMC Cancer* **2020**, *20*, 746. [CrossRef]
76. Bartlett, A.Q.; Vesco, K.K.; Purnell, J.Q.; Francisco, M.; Goddard, E.; DeBarber, A.; Leo, M.C.; Baetscher, E.; Rooney, W.; Naugler, W.; et al. Pregnancy and weaning regulate human maternal liver size and function. *bioRxiv* **2021**. [CrossRef]
77. Martinson, H.A.; Jindal, S.; Durand-Rougely, C.; Borges, V.F.; Schedin, P. Wound healing-like immune program facilitates postpartum mammary gland involution and tumor progression. *Int. J. Cancer* **2015**, *136*, 1803–1813. [CrossRef] [PubMed]
78. Lyons, T.R.; O'Brien, J.; Borges, V.F.; Conklin, M.W.; Keely, P.J.; Eliceiri, K.W.; Marusyk, A.; Tan, A.C.; Schedin, P. Postpartum mammary gland involution drives progression of ductal carcinoma in situ through collagen and COX-2. *Nat. Med.* **2011**, *17*, 1109–1115. [CrossRef] [PubMed]
79. Jindal, S.; Narasimhan, J.; Borges, V.F.; Schedin, P. Characterization of weaning-induced breast involution in women: Implications for young women's breast cancer. *NPJ Breast. Cancer* **2020**, *6*, 55. [CrossRef] [PubMed]

80. Tsujikawa, T.; Kumar, S.; Borkar, R.N.; Azimi, V.; Thibault, G.; Chang, Y.H.; Balter, A.; Kawashima, R.; Choe, G.; Sauer, D.; et al. Quantitative Multiplex Immunohistochemistry Reveals Myeloid-Inflamed Tumor-Immune Complexity Associated with Poor Prognosis. *Cell Rep.* **2017**, *19*, 203–217. [CrossRef] [PubMed]
81. Pennock, N.D.; Martinson, H.A.; Guo, Q.; Betts, C.B.; Jindal, S.; Tsujikawa, T.; Coussens, L.M.; Borges, V.F.; Schedin, P. Ibuprofen supports macrophage differentiation, T cell recruitment, and tumor suppression in a model of postpartum breast cancer. *J. Immunother. Cancer* **2018**, *6*, 98. [CrossRef] [PubMed]

Pregnancy and weaning regulate human maternal liver size and function

Alexandra Q. Bartlett[a], Kimberly K. Vesco[b], Jonathan Q. Purnell[c], Melanie Francisco[b], Erica Goddard[d], Xiangnan Guan[e], Andrea DeBarber[f], Michael C. Leo[b], Eric Baetscher[g], William Rooney[g], Willscott Naugler[h], Alexander R. Guimaraes[i], Patrick Catalano[j], Zheng Xia[k,e], and Pepper Schedin[a,l,m,1]

[a]Department of Cell, Developmental, and Cancer Biology, Oregon Health & Science University, Portland, OR 97239; [b]Center for Health Research, Kaiser Permanente Northwest, Portland, OR 97227; [c]Knight Cardiovascular Institute, Oregon Health & Science University, Portland, OR 97239; [d]Public Health Sciences Division/Translational Research Program, Fred Hutchinson Cancer Research Center, Seattle, WA 98109; [e]Computational Biology Program, Oregon Health & Science University, Portland, OR 97201; [f]Department of Chemical Physiology and Biochemistry, Oregon Health & Science University, Portland, OR 97239; [g]Advanced Imaging Research Center, Oregon Health & Science University, Portland, OR 97239; [h]Department of Medicine, Division of Gastroenterology and Hepatology, Oregon Health & Science University, Portland, OR 97239; [i]Department of Diagnostic Radiology, Oregon Health & Science University, Portland, OR 97239; [j]Mother Infant Research Institute, Department of Obstetrics and Gynecology, Tufts University School of Medicine, Boston, MA 02111; [k]Department of Molecular Microbiology and Immunology, Oregon Health & Science University, Portland, OR 97273; [l]Knight Cancer Institute, Oregon Health & Science University, Portland, OR 97201; and [m]Young Women's Breast Cancer Translational Program, University of Colorado Anschutz Medical Campus, Aurora, CO 80045

Edited by David D. Moore, University of California, Berkeley, CA, and approved October 14, 2021 (received for review April 16, 2021)

During pregnancy, the rodent liver undergoes hepatocyte proliferation and increases in size, followed by weaning-induced involution via hepatocyte cell death and stromal remodeling, creating a prometastatic niche. These data suggest a mechanism for increased liver metastasis in breast cancer patients with recent childbirth. It is unknown whether the human liver changes in size and function during pregnancy and weaning. In this study, abdominal imaging was obtained in healthy women at early and late pregnancy and postwean. During pregnancy time points, glucose production and utilization and circulating bile acids were measured. Independently of weight gain, most women's livers increased in size with pregnancy, then returned to baseline postwean. Putative roles for bile acids in liver growth and regression were observed. Together, the data support the hypothesis that the human liver is regulated by reproductive state with growth during pregnancy and volume loss postwean. These findings have implications for sex-specific liver diseases and for breast cancer outcomes.

liver | pregnancy | bile acids | maternal health

Sex-specific differences in liver disease have been attributed to sexual dimorphisms in steroid production, metabolic enzymes, and behavior patterns (1). Whether a pregnancy cycle contributes to sex-specific liver disease remains largely unexplored; however, a previously unrecognized liver biology linked to reproductive status has been reported in rodents (2). This rodent study found that during pregnancy and lactation, hepatocytes proliferated and entered a higher anabolic state accompanied by an overall increase in liver size. Upon weaning, hepatocytes rapidly underwent programmed cell death, liver metabolism shifted toward catabolism, and the liver regressed to its prepregnant size in a process referred to as weaning-induced liver involution (2). In mice, liver involution promoted breast cancer outgrowth in the liver, suggesting a pathophysiological consequence of liver involution (2, 3).

Notably, young women diagnosed with breast cancer in the postpartum period were found to be at increased risk for liver metastasis (2). Taken together, these findings suggest that weaning-induced liver involution, which we predict would return the enlarged liver to its prepregnant, prelactational state, may create a prometastatic liver niche in women. However, it is unknown whether the human liver changes in size and function across a reproductive cycle, as expected if the liver is tuned to meet the unique metabolic demands of pregnancy, lactation, and weaning. Such evidence would corroborate findings in rodents and would be foundationally important for future studies of liver health in women.

To investigate the impact of reproductive state on liver size and function in women, we conducted a prospective study of healthy pregnant women using magnetic resonance and spectroscopy imaging of the liver and compared findings to a validated rodent model. Here, we show that the human female liver is regulated in both size and function by reproductive state and provide evidence of weaning-induced liver involution in humans. Furthermore, our data provide a hypothesis to explain the increased liver metastasis observed in postpartum breast cancer patients, as well as having potentially broader implications for the understanding of sex-specific liver diseases.

Results

In total, 47 healthy pregnant women completed early (12 to 16 wk gestation) and late pregnancy (32 to 36 wk gestation) study visits (Fig. 1*A*). Study participants underwent liver MRI (Fig 1*A*), provided blood samples, had insulin sensitivity assessed via hyperinsulinemic-euglycemic clamp, and completed body composition analyses. Participant demographics are shown in *SI Appendix*, Table S1.

To assess whether liver size is increased during pregnancy, we measured livers via MRI and found that, on average, liver volumes increased 15% (182 cm^3 ± 197 cm^3) from early to late

Significance

These human data are consistent with reproductive control of liver size and function in women and concur with recent observations in rodents, suggesting a conserved liver biology. The question of whether this described liver biology has implications for maternal health during pregnancy or sex-specific risk for liver disease remains to be determined. However, our evidence suggestive of weaning-induced liver involution in women may lead to improved understanding of the high rates of liver metastasis observed in young postpartum breast cancer patients.

Author contributions: A.Q.B., K.K.V., J.Q.P., E.G., A.R.G., and P.S. designed research; A.Q.B., K.K.V., J.Q.P., E.G., X.G., A.D., E.B., W.R., W.N., and P.S. performed research; A.D. contributed new reagents/analytic tools; A.Q.B., K.K.V., J.Q.P., M.F., E.G., X.G., M.C.L., E.B., P.C., Z.X., and P.S. analyzed data; and A.Q.B. and P.S. wrote the paper.

The authors declare no competing interest.

This article is a PNAS Direct Submission.

[1]To whom correspondence may be addressed. Email: schedin@ohsu.edu.

This article contains supporting information online at http://www.pnas.org/lookup/suppl/doi:10.1073/pnas.2107269118/-/DCSupplemental.

Published November 22, 2021.

PHYSIOLOGY

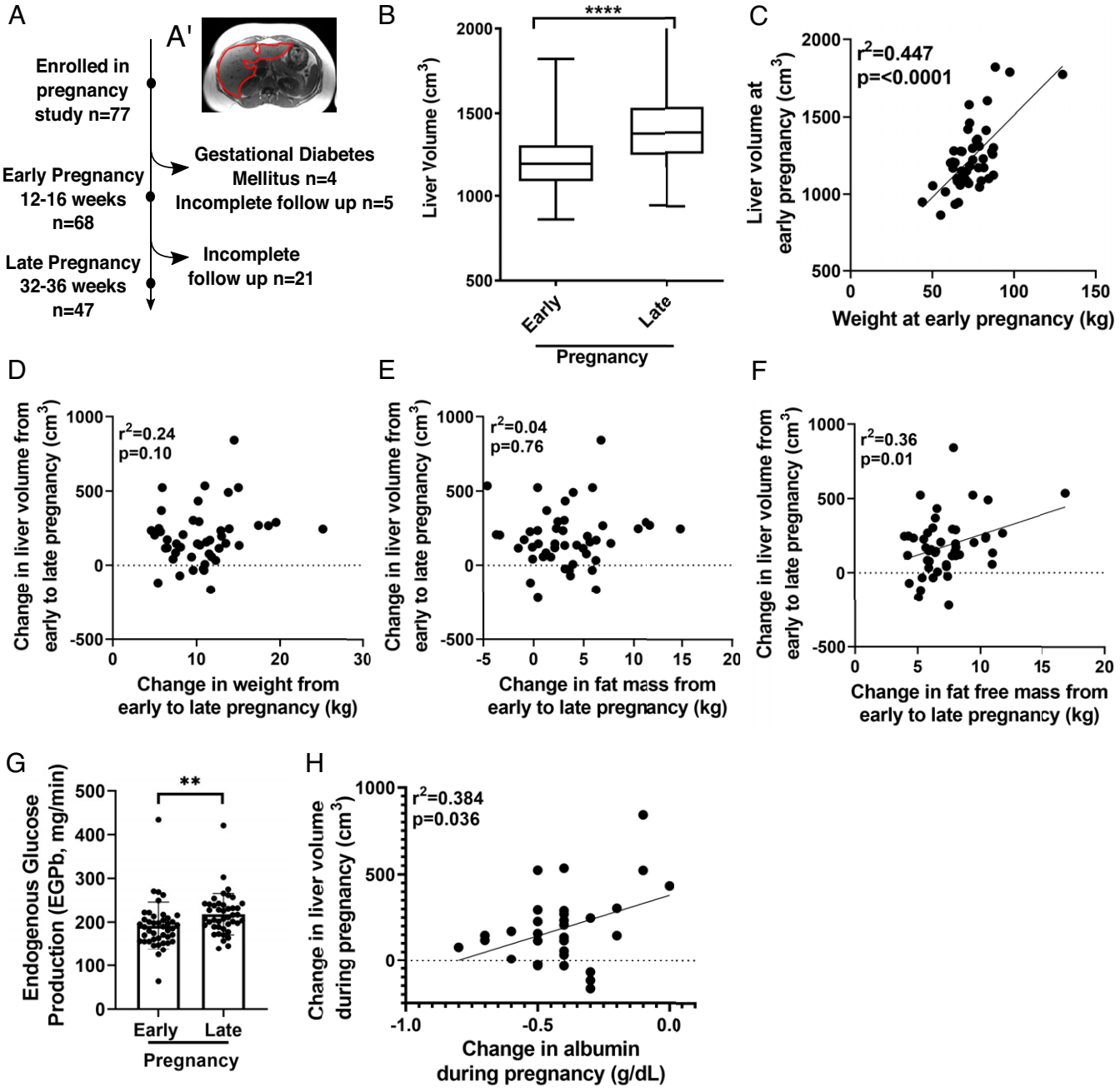

Fig. 1. Liver changes during pregnancy. (*A*) Diagram of the observational study. (*A'*) Liver MRI cross-section with liver outlined in red. (*B*) Average liver volume at early and late pregnancy ($n = 47$; $^{****}P < 0.0001$ by two-tailed paired *t* test). (*C*) Pearson's correlation of liver volume and BMI at early pregnancy ($n = 47$). Pearson's correlation of change in liver volume with change in weight (*D*), fat mass (*E*), and fat-free mass (*F*) ($n = 47$). (*G*) EGP-b at early and late pregnancy ($n = 47$; $^{**}P < 0.01$ by two-tailed paired *t* test). (*H*) Pearson's correlation of change in liver volume and change in albumin ($n = 30$).

pregnancy ($P < 0.0001$) (Fig. 1*B*). Average liver size at early pregnancy was 1,239 $cm^3 \pm 220.8$ cm^3 and at late pregnancy was 1,421 $cm^3 \pm 298.6$ cm^3 (Fig. 1*B*).

Because liver size is attuned to overall body size via the "hepatostat" (4), we next determined whether the increase in liver size from early to late pregnancy correlated with increased body mass of pregnancy. First, we investigated the existence of the "hepatostat" at baseline, using body weight at the early pregnancy visit as a baseline surrogate, as pregnancy-related weight gain is minimal at this time point (5). Liver volume at early pregnancy correlated with body weight (Fig. 1*C*), confirming previous studies in nonpregnant individuals (4). In contrast, the change in liver volume during pregnancy did not correlate with gestational weight gain (Fig. 1*D*). Furthermore, we found no relationships between pregnancy liver volume change and change in total fat mass (Fig. 1*E*), subcutaneous abdominal, or visceral adipose tissue (VAT) volumes (Table 1). However, the change in a woman's fat-free mass, which includes liver, fetal tissue, placenta, and plasma, did correlate with change in liver size (Fig. 1*F*). The association between change in fat-free mass and

Table 1. Change in liver volume correlated with measures of body composition and metabolism

Variable	Mechanism of collection	Sample size	Pearson correlation coefficient	*P* value
Body composition				
Change in weight	Scale	47	0.260	0.078
Change in BMI	Scale, stadiometer	47	0.213	0.150
Change in fat mass	BODPOD	47	0.077	0.605
Change in fat-free mass	BODPOD	47	**0.335**	**0.021**
Change in SAT	MRI	47	0.123	0.409
Change in VAT	MRI	47	0.245	0.097
Change in IHL	H-MR spectroscopy	47	−0.035*	0.814*
Metabolism				
Change in M value	Hyperinsulinemic-euglycemic clamp	43	−0.015	0.926
Change in EGP	Hyperinsulinemic-euglycemic clamp	43	−0.047*	0.763*
Change in Rd	Hyperinsulinemic-euglycemic clamp	43	0.053	0.736
Change in fasting insulin	Blood draw	45	0.095	0.537
Change in total cholesterol	Blood draw	45	0.062	0.684
Change in triglycerides	Blood draw	45	0.176	0.248
Change in LDL	Blood draw	45	−0.119	0.438
Change in HDL	Blood draw	45	0.103	0.500
Change in very low density lipoprotein	Blood draw	45	−0.103	0.500

Bold text indicates that the change fat free mass was the only variable that reached statistical significance.
*These analyses were done with Spearmen Correlation.

liver volume is confounded as fat-free mass is not an independent variable from liver mass. In sum, these data suggest that liver size increase during pregnancy is unlinked to overall body size; that is, it is not controlled by the "hepatostat" mechanism. Rather, these data may reflect an unrecognized, reproductive state–controlled program regulating liver size during pregnancy.

We next asked if metabolic measures were associated with liver volume change and found no relationship with cholesterol concentrations or with measures of insulin sensitivity, that is, endogenous glucose production (EGP) and glucose disposal rate (Rd) (Table 1). We also found no relationship between change in liver volume and change in intrahepatic lipid (IHL) content (Table 1). Assessment of IHL content in rodents also showed no change in IHL during pregnancy (*SI Appendix*, Fig. S1). In sum, we observed that the increase in human liver volume with late pregnancy occurred independent of weight gain of pregnancy, various other measures of body composition, circulating metabolites, and IHL storage.

In rodents, hepatocyte proliferation contributes to increased liver size and metabolic output during pregnancy and lactation (2, 6). Obtaining timed liver biopsies would be the most direct way to investigate hepatocyte proliferation during pregnancy in women; however, liver biopsies were not performed in our study for participant safety. Thus, we indirectly assessed for increased hepatocyte number by evaluating hepatocyte function. We found evidence for increased liver output as measured by increases in EGP (Fig. 1*G*) and serum albumin concentration (Fig. 1*H*), two surrogates of liver function (7, 8). Of note, an additional contributor to increased liver volume during pregnancy is increased blood flow, which rises ∼50% by late pregnancy (9). However, increased blood flow during pregnancy is not reported to associate with elevated hepatocyte metabolic output. In sum, these data are consistent with an increase in liver size and synthetic capacity during pregnancy, which may be due to increased hepatocyte proliferation as observed in rodents. Additional studies are required to determine if hepatocyte proliferation is increased during pregnancy in women.

We next looked for evidence of weaning-induced liver involution in women, a biology not previously described in humans. Of the 47 women who participated in our pregnancy study, 36% completed a liver MRI >3 mo postwean (median 5.7 mo) (Fig. 2*A*). Liver volumes trended toward a decrease in size between late pregnancy and postwean (Fig. 2*B*), and postwean liver volumes were similar to early pregnancy, indicative of a return to baseline (Fig. 2*C*). These data provide evidence of postpartum liver involution in women.

While our data showed a statistically significant increase in liver size during pregnancy and a trend toward decrease after weaning, there was heterogeneity in how an individual's liver size changed with pregnancy and postwean. During pregnancy, we found that 72% (34/47) of women had an average increase in liver volume of ∼20% (Fig. 2*D*, black bars). However, 21% of participants (10/47) had no measurable liver volume change and 6% (3/47) had a reduction in liver volume (Fig. 2*D*, black bars, *SI Appendix*, Table S2). We saw similar heterogeneity with regard to liver volume change from late pregnancy to postwean (Fig. 2*D*, gray bars).

Considering the heterogeneity in liver volume change and what is known about normal rodent liver biology (i.e., liver weight gain with pregnancy and loss postwean) (2), we performed subgroup analyses. We delineated the participants into two groups: "gain-loss," the observed pattern in the normal rodent, or "not gain-loss" for those that did not display the rodent pattern. 53% of women displayed the anticipated liver "gain-loss" pattern (Fig. 2*E*). The "not gain-loss" group comprised heterogeneous patterns and included three women who lost liver volume during pregnancy and regained postwean, three women with no significant liver volume changes, and one woman each with either continuous liver size loss or gain across the three visits (Fig. 2*F*). Of note, liver volume patterns with pregnancy and postwean did not correlate with a woman's overall weight gain of pregnancy (*SI Appendix*, Fig. S2).

Upon further exploration, we found that none of the women whose liver changes were similar to the normal rodent pattern of "gain-loss" had gestational hypertension, yet 50% of the "not gain-loss" group did (Fig. 2*F*, dashed lines). Furthermore, measures of insulin sensitivity differed between these groups. Specifically, we found the "gain-loss" participants had greater EGP at late pregnancy (Fig. 2*G*), consistent with published data showing elevated EGP in healthy pregnancy (10). We also found greater glucose disposal rates at late pregnancy in the "gain-loss" group (Fig. 2*H*), consistent with greater insulin

PHYSIOLOGY

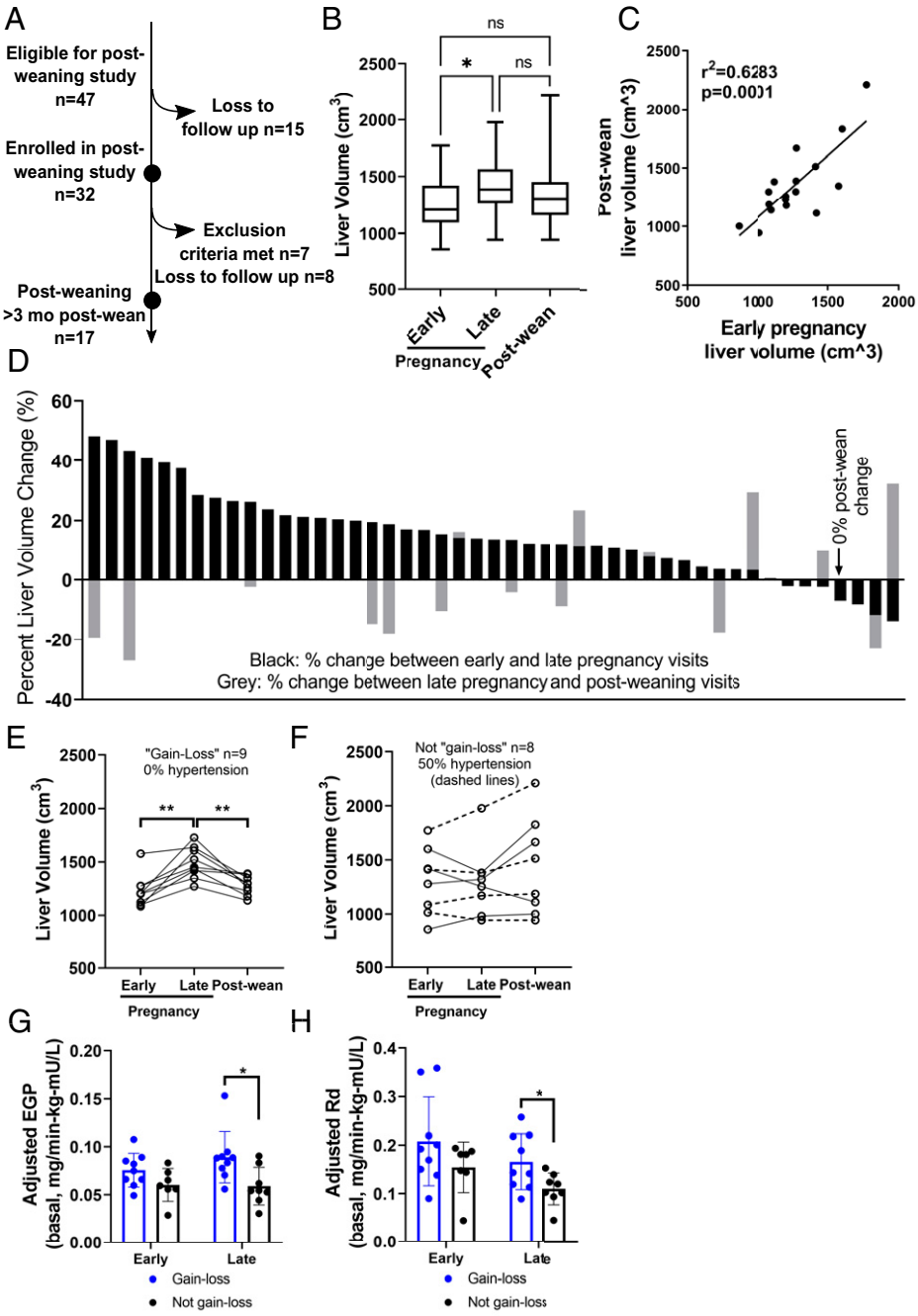

Fig. 2. Human liver volumes postwean. (*A*) Diagram for postwean observational study. (*B*) Liver volume at early, late, and postwean time points ($n = 17$). (*C*) Pearson's correlation of liver volumes at early pregnancy and postwean ($n = 17$). (*D*) Liver volume change between early and late pregnancy (black bars) and between late pregnancy and postwean (gray bars) per participant. Primary pattern (*E*) and secondary patterns (*F*) of liver volume change with pregnancy and postwean. Dashed lines show participants with hypertension (paired *t* test). EGP (*G*) and glucose disposal rate, Rd, (*H*) in women in gain–loss group compared to women not in gain–loss group. Pearson's correlation. *P* value: * < 0.05, ** < 0.01.

sensitivity in the muscle. These data suggest that the "not gain-loss" pattern may be associated with suboptimal gestational metabolic health and gestational hypertension. One question is whether these metabolic parameters impact fetal outcomes. In this cohort, maternal liver size patterns did not correlate with newborn weight, length, or Ponderal index, three common neonatal health measures.

To investigate the mechanistic relationship between reproductive state and liver size, we utilized a rat model, as previously described (2). We found liver weight increases during pregnancy were greater than expected due to gestational weight gain alone (Fig. 3*A*). These data suggest rat liver weight during pregnancy is unlinked from the "hepatostat," corroborating our human data (Fig. 1*D*). Next, we confirmed maximum hepatocyte proliferation in the rat livers to occur during pregnancy (Fig. 3*B*), consistent with previous reports (2, 6). Together, these data suggest a physiological model in which increased liver volume of pregnancy is due to increased hepatocyte proliferation that is activated via an unrecognized, pregnancy-mediated developmental program.

As a possible mechanism underlying a pregnancy-associated liver growth program, we investigated bile acid metabolism in

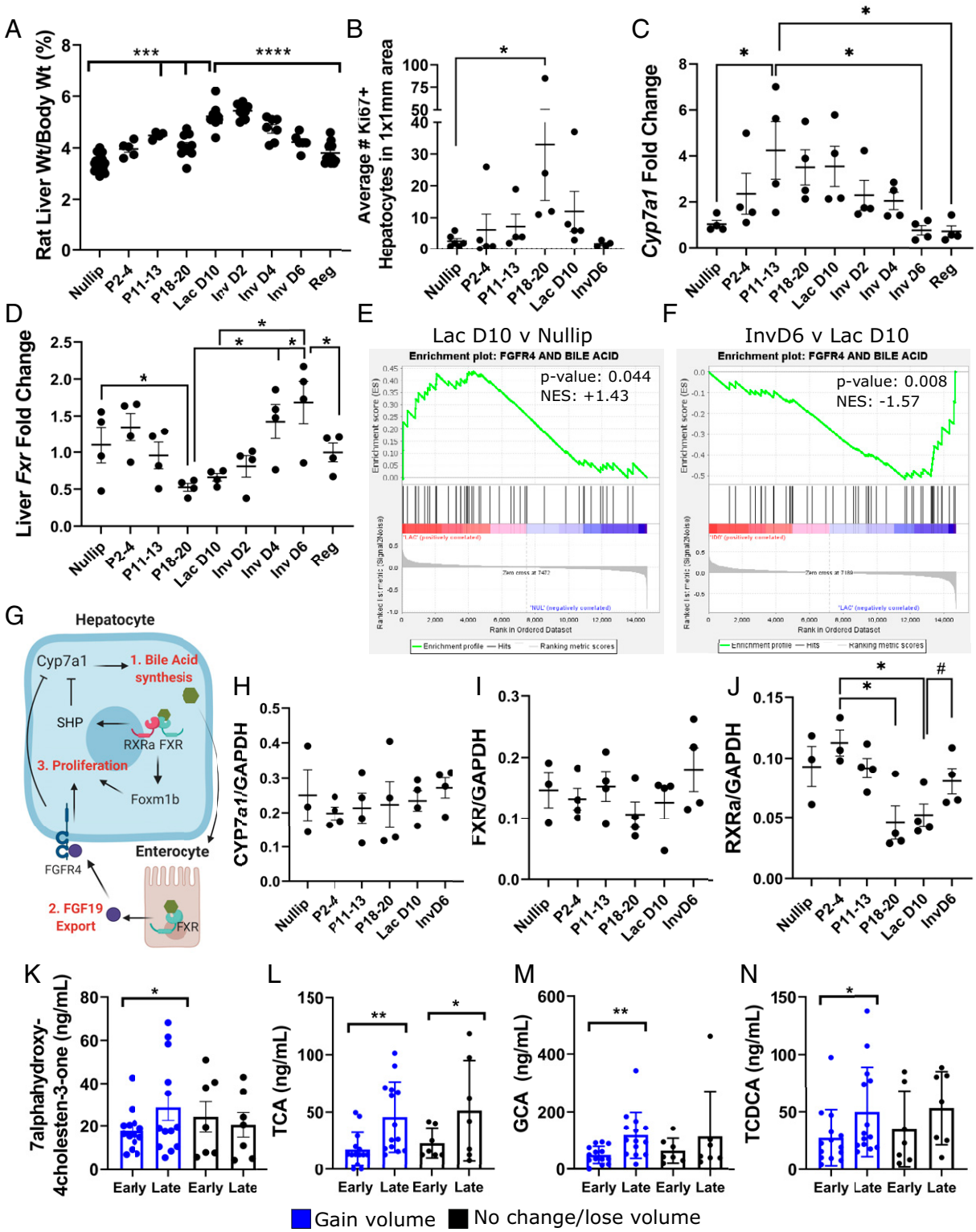

Fig. 3. Hepatic bile acid signaling and liver size. (*A*) Rat liver weight normalized to body weight: nulliparous (nullip) $n = 24$; early (P2-4) $n = 5$; middle (P11-13) $n = 4$; and late (P18-20) pregnancy $n = 10$; lactation day 10 (Lac D10) $n = 9$; involution (Inv) D2 $n = 9$; InvD4 $n = 7$; InvD6 $n = 6$; Regressed (Reg) $n = 14$; one-way ANOVA. (*B*) Ki67+ hepatocytes in rat livers, $n = 3$ to 5/group. (*C*) *Cyp7a1* and (*D*) *FXR* mRNA fold change in liver, $n = 4$ per group; one-way ANOVA. Gene set enrichment analysis plots of FGFR4–bile acid gene pathway for (*E*) lactation day 10 versus nulliparous groups and (*F*) involution day 6 versus lactation day 10 groups. (*G*) Model for pregnancy enlargement of liver due to hepatocyte proliferation downstream of bile acid signaling. Protein abundance in whole rat liver of (*H*) CYP7A1, (*I*) FXR, and (*J*) RXRalpha. Data are normalized to GAPDH protein abundance; nullip $n = 3$, P2-4, P11-13, P18-20, Lac D10, and InvD6 $n = 4$/group; $^*P < 0.05$ by one-way ANOVA; # $P < 0.05$ by Student's t test. (*K*) Human 7α-hydroxy-4cholesten-3-one plasma concentrations at early and late pregnancy, separated by liver gain ($n = 14$) and no gain ($n = 7$). Human plasma concentrations of bile acids TCA (*L*), GCA (*M*), and TCDCA (*N*) paired t test, P value: * < 0.05, ** < 0.01, *** < 0.001, **** < 0.0001.

rodents. Bile acid signaling contributes to liver regeneration following partial hepatectomy and can control liver size independent of body size (11, 12). Furthermore, bile acids have been shown to regulate hepatocyte proliferation in a pathway dependent on enterocyte-derived fibroblast growth factor 15/19 (11, 13, 14). To investigate if the bile acid pool is modulated by reproductive state, we measured liver *Cyp7a1*, the gene that encodes rate limiting enzyme in bile acid synthesis. We found a three- to fourfold increased expression of *Cyp7a1* with pregnancy, which remained elevated during lactation, followed by a rapid decline with weaning (Fig. 3*C*). Since hepatic FXR signaling acts as a negative regulator of Cyp7a (Fig. 3*D*), we measured hepatic *Fxr*. We found *Fxr* was down-regulated during late pregnancy, when *Cyp7a1* was high, and increased with weaning, when *Cyp7a1* was low (Fig. 3*D*). To further investigate the hypothesis that elevated bile acids contribute to hepatocyte proliferation through activation of FGFR4 signaling, we analyzed an RNA-sequencing dataset from mouse liver at various reproductive stages. We performed gene set enrichment analysis using a custom gene set composed of genes in bile acid metabolism and FGFR4 downstream signaling pathways. Consistent with our hypothesis, we found an enrichment for bile acid–FGFR4 signaling pathways in lactation stage mice compared to nulliparous (Fig. 3*E* and *SI Appendix*, Fig. S3). Additionally, at involution day 6 this bile acid–FGFR4 gene signature was significantly decreased compared to lactation (Fig. 3*F* and *SI Appendix*, Fig. S3). Furthermore, we identified the up-regulation of individual genes involved with bile acid synthesis (*Cyp7a1*, *Cyp8b1*) and proliferation (*Foxm1*) during lactation, which were subsequently down-regulated with involution (*SI Appendix*, Fig. S3). Conversely, genes involved with inhibiting bile acid synthesis (*Rxra*, *Shp*) were reduced during lactation and elevated during involution (*SI Appendix*, Fig. S3). A model depicting a proposed mechanism by which bile acid–FGFR4 signaling increases hepatocyte proliferation is shown (Fig. 3*G*). Because gene expression and protein concentration are not always linked, we evaluated protein abundance for CYP7A1 and FXR. We were unable to validate reproductive-stage regulation of *Cyp7a1* and *FXR* at the protein level (Fig. 3 *H* and *I*). However, based on our mouse RNA-sequencing data that showed regulation of *RXRa* by reproductive stage (*SI Appendix*, Fig. S3), we also measured RXRa protein concentration. RXRa is a known binding partner for FXR that acts as a co-negative regulator of *Cyp7a1* (15, 16). We found that RXRa was significantly reduced at pregnancy days 18 to 20 and lactation day 10, then was increased at involution day 6 (Fig. 3*J*). The decreased gene expression and protein abundance of RXRa might be sufficient to activate *Cyp7A1* gene expression without a corresponding decrease in FXR protein. In sum, these data associate increased bile acids with the physiologic expansion of the liver during pregnancy—consistent with a previous report (12)—and extend these observations to suggest a role for bile acids in regulating liver size during pregnancy, lactation, and weaning.

We then examined associations between liver growth and the bile acid pool in pregnant women by measuring a biomarker of bile acid production and serum bile acid concentrations at early and late pregnancy. Serum concentrations of 7α-hydroxy-4-cholestene-3-one (7αC4), a readout for cholesterol 7α-hydroxylase (Cyp7a1) enzyme activity (17), were significantly increased at late compared to early pregnancy only in the women who had an increase in liver volume during pregnancy (Fig. 3*F*). This finding supports the hypothesis that increased bile acid production during pregnancy may be required for liver size increase. Furthermore, among the women whose liver increased in size during pregnancy, we found increases in several primary bile acids and their conjugates (Fig. 3 *G–I*). Of note, changes in secondary bile acids, which are metabolic products of gut bacteria, only weakly correlated with liver volume change (*SI Appendix*, Table S3). In this human cohort, we did not find associations between concentration of plasma FGF19, an enterocyte product shown to induce hepatocyte proliferation and liver growth in rodents (*SI Appendix*, Fig. S4). One potential caveat to our FGF19 analysis is that plasma concentrations of FGF19 may not reflect concentration in the portal vein that links the gut and liver. In sum, these human data are consistent with an increased bile acid pool during pregnancy, which may contribute to the increased liver size observed in pregnancy.

Discussion

In this study, we find evidence for a previously unreported liver biology in women—namely that during the course of a normal pregnancy cycle liver volume increases during gestation and decreases postwean. Multiple observations and reports demonstrate tight control of liver size in proportion to body size, a phenomenon that has been referred to as the "hepatostat" (4). Yet, in our study, increased liver volume during pregnancy is not accounted for by change in body size. Since liver size is presumed to be directly linked to a physiologic function of the liver (18), our data suggest that a metabolic demand above and beyond body size accounts for increased liver size during pregnancy. Consistent with this hypothesis, in rodents we find that liver size remains elevated through lactation even though body size is reduced compared to late pregnancy.

One potential mechanism controlling liver size during a pregnancy cycle is the circulation of bile acids, which have been shown to modulate liver size independent of the body size hepatostat (19, 20). Such a paradigm where liver size is controlled by bile acid flux would allow for a situation in which body size could become "unlinked" from liver size. The data presented here obtained from rodent models and human correlates support the idea that increased production of primary bile acids during pregnancy and lactation via the Cyp7a1 synthetic pathway leads to hepatocyte proliferation and thus a larger liver. Since the primary function of bile acids is to facilitate fat absorption in the intestine, an increase in liver parenchyma capable of bile acid synthesis would make sense given increased caloric demand during pregnancy and lactation. In sum, our human data are consistent with dynamic size regulation of the liver to accommodate the unique metabolic demands of pregnancy and lactation. Furthermore, our combined human and rodent data suggest a mechanism whereby physiologically regulated bile acid synthesis underlies liver size changes across a pregnancy cycle. Future studies directly testing this mechanism are needed.

Additional factors that could contribute to increased liver size with pregnancy include hormones, such as thyroid hormone, estrogen, and progesterone. Thyroid hormone can induce hepatocyte proliferation (21), yet thyroid hormone does not associate with significant growth of the liver nor is it required for liver regeneration (22). Furthermore, thyroid hormone is known to decrease between early and late pregnancy (23, 24), which is a pattern of expression inconsistent with a role in hepatocyte proliferation. Additionally, previous work has evaluated the impact of estrogen and progesterone on liver size. Administration of pregnancy-relevant concentrations of estrogen and progesterone did not induce liver growth, suggestive that these hormones are not key for increasing liver size during pregnancy (25). Prolactin, which increases through pregnancy and peaks during lactation (26, 27), is known to stimulate hepatocyte proliferation and is associated with accelerated liver regeneration following partial hepatectomy (28–30). A limitation of our study is lack of identification of the molecular mechanism upstream of increased bile acid production during pregnancy and lactation, of which pregnancy hormones could contribute.

Intriguingly, there is evidence that prolactin can stimulate bile acid synthesis (31). These prolactin data and our observation that RXRa, a member of the steroid receptor super family, is regulated in a manner consistent with bile acid regulation of liver size, may generate new avenues to pursue.

While the pattern of liver size gain with pregnancy and loss upon weaning was observed in the majority of women in this pregnancy study, we also identified a subset of women for whom liver size did not follow a "gain-loss" pattern. Gestational hypertension and reduced liver insulin sensitivity were more common in this subset. Therefore, an intriguing hypothesis is that a facet of healthy pregnancy is the gain-loss pattern of liver volume. A corollary to this hypothesis is that preexisting and/or pregnancy-specific conditions such as gestational hypertension could underlie the inability of the liver to appropriately respond to pregnancy (32). Of note, gestational hypertension affects 5 to 10% of pregnancies and can progress to preeclampsia with known pathogenic liver involvement in ∼15 to 20% of cases (33). Gestational hypertension is attributed to a vascular disorder that is initiated at the placental interface, specifically due to incomplete maturation of the maternal spiral arteries (34). If related, the question of whether the same pathophysiology that leads to gestational hypertension can also impair the normal liver response to growth cues of pregnancy, or vice versa, remains unknown. On the other hand, albeit a small study, our data show that liver gain with pregnancy is not a requisite for normal fetal growth, as we observed no differences in newborn size between women who did and did not experience liver gain with pregnancy. Future studies would be required to determine if there are any long-term impacts due to a lack of maternal liver growth during gestation, as has been described for other variations in neonatal nutrition and lifetime risk of disease (35–37).

The data presented here show that the human liver responds to a pregnancy cycle in a similar manner to rodents, namely, increased size with pregnancy and lactation, followed by a decrease in size postwean. The process that returns the rodent liver to its prepregnant state, weaning-induced liver involution, promotes breast cancer metastasis to the liver (2, 3). Given that women have an increased risk of liver metastasis if diagnosed with breast cancer within 5 y of pregnancy, we speculate that weaning-induced liver involution creates a prometastatic microenvironment in the liver. Although we cannot definitively demonstrate liver involution in humans, it has recently been demonstrated that the breast undergoes weaning-induced involution in women similar to rodents (38, 39). Therefore, we theorize that there is a conserved mammalian developmental program that links the mammary gland and the liver through a pregnancy cycle, putatively to meet the elevated metabolic demands of pregnancy and lactation. The potential importance of this biology for supporting reproduction and infant health are apparent; however, weaning-induced breast and liver involution may have unanticipated consequences, including the transient increased risk of breast cancer and liver metastasis (2, 40–43). Additional impacts on risk for liver disease may be anticipated given known disparities in liver disease by sex, including increased risk for acute liver failure and autoimmune liver conditions in women (1).

A key strength of our study is that each woman serves as her own control, allowing us to see how an individual's liver changes during a pregnancy cycle. However, our human cohort study cannot draw mechanistic conclusions because it was purely observational. Additionally, these data were generated in a small, predominately White, non-Hispanic cohort and require validation in a larger study with a diverse population to generalize these findings.

In summary, this work describes an observation in normal women, specifically increased liver size with pregnancy and decreased size postwean, putatively to accommodate the dramatic changes in metabolic demands across a pregnancy–lactation–wean cycle. These findings demonstrate reproductive control of liver size and function in women and concur with recent observations in rodents, suggesting a conserved liver biology. The question of whether this described liver biology has implications for maternal health during pregnancy or sex-specific risk for liver disease remains to be determined (1, 44, 45). However, our evidence suggest weaning-induced liver involution in women, which if validated, may lead to improved understanding of the high rates of liver metastasis observed in young postpartum breast cancer patients (2).

Materials and Methods

Recruitment.

Prospective cohort. We conducted a prospective cohort study of pregnant women receiving care at Kaiser Permanente Northwest (KPNW) or Oregon Health & Science University (OHSU). All study activities were approved by Institutional Review Boards at KPNW (no. 3993) and OHSU (no. 10438 and 15264). Recruitment started in December 2014 and was completed in August 2017. KPNW members who met the study inclusion criteria were identified weekly using the electronic health record (EHR). Eligible participants were mailed a recruitment letter and received a follow-up phone call a week later. During this telephone call, study personnel conducted additional eligibility screening and scheduled an explanatory visit. If patients consented at the explanatory visit, this was followed by two visits between 12 to 16 wk of gestation and two visits between 32 to 36 wk of gestation. Participants who completed all pregnancy study visits had the option to complete a postwean study visit, between 3–12 mo after weaning.

Inclusion/exclusion criteria. Patients were eligible for the study if they were between 18 to 45 y of age, were less than 12 wk pregnant with a singleton gestation at time of enrollment, had a body mass index (BMI) between 18.5 kg/m^2 and 38 kg/m^2, and were fluent English speakers. Participants were excluded if they had any of the following conditions or symptoms: contraindications to MRI study (e.g., claustrophobia, metal implants); pregestational diabetes; gestational diabetes; history of bariatric surgery or other medical conditions requiring specialized nutritional care; anemia; current history of drug, tobacco, or alcohol use; maternal rheumatologic or chronic inflammatory state; or chronic hypertension.

Measures. Data for this paper were collected at three study visits: one at 12 to 16 wk of gestation, one at 32 to 37 wk of gestation, and one between 3–12 mo postwean. Height was measured at the first visit to allow for calculation of BMI; weight was measured using a calibrated scale at each visit. Demographic variables, including parity and preconception BMI, were extracted from the EHR.

Air Displacement Plethysmography. Air displacement plethysmography (BOD POD, COSMED USA, Inc.) was used to determine participants' fat mass, fat-free mass, and percent body fat at each visit. Participants first changed into a bathing suit or spandex clothing and a swimming cap. They then sat inside the BOD POD while the air displaced by the body was measured. Results included total mass and body density. Fat mass and fat-free mass were estimated using van Raaj's pregnancy equations to account for changes in the density of fat-free mass during pregnancy (47, 48).

MRI Acquisition. MRI and spectroscopy data were collected using a Siemens Prisma Fit 3T whole-body system (Siemens Healthineers) at the Advanced Imaging Research Center at OHSU. Abdominal MR data were acquired in two stations, the first centered at umbilicus and the second centered over the xyphoid process, to acquire MRI and liver magnetic resonance spectroscopy (MRS). Siemens flexible 18-channel array and spine array receiver coils with body-coil transmission were used. The abdominal MRI protocol included a T1-weighted gradient-echo sequence (TE = 2.5 ms, TR = 140 ms, flip-angle = 90°, $(1.25\ mm)^2$ in plane resolution, 30 slices with 6 mm thickness) acquired in two-breath holds of ∼18 s each. The liver T1-weighted MRI protocol was acquired with identical parameters to the abdominal T1 volume but with a variable number of slices to cover the entire extent of the liver.

MRI Processing. The T1-weighted MRI data sets of abdomen and liver were manually spliced together with affine transformations and overlapping slice elimination. The top of the liver and the L-4/5 intervertebral disk were identified as the upper and lower bounds, respectively, for the segmentation analysis for abdominal visceral and subcutaneous fat volumes.

Abdominal T1-w MRI volumes were segmented into five classes: unlabeled, subcutaneous adipose tissue (SAT), VAT, muscle, and organ (including all other abdominal volume). A custom Python pipeline was used to create an initial automated segmentation using inputs from the umbilicus T1-weighted volumes, the liver T1-weighted volumes, and an 11-slice manual segmentation label map, the merged T1-weighted MRI data set, and the affine transforms that map individual volume acquisitions to the merged image space. Manually generated uterus/placenta and liver masks were created as these two regions have high rates of false positives for classification as adipose tissue.

Processing within the pipeline made use of the following Python libraries: Nipype (49), the Advanced Normalization Tools (50), the Insight Toolkit (51), Scikit-image (52), Scikit-learn (53), and SciPy (54). Following N4 bias field correction, steps in the segmentation pipeline relied upon intensity thresholding and morphological operations. The muscle mask was generated with a compact watershed algorithm seeded with the muscle mask from the 11-slice segmentation. SAT masking made use of the geodesic active contours algorithm (55), coupled with dilation and erosion steps to distinguish the SAT from internal VAT. VAT was taken as the difference between the total adipose mask and the SAT mask. Segmentation masks output from the automated pipeline subsequently underwent slice-by-slice manual review followed by manual refinement by a single analyst (J.Q.P.) using the 3D Slicer software package to ensure accuracy of VAT and SAT masks placements.

Liver segmentation was manually conducted separately using the OsiriX and Image J software programs.

Liver Volume Determination. Image analysis was performed using OsiriX (OsiriX Imaging Software) software and Image J software (NIH). For volume estimation, 3D-VIBE (a T1-weighted FLASH technique with fat selective prepulse) sequences were used. The liver was identified on each image, and the outline of the liver tissue annotated by freehand region of interest estimation by operators trained by a body radiologist with over 10 y of experience in MRI of the liver. This allowed for the generation of a liver area on each slice. Liver volume was calculated by multiplying the estimated area of each slice by the interval between slices, summing all volumes containing liver for the total liver volume (46).

Liver volume determinations were performed by two blinded operators. Operators independently measured liver volumes for five cases with two MRI scans per case (early and late pregnancy). The observed interoperator variability (*SI Appendix*, Table S2) was used to benchmark values that are within the range of measurement error, in this case +7 to −7%.

MRS. IHL was measured using 1H single-voxel MRS, following MRI. Liver MRS voxels were positioned within the right lobe with voxel sizes ranging from 18 to 24 cm^3.

Liver spectra were collected using a point-resolved spectroscopy single-voxel spectroscopy sequence (TR = 5 s, TE = 30 ms, 1,024 points, 2,000 Hz spectral width). The long repetition time ensured fully relaxed water signal (99.2%), because it serves as an internal standard for quantification. Three separately acquired MRS series were run, each during a 10-s breath hold.

MRS analysis was conducted using the advanced method for accurate, robust, and efficient spectral time-domain fitting module within the jMRUI software program. All spectral fits were inspected and rerun with additional constraints if fitting contained errors. IHL is expressed as a proportion of primary lipid peak to water peak areas.

Hyperinsulinemic-Euglycemic Clamp. Hyperinsulinemic-euglycemic clamp with coinfusion of [6,6-2H2] glucose was used to determine whole-body and skeletal muscle insulin sensitivity (Rd) and EGP (56, 57). Subjects were advised regarding a standard diet consisting of 30% of total calories from fat sources, 15% from protein, and 55% from carbohydrates for the 3 d before study. Following an 11-h overnight fast, subjects were admitted to the OHSU Clinical and Translational Research Center where a hyperinsulinemic-euglycemic clamp was performed. At 0600, an intravenous catheter was placed in one arm for infusions and in the contralateral hand for blood withdrawal and warmed to 70 °C using a warming mitt for sampling of arterialized venous blood. A primed constant infusion of [6,6-2H2] glucose (Cambridge Isotope Laboratories) was infused at 0.133 mL/min and an enrichment intended to achieve ∼1.0 mol percent excess for all subjects. The basal infusion of [6,6-2H2] glucose was continued for 2 h, and plasma samples were obtained from 90 to 120 min to estimate basal EGP and fasting insulin concentration. Basal EGP was calculated according to the steady-state equations of Steele (58). At the completion of the 2-h infusion glucose isotope, a primed, constant infusion of regular insulin at 40 mU/m2/min was started. Plasma glucose was maintained at 90 mg/dL for the remaining 2 h. During the final 30 min of the clamp, blood samples were obtained every 5 min for isotope analysis. Suppression of EGP by insulin infusion during the 2-h clamp was estimated using the method developed by Black (59). EGP, Rd, and M value were adjusted for insulin level (mU/L) and fat-free mass (kg).

Labs. Venipuncture was used to obtain blood samples with participants in the fasting state. The following measures were assessed and run in the Laboratory Core of the Oregon Clinical and Translation Research Institute: comprehensive metabolic panel, lipid panel, free fatty acids, liver function tests, glucose, and insulin. Insulin was assessed by radioimmunoassay (Mercodia AB) and glucose by a Hexokinase based colorimetric assay (Stanbio laboratory).

Bile Acid Profiling. Bile acid profiling was performed in the OHSU Bioanalytical Shared Resource/Pharmacokinetics Core. Plasma samples from early and late pregnancy were utilized to quantify plasma bile acids and 7α-hydroxy-4-cholesten-3-one using liquid chromatography–tandem mass spectrometry (LC-MS/MS). Quantification of plasma bile acids was performed with a 4000 QTRAP hybrid triple quadrupole-linear ion trap mass spectrometer (SCIEX) operating with electrospray ionization (ESI) in the negative mode. The mass spectrometer was interfaced to a Shimadzu high-performance liquid chromatography (HPLC) system consisting of SIL-20AC XR auto-sampler and LC-20AD XR LC pumps. Analyte separation was achieved using a gradient HPLC method and Luna 2.5u C18 (2)-HST 50 × 2 mm column (Phenomenex) kept at 50 °C with a Shimadzu CTO-20AC column oven.

The stable isotope dilution LC-MS/MS method to quantify plasma bile acids was previously described (60). In brief, plasma was spiked with internal standards, and bile acids were measured following protein precipitation and extraction with methanol, centrifugation, and filtration of the supernatant. Calibrants were prepared in charcoal stripped matrix (SP1070 from Golden West Biological) using authentic bile acid and conjugate standards (obtained from Toronto Research Chemicals and Cerilliant).

Data were acquired using SCIEX Analyst 1.6.2 and analyzed using SCIEX MultiQuant 3.0.3 software. Sample values were calculated from calibration curves generated from the peak area ratio of the analyte to internal standard versus analyte concentration that was fit to a linear equation with 1/× weighting. The following bile acids were measured: Taurocholic acid (TCA), Glycocholic acid (GCA), Taurochenodeoxycholic acid (TCDCA), Glycochenodeoxycholic acid (GCDCA), Ursodeoxycholic acid (UDCA), Cholic acid (CA), Chenodeoxycholic acid (CDCA), Deoxycholic acid (DCA), and Lithocholic acid (LCA). Compounds were quantified with multiple reaction monitoring and transitions optimized by infusion of pure compounds.

Plasma 7α-hydroxy-4-cholesten-3-one was determined by LC-MS/MS following protein precipitation and extraction with acetonitrile. To each 100 μL sample of EDTA plasma was added 1 ng of internal standard 7α-hydroxy-4-cholesten-3-one-d7 (prepared at 0.2 ng/μL in methanol) and 300 μL of acetonitrile. The samples were vortex mixed and centrifuged at 12,000 × *g* for 10 min. The supernatant was removed and filtered prior to injection for analysis with LC-MS/MS.

Calibration standards were prepared across the range 1 to 100 ng/mL in charcoal stripped plasma SP1070 (Golden West Biological) using authentic 7α-hydroxy-4-cholesten-3-one (obtained from Toronto Research Chemicals).

LC-MS/MS was performed using a 5500 QTRAP hybrid triple quadrupole-linear ion trap mass spectrometer (SCIEX) with ESI in the positive mode. The mass spectrometer was interfaced to a Shimadzu HPLC system consisting of SIL-20AC XR auto-sampler and LC-20AD XR LC pumps. The 5500 QTRAP was operated with the following settings: source voltage 4500 kV, GS1 40, GS2 30, CUR 40, TEM 650, and CAD gas high.

Analyte separation was achieved using a Gemini 3u C6-Phenyl 110A 100 × 2 mm column (Phenomenex) kept at 35 °C using a Shimadzu CTO-20AC column oven. The gradient mobile phase was delivered at a flow rate of 0.4 mL/min and consisted of two solvents: A, 0.1% formic acid in water; B: 0.1% formic acid in acetonitrile. The initial concentration of solvent B was 40% followed by a linear increase to 95% B in 10 min, this was held for 2 min, then decreased back to 40% B over 0.1 min, then held for 3 min. The retention time for 7α-hydroxy-4-cholesten-3-one was 8.2 min.

Data were acquired using SCIEX Analyst 1.6.2 and analyzed using SCIEX MultiQuant 3.0.3 software. Sample values were calculated from calibration curves generated from the peak area ratio of the analyte to internal standard versus analyte concentration that was fit to a linear equation with 1/× weighting.

FGF19 ELISA. Human serum concentration of FGF-19 was determined using the Human FGF-19 Quantikine enzyme-linked immunoassay (ELISA) (R&D Systems, DF1900). Assay was completed according to manufacturer's instructions with samples run in duplicate.

Rodent Studies.

Postpartum rodent model. The University of Colorado Anschutz Medical Campus approved rat procedures. Age-matched Sprague Dawley female rats

(Harlan) were housed and bred as described (61). For tissue collection, rats were euthanized across groups by CO_2 asphyxiation and cardiac puncture. Whole livers were removed, washed 3× in 1× phosphate-buffered saline (PBS), and tissues weighed. Left lobes were fixed in 10% neutral buffered formalin (Anatech ltd) and processed for formalin fixed, paraffin embedded, and caudate lobes were flash frozen on liquid nitrogen for protein and RNA extraction. Oregon Health & Science University Institutional Animal Care and Use Committees approved mouse procudures. Age-matched Balb/c female mice (Charles River Laboratories, The Jackson Laboratory) were housed and bred as described (61). For tissue collection, mice were euthanized across groups by CO_2 asphyxiation and cardiac puncture. Whole livers were removed, washed 3× in 1× PBS and tissues weighed. Caudate lobes were flash frozen on liquid nitrogen for RNA extraction.

Immunohistochemistry. Immunohistochemical detection was performed as described (62). Briefly, tissues were deparaffinized, rehydrated, and heat-mediated antigen retrieval was performed with EDTA for 5 min at 125 °C. Primary antibodies used were as follows: Ki67 (Neomarkers RM-9106-s, 1:50) for 2 h at room temperature (RT) and Adipophilin (LS-B2168/34250 Lifespan Biosciences, 1:400) for 1 h at RT. Secondary antibody was anti-rabbit (Agilent Envision+ K4003, RTU), used for Ki67 at 1 h at RT and for Adipophilin at 30 min at RT. DAB chromogen (Agilent, K346889-2) with hematoxylin counter stain (Agilent, S330130-2) was used to visualize positive stain. Stained sections were scanned using the Aperio AT2 slide scanner (Leica Biosystems). Number of Ki67+ hepatocytes were counted in five 1 × 1 mm areas. Adipophilin signal quantification was performed by Aperio ImageScope version 12.1.0.5029 as described previously (63). All analyses were done by investigators blinded to group.

Real-time qRT-PCR. RNA was isolated from flash frozen rat liver for complementary DNA (cDNA) synthesis and qPCR. One microgram total RNA was used for RT-mediated synthesis of cDNA using SuperScript II RT (Invitrogen) and random hexamer primers for Cyp7a and SuperScript IV (Invitrogen) for FXR. qPCR for rat Cyp7a and reference gene GAPDH was performed using FastStart Essential DNA Green Master (Roche) in an Applied Biosystems theromocycler with 45 cycles of 95 °C for 20 s, 60 °C for 40 s, and 72 °C for 20 s. Rat primer sequences were as follows: Cyp7a, forward CTGTCATACCACAAAGTCTTATG TCA and reverse ATGCTTCTGTGTCCAAATGCC; GAPDH forward CGCTGGTG CTGAGTATGTCG and reverse CTGTGGTCATGAGCCCTTCC.

qPCR for rat FXR and reference gene GAPDH was performed using SsoAdvanced Unviersal SYBR Green Supermix (BioRad) in the ViiA 7 Real-Team PCR System (Thermo Fisher) with the following times: 95 °C for 2 min, 40 cycles of 95 °C for 15 s and 56 °C for 60 s, then 95 °C for 15 s, 61 °C for 60 s, and 95 °C for 15 s. Rat primer sequences were as follows: FXR, forward AGGCCATGTTCCTT CGTTCA and reverse TTCAGCTCCCCGACACTTTT; GAPDH, forward ACCACAGT CCATGCCATCAC and reverse TCCACCACCCTGTTGCTGTA.

Immunoblotting. Rat liver protein lysates in radioimmunoprecipitation assay buffer were separated by Wes automated gel electrophoresis system (Protein Simple). Primary antibodies and dilutions were as follows: CYP7A1 (Abcam no. ab234982, 1:20), FXR (Thermo Fisher Invitrogen no. 417200, 1:50), RXRa (Abcam no. ab125001, 1:20), and GAPDH (Cell Signaling Technology no. 2118, 1:20). Protein input for CYP7A1 and FXR assays was 0.25 mg/mL. Protein input for RXR assay was 0.5 mg/mL. GAPDH assays used both 0.25 mg/mL and 0.5 mg/mL protein input. Anti-rabbit (Protein Simple no. 042-206, RTU) or anti-mouse (Protein Simple no. 042-205, RTU) horseradish peroxidase–conjugated secondary antibodies were utilized, followed by chemiluminescent substrate (Protein Simple no. PS-CS01, Luminol-S, Peroxide). Signal was detected using the Wes System camera. Immunoblot electrophoretograms were analyzed by Compass Software (Protein Simple).

RNA-sequencing. RNA was isolated from flash frozen whole murine liver using the Direct-zol RNA MiniPrep kit (Zymo Research no. R2051). An input of 100 ng RNA was used for library preparation. Library construction was performed by Novogene using a NEBNext Ultra RNA Library Prep Kit for Illumina (cat no. E7420S, New England Biolabs) according to the manufacturer's protocol. Briefly, messenger RNA (mRNA) was enriched using oligo(dT) beads followed by two rounds of purification and fragmented randomly by adding fragmentation buffer. The first-strand cDNA was synthesized using random hexamers primer, after which a custom second-strand synthesis buffer (Illumina), dNTPs, RNase H, and DNA polymerase I were added to generate the second-strand (double stranded cDNA). After a series of terminal repair, polyadenylation, and sequencing adaptor ligation, the double-stranded cDNA library was completed following size selection and PCR enrichment. The resulting 250- to 350-base pair (bp) insert libraries were quantified using a Qubit 2.0 fluorometer (Thermo Fisher Scientific) and qPCR. Size distribution was analyzed using an Agilent 2100 Bioanalyzer (Agilent Technologies). Qualified libraries were sequenced on an Illumina Novaseq6000 Platform (Illumina) using a paired-end 150 run (2 × 150 bases). The raw fastq files were first quality checked using FastQC (version 0.11.8) software. Fastq files were aligned to mm10 mouse reference genome (GRCm38.39) and per-gene counts quantified by RNA-Seq by Expectation-Maximization (RSEM) (version 1.3.1) based on the gene annotation Mus_musculus.GRCm38.89.chr.gtf. Differential gene expression analysis was performed using DESeq2 (version 1.22.2) (64). Gene expression differences were considered significant if passing the following criteria: adjusted P value < 0.05, log2(fold change) ≥ 1. Custom gene set for GSEA analysis was built from curated gene lists available from Molecular Signature Database (http://www.gsea-msigdb.org/gsea/index.jsp). Specifically, the gene set was composed from the following: REACTOME_DOWNSTREAM_SIGNALING_OF_ACTIVATED_FGFR4 and REACTOME_BILE_ACID_AND_BILE_SALT_METABOLISM. Gene Set Enrichment Analysis (GSEA) analysis was performed with GSEA software developed by the University of California San Diego and Broad Institute (65, 66).

Data Availability. Raw RNA-sequencing data of mouse liver tissues performed in this study have been deposited in the Gene Expression Omnibus database under accession code GSE188680. All other study data are included in the article and/or *SI Appendix*.

ACKNOWLEDGMENTS. We want to thank Mara Kalter and Claire Dorfman for participant outreach and scheduling and thank our study participants, whose generous gift of time and trust made this study possible. We acknowledge the OHSU Bioanalytical Shared Resource for providing technical assistance and access to analytical instrumentation. We are grateful to Dr. Gordon Mills for constructive review of the manuscript and Weston Anderson for outstanding assistance with manuscript writing, editing, and preparation. Funding was received from the following: OHSU Center for Women's Health Circle of Giving to P.S., K.K.V., and J.Q.P.; DoD Grant No. BC170206 to P.S.; OHSU School of Medicine Dean's Fund to P.S., A.D., and A.Q.B.; and National Institute of Diabetes and Digestive and Kidney Diseases, No. R01DK098707 to K.K.V.

1. J. Guy, M. G. Peters, Liver disease in women: The influence of gender on epidemiology, natural history, and patient outcomes. *Gastroenterol. Hepatol. (N. Y.)* **9**, 633–639 (2013).
2. E. T. Goddard *et al.*, The rodent liver undergoes weaning-induced involution and supports breast cancer metastasis. *Cancer Discov.* **7**, 177–187 (2017).
3. A. Q. Bartlett, N. D. Pennock, A. Klug, P. Schedin, Immune milieu established by postpartum liver involution promotes breast cancer liver metastasis. *Cancers (Basel)* **13**, 1698 (2021).
4. G. K. Michalopoulos, Hepatostat: Liver regeneration and normal liver tissue maintenance. *Hepatology* **65**, 1384–1392 (2017).
5. K. M. Rasmussen, A. L. Yaktine, Eds., *Weight Gain During Pregnancy: Reexamining the Guidelines* (The National Academies Collection: Reports funded by National Institutes of Health, 2009).
6. G. Dai *et al.*, Maternal hepatic growth response to pregnancy in the mouse. *Exp. Biol. Med. (Maywood)* **236**, 1322–1332 (2011).
7. J. R. Carvalho, M. Verdelho Machado, New insights about albumin and liver disease. *Ann. Hepatol.* **17**, 547–560 (2018).
8. J. E. Gerich, Role of the kidney in normal glucose homeostasis and in the hyperglycaemia of diabetes mellitus: Therapeutic implications. *Diabet. Med.* **27**, 136–142 (2010).
9. F. Hytten, Blood volume changes in normal pregnancy. *Clin. Haematol.* **14**, 601–612 (1985).
10. P. M. Catalano *et al.*, Longitudinal changes in basal hepatic glucose production and suppression during insulin infusion in normal pregnant women. *Am. J. Obstet. Gynecol.* **167**, 913–919 (1992).
11. W. Huang *et al.*, Nuclear receptor-dependent bile acid signaling is required for normal liver regeneration. *Science* **312**, 233–236 (2006).
12. A. Milona *et al.*, Raised hepatic bile acid concentrations during pregnancy in mice are associated with reduced farnesoid X receptor function. *Hepatology* **52**, 1341–1349 (2010).
13. X. Wu *et al.*, FGF19-induced hepatocyte proliferation is mediated through FGFR4 activation. *J. Biol. Chem.* **285**, 5165–5170 (2010).
14. T. Inagaki *et al.*, Fibroblast growth factor 15 functions as an enterohepatic signal to regulate bile acid homeostasis. *Cell Metab.* **2**, 217–225 (2005).
15. B. M. Forman *et al.*, Identification of a nuclear receptor that is activated by farnesol metabolites. *Cell* **81**, 687–693 (1995).
16. M. Makishima *et al.*, Identification of a nuclear receptor for bile acids. *Science* **284**, 1362–1365 (1999).
17. C. Gälman, I. Arvidsson, B. Angelin, M. Rudling, Monitoring hepatic cholesterol 7alpha-hydroxylase activity by assay of the stable bile acid intermediate 7alpha-hydroxy-4-cholesten-3-one in peripheral blood. *J. Lipid Res.* **44**, 859–866 (2003).
18. J. Huang, D. A. Rudnick, Elucidating the metabolic regulation of liver regeneration. *Am. J. Pathol.* **184**, 309–321 (2014).
19. W. E. Naugler, Bile acid flux is necessary for normal liver regeneration. *PLoS One* **9**, e97426 (2014).

20. W. E. Naugler *et al.*, Fibroblast growth factor signaling controls liver size in mice with humanized livers. *Gastroenterology* **149**, 728–40.e15 (2015).
21. M. Pibiri *et al.*, Cyclin D1 is an early target in hepatocyte proliferation induced by thyroid hormone (T3). *FASEB J.* **15**, 1006–1013 (2001).
22. R. López-Fontal *et al.*, Mice lacking thyroid hormone receptor Beta show enhanced apoptosis and delayed liver commitment for proliferation after partial hepatectomy. *PLoS One* **5**, e8710 (2010).
23. R. Stricker *et al.*, Evaluation of maternal thyroid function during pregnancy: The importance of using gestational age-specific reference intervals. *Eur. J. Endocrinol.* **157**, 509–514 (2007).
24. J. J. Endendijk, H. A. A. Wijnen, V. J. M. Pop, A. L. van Baar, Maternal thyroid hormone trajectories during pregnancy and child behavioral problems. *Horm. Behav.* **94**, 84–92 (2017).
25. A. Milona *et al.*, The normal mechanisms of pregnancy-induced liver growth are not maintained in mice lacking the bile acid sensor Fxr. *Am. J. Physiol. Gastrointest. Liver Physiol.* **298**, G151–G158 (2010).
26. D. R. Grattan, "The actions of prolactin in the brain during pregnancy and lactation" in *Progress in Brain Research,* J. A. Russell, A. J. Douglas, R. J. Windle, C. D. Ingram, Eds. (Elsevier, 2001), pp. 153–171.
27. Y. Hu, Y. Ding, M. Yang, Z. Xiang, Serum prolactin levels across pregnancy and the establishment of reference intervals. *Clin. Chem. Lab. Med.* **56**, 838–842 (2018).
28. J. J. Berlanga, J. A. Fresno Vara, J. Martín-Pérez, J. P. García-Ruiz, Prolactin receptor is associated with c-src kinase in rat liver. *Mol. Endocrinol.* **9**, 1461–1467 (1995).
29. I. M. Olazabal *et al.*, Prolactin's role in the early stages of liver regeneration in rats. *J. Cell. Physiol.* **219**, 626–633 (2009).
30. B. Moreno-Carranza *et al.*, Prolactin promotes normal liver growth, survival, and regeneration in rodents: Effects on hepatic IL-6, suppressor of cytokine signaling-3, and angiogenesis. *Am. J. Physiol. Regul. Integr. Comp. Physiol.* **305**, R720–R726 (2013).
31. J. Cao *et al.*, Differential regulation of hepatic bile salt and organic anion transporters in pregnant and postpartum rats and the role of prolactin. *Hepatology* **33**, 140–147 (2001).
32. R. H. Westbrook, G. Dusheiko, C. Williamson, Pregnancy and liver disease. *J. Hepatol.* **64**, 933–945 (2016).
33. P. Saudan, M. A. Brown, M. L. Buddle, M. Jones, Does gestational hypertension become pre-eclampsia? *Br. J. Obstet. Gynaecol.* **105**, 1177–1184 (1998).
34. J. A. Hutcheon, S. Lisonkova, K. S. Joseph, Epidemiology of pre-eclampsia and the other hypertensive disorders of pregnancy. *Best Pract. Res. Clin. Obstet. Gynaecol.* **25**, 391–403 (2011).
35. D. J. Barker, The origins of the developmental origins theory. *J. Intern. Med.* **261**, 412–417 (2007).
36. D. J. Barker, K. L. Thornburg, The obstetric origins of health for a lifetime. *Clin. Obstet. Gynecol.* **56**, 511–519 (2013).
37. T. P. Fleming *et al.*, Origins of lifetime health around the time of conception: Causes and consequences. *Lancet* **391**, 1842–1852 (2018).
38. S. Jindal, J. Narasimhan, V. F. Borges, P. Schedin, Characterization of weaning-induced breast involution in women: Implications for young women's breast cancer. *NPJ Breast Cancer* **6**, 55 (2020).
39. T. Stein, N. Salomonis, B. A. Gusterson, Mammary gland involution as a multi-step process. *J. Mammary Gland Biol. Neoplasia* **12**, 25–35 (2007).
40. E. T. Goddard *et al.*, Association between postpartum breast cancer diagnosis and metastasis and the clinical features underlying risk. *JAMA Netw. Open* **2**, e186997 (2019).
41. D. T. Janerich, M. B. Hoff, Evidence for a crossover in breast cancer risk factors. *Am. J. Epidemiol.* **116**, 737–742 (1982).
42. M. Lambe *et al.*, Transient increase in the risk of breast cancer after giving birth. *N. Engl. J. Med.* **331**, 5–9 (1994).
43. P. Schedin, Pregnancy-associated breast cancer and metastasis. *Nat. Rev. Cancer* **6**, 281–291 (2006).
44. A. Lonardo *et al.*, Sex differences in nonalcoholic fatty liver disease: State of the art and identification of research gaps. *Hepatology* **70**, 1457–1469 (2019).
45. S. Wagnerberger *et al.*, Sex-specific differences in the development of acute alcohol-induced liver steatosis in mice. *Alcohol Alcohol.* **48**, 648–656 (2013).
46. S. Perandini, N. Faccioli, M. Inama, R. Pozzi Mucelli, Freehand liver volumetry by using an electromagnetic pen tablet: Accuracy, precision, and rapidity. *J. Digit. Imaging* **24**, 360–365 (2011).
47. J. M. van Raaij, M. E. Peek, S. H. Vermaat-Miedema, C. M. Schonk, J. G. Hautvast, New equations for estimating body fat mass in pregnancy from body density or total body water. *Am. J. Clin. Nutr.* **48**, 24–29 (1988).
48. N. E. Marshall *et al.*, Comparison of multiple methods to measure maternal fat mass in late gestation. *Am. J. Clin. Nutr.* **103**, 1055–1063 (2016).
49. K. Gorgolewski *et al.*, Nipype: A flexible, lightweight and extensible neuroimaging data processing framework in Python. *Front. Neuroinform.*, 10.3389/fninf.2011.00013 (2011).
50. B. B. Avants, N. Tustison, G. Song, Advanced normalization tools (ANTS). *Insight j.* **2**, 1–35 (2009).
51. M. McCormick, X. Liu, J. Jomier, C. Marion, L. Ibanez, ITK: Enabling reproducible research and open science. *Front. Neuroinform.* **8**, 13 (2014).
52. S. van der Walt *et al.*; scikit-image contributors, scikit-image: Image processing in Python. *PeerJ* **2**, e453 (2014).
53. F. Pedregosa *et al.*, Scikit-learn: Machine learning in Python. *J. Mach. Learn. Res.* **12**, 2825–2830 (2011).
54. P. Virtanen, *et al.;* SciPy 1.0 Contributors, SciPy 1.0: Fundamental algorithms for scientific computing in Python. *Nat Methods* **17**, 261–272 (2020).
55. L. Alvarez, L. Baumela, P. Henriquez, P. Marquez-Neila, A real time morphological snakes algorithm. *Image Processing On Line*, 10.5201/ipol.2012.abmh-rtmsa (2012).
56. J. P. Kirwan, L. Huston-Presley, S. C. Kalhan, P. M. Catalano, Clinically useful estimates of insulin sensitivity during pregnancy: Validation studies in women with normal glucose tolerance and gestational diabetes mellitus. *Diabetes Care* **24**, 1602–1607 (2001).
57. P. M. Catalano *et al.*, Carbohydrate metabolism during pregnancy in control subjects and women with gestational diabetes. *Am. J. Physiol.* **264**, E60–E67 (1993).
58. R. Steele, Influences of glucose loading and of injected insulin on hepatic glucose output. *Ann. N. Y. Acad. Sci.* **82**, 420–430 (1959).
59. P. R. Black, D. C. Brooks, P. Q. Bessey, R. R. Wolfe, D. W. Wilmore, Mechanisms of insulin resistance following injury. *Ann. Surg.* **196**, 420–435 (1982).
60. K. L. Calkins *et al.*, Intravenous fish oil and pediatric intestinal failure-associated liver disease: Changes in plasma phytosterols, cytokines, and bile acids and erythrocyte fatty acids. *JPEN J. Parenter. Enteral Nutr.* **42**, 633–641 (2018).
61. S. M. McDaniel *et al.*, Remodeling of the mammary microenvironment after lactation promotes breast tumor cell metastasis. *Am. J. Pathol.* **168**, 608–620 (2006).
62. Q. Guo *et al.*, Physiologically activated mammary fibroblasts promote postpartum mammary cancer. *JCI Insight* **2**, e89206 (2017).
63. T. R. Lyons *et al.*, Postpartum mammary gland involution drives progression of ductal carcinoma in situ through collagen and COX-2. *Nat. Med.* **17**, 1109–1115 (2011).
64. M. I. Love, W. Huber, S. Anders, Moderated estimation of fold change and dispersion for RNA-seq data with DESeq2. *Genome Biol.* **15**, 550 (2014).
65. A. Subramanian *et al.*, Gene set enrichment analysis: A knowledge-based approach for interpreting genome-wide expression profiles. *Proc. Natl. Acad. Sci. U.S.A.* **102**, 15545–15550 (2005).
66. V. K. Mootha *et al.*, PGC-1alpha-responsive genes involved in oxidative phosphorylation are coordinately downregulated in human diabetes. *Nat. Genet.* **34**, 267–273 (2003).